DYNAMICS OF FLUID-CONVEYING TIMOSHENKO PIPES

A Thesis

by

RYAN CURTIS PETRUS

Submitted to the Office of Graduate Studies of
Texas A&M University
in partial fulfillment of the requirements for the degree of

MASTER OF SCIENCE

May 2006

Major Subject: Mechanical Engineering

DYNAMICS OF FLUID-CONVEYING TIMOSHENKO PIPES

A Thesis

by

RYAN CURTIS PETRUS

Submitted to the Office of Graduate Studies of
Texas A&M University
in partial fulfillment of the requirements for the degree of

MASTER OF SCIENCE

Approved by:

Chair of Committee,	J.N. Reddy
Committee Members,	Ray M. Bowen
	Jose Roesset
Head of Department,	Dennis L. O'Neal

May 2006

Major Subject: Mechanical Engineering

ABSTRACT

Dynamics of Fluid-Conveying Timoshenko Pipes. (May 2006)

Ryan Curtis Petrus, B.S., B.S., Louisiana Tech University

Chair of Advisory Committee: Dr. J.N. Reddy

Structures conveying mass lose stability once the mass exceeds a certain critical velocity. The type of instability observed depends on the nature of the supports that the structure has. If the structure (beam or pipe) is cantilevered (thereby deeming it a non-conservative system), “garden-hose-like” flutter instability is observed once a critical velocity is exceeded. When studying the flutter instability of a cantilevered pipe (including shear deformation) by strictly a linear theory, it has been demonstrated through numerical integration that the values of the critical velocity are only valid for small values of the mass ratio (mass of the fluid divided by the total mass) (approximately $\beta < 0.1$). This fact is also true if shear deformation is neglected. Also, linear theory predicts the pipe to oscillate unboundedly as time progresses, which is physically impossible. Therefore, shortly after the pipe goes unstable, the linear theory is no longer applicable. If non-linear terms are taken into account from the beginning, it can be shown that the pipe oscillates into a limit cycle.

This thesis, along with the rest of my degrees, is dedicated to my Dad. He has supported every decision I have made throughout college (and life) and he has helped me in every way possible. He has always taught me to work hard at everything and reach every goal set.

ACKNOWLEDGEMENTS

When I came to Texas A&M University in 2004, I had no background in mechanical engineering and thus, had no particular interests. Because I had to be taught from square one, I would like to acknowledge every professor that helped me gain knowledge (and interest) in mechanics and dynamics. Therefore, I would like to give my appreciation to Professors Reddy, Srinivasa, Bowen, Palazzolo, and Roesset.

TABLE OF CONTENTS

CHAPTER Page

LIST OF TABLES

TABLE Page

LIST OF FIGURES

FIGURE Page

FIGURE Page

CHAPTER I

INTRODUCTION

The stability of structures conveying mass has interested engineers over the past century; such applications include exhaust pipes, stacks of flue gases, air-conditioning ducts, offshore piping, traveling chains, nuclear reactors, and jet pumps. A particular area of interest that has received attention over the past few decades is the stability of elastic pipes conveying fluid. The dynamic interaction between the fluid (water, gas, etc.) and the pipe causes energy to be transferred to the pipe, and after a sufficient amount of energy exchange, stability of the pipe is lost.

When formulating the equations of motion for elastic pipes, three accelerations associated with the inertial axial transport of mass appear: (i) transverse acceleration of the fluid, (ii) the Coriolis acceleration associated with the change of angular velocity, and (iii) the centripetal acceleration associated with the deformed (curved) shape of the pipe. The new forces, respectively, are

$$F_{transverse} = m_f \frac{\partial^2 w_0}{\partial t^2} \tag{1.1}$$

$$F_{Coriolis} = 2m_f \frac{\partial^2 w_0}{\partial t \partial x} \tag{1.2}$$

$$F_{centripetal} = m_f v^2 \frac{\partial^2 w_0}{\partial x^2} \tag{1.3}$$

This thesis follows the style of *Journal of Sound and Vibration.*

where m_f is the mass per unit length of the fluid, w_0 is the transverse deflection of the beam, and v is the magnitude of the fluid's velocity vector. These new forces cause different types of instability depending solely on the boundary conditions present.

Once these linear equations of motion are formulated, the free-vibration eigenvalue problem is formulated. The imposition of the boundary conditions (simply-supported or cantilevered) will now determine what type of instability is present. If the beam is simply-supported/cantilevered, it can loose stability by buckling/flutter. When the beam is simply supported, the buckling phenomenon is characterized by the domination of the stiffening centripetal force (buckling load) over the Coriolis restoring (damping) force for some critical velocity. When the beam is cantilevered, the flutter phenomenon is characterized by the combination of the work done by the Coriolis force and extra energy added by the fluid; these two energy inputs cause negative damping to occur at some critical velocity. Paidoussis [1] stated (proved by Benjamin [2]) that the rate of work done by the fluid forces over a period of oscillation is

$$\frac{dW}{dt} = -\int_0^L \frac{\partial w_0}{\partial t} m_f \left(\frac{\partial}{\partial t} + v \frac{\partial}{\partial x} \right)^2 w_0 dx \tag{1.4}$$

where w_0 is the transverse displacement, m_f is the mass per unit length of the fluid, and v is the velocity of the fluid. The work done over a cycle T is thus

$$\Delta W = -m_f v \int_0^T \left[\left(\frac{\partial w_0}{\partial t} \right)^2 + v \left(\frac{\partial w_0}{\partial t} \right) \left(\frac{\partial w_0}{\partial x} \right) \right]_0^L dt \tag{1.5}$$

Consequently, the virtual work for the left end either simply supported or cantilevered is

$$\delta W = -\int_0^T \left[m_f v \left(\frac{\partial w_0}{\partial t} + v \frac{\partial w_0}{\partial x} \right) \delta w_0 \right]_{x=L} dt \tag{1.6}$$

This work will vanish if the right end is simply supported; therefore no extra energy will be added. Because of the aforementioned description of transfer of energy, the simply-supported cantilevered beams are conservative and non-conservative, respectively.

Because cantilevers will be of most interest in this work, the flutter (single-degree-of-freedom) instability for strictly a linear theory will only be studied. When the beam goes into this "garden-hose like" flutter instability (i.e. a Hopt bifurcation), the beam will not oscillate infinitely as linear theory predicts. Instead, the system goes into a limit cycle which can only be explained by non-linear theory. Hence, at the instant the beam reaches this Hopt bifurcation, linear theory abruptly ends. Because only the linear theory is being studied, non-linear aspects (such as limit cycles) will not be studied.

The aim of the first half of this study is to derive the non-dimensional governing equations of motions for the linear Timoshenko beam theory, formulate the Bubnov-Galerkin eigenvalue problem for cantilevered end conditions, solve this eigenvalue problem via basis functions that satisfy the "non-fluid" essential and natural boundary conditions, and determine the non-dimensional critical velocities at which the system goes unstable. Once the critical velocities are ascertained, the second half will begin with a time-dependent finite element model and conclude with numerical integration of a set of coupled ordinary time-dependent differential equations whose unknowns are the total number degrees of freedom taken in the beam. Once this degree of freedom vector is obtained, the transverse degree of freedom (response) at the rightmost end versus time

will be plotted numerically for certain stable and unstable parameters. This numerical process will be repeated for each thickness (slenderness ratio) of the beam.

CHAPTER II

EARLY HISTORY AND LITERATURE REVIEW

As early as 1878, Aitken conducted experiments on traveling chains and elastic cords. In 1885, Brillouin first recognized the self-excited oscillations of a pipe conveying fluid. The first to theoretically derive the governing equations of motion was Bourrieres (one of Brillouin's students) in 1939; he examined the instability (fluttering) of cantilevered pipes both theoretically and experimentally [3]. Bourrieres published a paper that remained unknown to subsequent authors until it was discovered by Paidoussis in 1972.

In the 1950's and 1960's, researchers such as: Feodos'ev, Handelman, Heinrich, Housner, Niordson, and Bolotin, in ignorance of Bourrieres work, re-derived the equations of motion and studied the buckling problem and verified their results experimentally [4]. In 1955, Long [5] studied cantilevered pipes but did not find instabilities because his method was only applicable to small flow velocities.

In 1961, Benjamin [2] was the first to provide a comprehensive study on pipe vibrations. Benjamin derived the correct and complete Lagrange function and the correct equations of motion for articulated pipes, which were verified experimentally also. In 1963 Gregory and Paidoussis also took a serious interest, theoretically and experimentally, in cantilevered pipes. They were the first to obtain critical velocities by approximate and exact methods, which were confirmed by experiments. Authors such as: Blevins (1977), Chen (1987), Paidoussis & Li (1992), and Paidoussis (1998) reported non-monotonic plots of the critical velocity versus the mass ratio [3]. In 2004,

Vittori [3] was the first to prove the non-existence of these non-monotonic results for Euler-Bernoulli beam theory; he instead observed "jumps" occurring at certain values of the mass ratio. He also showed that the number of jumps depended on the terms taken in the approximation. Quoting Elishakoff (Vittori's advisor) [3]: "From a linear differential equation of motion one ought to expect to get results of monotonic critical flow velocities for each non-dimensional parameter β," where β is the mass of the fluid divided by the total mass.

Because of the vast amount of literature available, the present author will not attempt to perform an exhaustive survey; instead, a few key papers will be listed relating to the present work. If interested in the equations of motions and dynamics of linear Euler-Bernoulli pipes (simply-supported and cantilevered), see [2, 5, 6, 7, 8, 9, 10, 11, 12, 13]. Paidoussis and Laithier [4, 14, 15] were the first to correctly derive and non-dimensionalize the linear equations of motion for Timoshenko beam theory assuming a plug-flow model. These equations were derived via the Newtonian approach and solved via the variational principle [16] in order to obtain critical velocities and frequencies for simply supported and cantilevered boundary conditions. Later on, Paidoussis, Luu, and Laithier [17] refined the Timoshenko model for several other outflow models. These equations were solved via a Bubnov-Galerkin and Fourier Transform method.

In reviewing all the Finite Element models for Timoshenko cantilevered beams only, two papers [18, 19] explicitly account for the correct non-conservative energy boundary terms when deriving the finite element model from the energy formulation. Chu and Lin in [19] used the correct methodology in deriving the mass, damping, and

stiffness matrices, but errors exist in the paper that were fixed in a later paper [20]. Pramila, Laukkanen, and Liukkonen [18] use linear interpolation of the rotation and deflection (which requires reduced integration of the rotation) and give explicit dimensional values for the additions into the stiffness and damping matrices. Chu and Lin [19] use an inner-dependent (super-convergent) interpolation for the rotation and deflection and give explicit dimensional values for the additions into the stiffness and damping matrices (i.e. the non-conservative boundary terms). Stack, Garnett, and Pawlas [21] use a conservative energy formulation and derive the correct element matrices, but do not account for the added energy boundary term. Reddy and Wang [22] start with the non-conservative energy formulation (i.e. principal of virtual work). Through integration by parts, the resulting element matrices and boundary terms are correct, but the boundary terms are not explicitly shown. None of the aforementioned authors start the finite element formulation from the weak form (which would also give the correct boundary terms).

Numerous authors have derived the non-linear equations of motion (Euler-Bernoulli and Timoshenko beam theories) from numerous assumptions. Being that there are many non-linear techniques available (Floquet theory, Liapunov's method, Krylov-Bogoliubov's (K-B) method, Finite Element Method…), there are many different routes that could be taken in order to determine equilibrium points, stability, and bifurcations. Through these different methods, the authors from [20, 23, 24, 25, 26, 27, 28] have concluded that the system approached a limit cycle after the onset of instability after a Hopt bifurcation.

CHAPTER III

ENERGY FORMULATION AND EQUATIONS OF MOTION

The purpose of this chapter is to derive the governing equations of motion of a fluid-conveying Timoshenko beam and a fluid-conveying bar via the dynamic virtual work statement (Hamilton's principle; see Reddy [12]). Once the three equations of motion are established, the two transverse beam equations will be non-dimensionalized and utilized hereafter. No boundary conditions will be considered in this chapter.

A. Displacements and Strains

In the classical Euler-Bernoulli beam theory, three assumptions are stated in the hypothesis relating to the plane cross sections (perpendicular to the neutral axis) of the beam after deformation [12]. The plane cross sections remain: (1) plane (no curvature), (2) rigid (not deformed), and (3) perpendicular to the neutral axis (which is chosen to coincide with the centerline) after deformation. Assumption (3) says the angle at which the cross-section rotates about the *y*-axis at a point on the neutral axis is equal to the slope of the neutral axis at that point, or simply $\theta = -\frac{\partial w}{\partial x}$. Due these assumptions, shear strain is neglected as well as the Poisson effect. In addition to the aforementioned assumptions, small strains and rotations are also assumed which leads to a linear relationship between the strains and displacements. In Timoshenko beam theory, assumption (3) is lifted and rotation of the cross-section is no longer equal to the rotation of the neutral axis; rather it is treated as an independent variable ϕ. Again, a linear relationship between the strains and displacements (small rotations and displacements) is

assumed. Using Reddy's notation in [12, 22, 29] (see Fig. 3.1), the displacement field of Timoshenko beam theory is expressed as

$$u(x,z,t) = u_0(x,t) + z\phi(x,t) \tag{3.1}$$

$$w(x,z,t) = w_0(x,t) \tag{3.2}$$

where the transverse displacement, $w_0(x,t)$ (the displacement of a point on the neutral axis) is assumed to be approximately the same as the transverse displacement of an arbitrary point on the transverse normal (which is perpendicular to the neutral axis and thus lies on the cross-section plane).

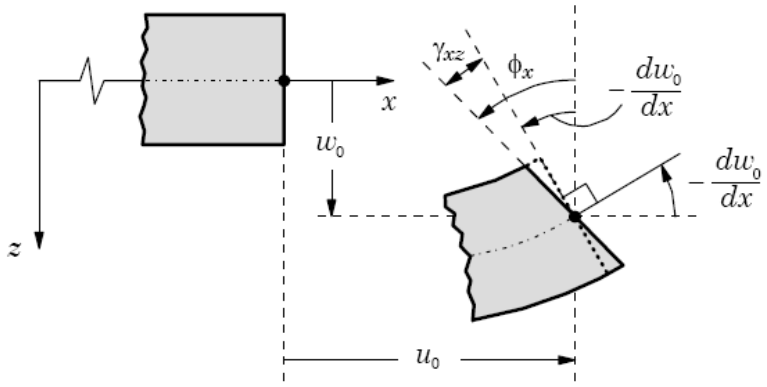

Fig. 3.1. A typical deformed element according to Timoshenko beam theory

The linear strain-displacement relations are

$$\varepsilon_{xx} = \frac{\partial u_0}{\partial x} + z\left(\frac{\partial \phi}{\partial x}\right) \tag{3.3}$$

$$2\varepsilon_{xz} = \gamma_{xz} = \frac{\partial w_0}{\partial x} + \phi \tag{3.4}$$

where, unlike the classical Euler-Bernoulli beam theory, the shear strain γ_{xz} is no longer equal to zero. Although the shear strain in Euler-Bernoulli beam theory is zero, there is still nonetheless a shear force (which must be calculated from the equilibrium equations $\sigma_{ij,j} = 0$) in order to keep equilibrium. All other strains are zero.

B. Virtual Work

Before formulating the virtual work statement, more assumptions in this work must be stated first. It is assumed that an incompressible fluid is flowing through a hollow circular pipe with a constant velocity (see Fig. 3.2), and no distributed axial or transverse loads (such as the weight of the fluid or beam) are applied; no point loads are applied to the beam also. Since the beam will assumed to be straight and horizontal (not resting on an elastic foundation), gravitational effects will be neglected. Finally, no internal frictional forces, outside pressure forces, or end tension forces will be present. All of notation used in formulating the virtual work and equations of motion is borrowed again from Reddy [22].

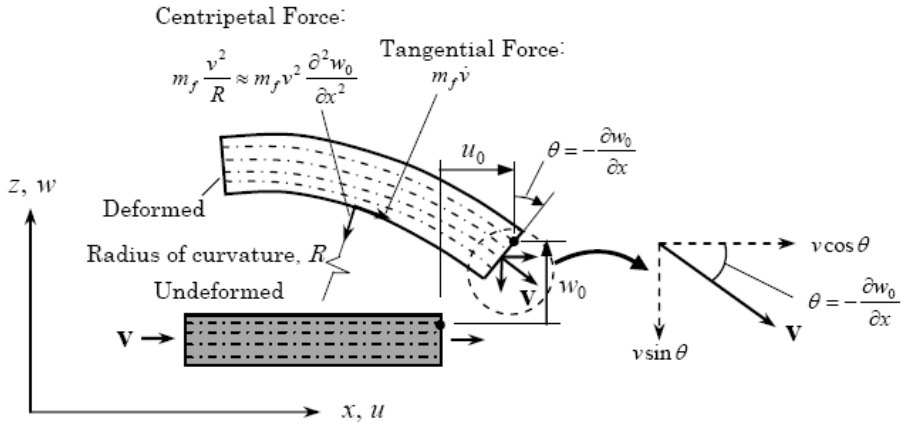

Fig. 3.2. A typical deformed element conveying fluid according to Euler-Bernoulli beam theory

The velocity vector of the fluid is of the form

$$\mathbf{v} = (v\cos\theta + \dot{u}_0)\hat{\mathbf{i}} + (-v\sin\theta + \dot{w}_0)\hat{\mathbf{j}},\ \theta = -\frac{\partial w_0}{\partial x} \tag{3.5}$$

where the over dot represents partial differentiation with respect to time. Due to the fluid velocity, an additional force appears in the virtual external work (δV), which is a part of the total virtual work statement. The force due to the centripetal acceleration of the fluid is

$$F_c = m_f \frac{v^2}{R} \approx m_f v^2 \frac{\partial^2 w_0}{\partial x^2} \tag{3.6}$$

where the curvature of the deformed beam is assumed to be equal to the inverse of the radius of the deformed beam, m_f is the mass per unit length of the fluid, and v is the magnitude of the velocity vector in (3.5). Since the fluid velocity is assumed to be constant, the tangential force is equal to zero. It is implicitly assumed that the Coriolis

force does no work on the free motions of the pipe. The fluid velocity also contributes an additional term in the virtual kinetic energy (δK).

The time-dependent (dynamic) virtual work statement (i.e. Hamilton's principle) for deformable bodies is

$$\int_0^T [(\delta U - \delta V) - \delta K]dt = 0 \tag{3.7}$$

where δU is the internal virtual work due only to the internal beam forces, δV is the external virtual work due to the beam external forces as well as the fluid forces, and δK is the virtual kinetic energy due to the beam forces and the fluid forces. Here

$$\delta U = \int_0^L \int_{A_p} [\sigma_{xx}\delta\varepsilon_{xx} + \sigma_{xz}\delta\gamma_{xz}]dAdx \tag{3.8}$$

$$\delta V = \int_0^L [-m_f v^2 \frac{\partial^2 w_0}{\partial x^2}(\sin\theta\delta u_0 + \cos\theta\delta w_0]dx \tag{3.9}$$

$$\begin{aligned}\delta K = &\int_0^L \int_{A_p} \rho_p[(\dot{u}_0 + z\dot{\phi})(\delta\dot{u}_0 + z\dot{\phi}) + \dot{w}_0\delta\dot{w}_0]dAdx \\ &+ \int_0^L \int_{A_f} \rho_f[\mathbf{v}\cdot\delta\mathbf{v} + z^2\dot{\phi}\delta\dot{\phi}]dAdx\end{aligned} \tag{3.10}$$

where ρ_f is the mass per unit length of the fluid, ρ_p is the mass per unit length of the beam, A_f is the cross-sectional area of the fluid, and A_p is the cross-sectional area of the beam. Note that (3.7) can always be written (where the variational symbol δ stays inside the integral) as opposed to taking the δ outside the integral; this is due to the $\sin\theta$ and $\cos\theta$ in δV.

Define the internal axial force per unit length, internal moment per unit length, and internal shear force per unit length, respectively, as

$$N_{xx} = \int_{A_p} \sigma_{xx} dA \tag{3.11}$$

$$M_{xx} = \int_{A_f} z\sigma_{xx} dA \tag{3.12}$$

$$Q_x = K_s \int_{A_p} \sigma_{xz} dA \tag{3.13}$$

where K_s is the shear correction factor. The reason behind introducing this correction factor is because the shear stress distribution is taken to be constant which contradicts its parabolic distribution calculated from elementary beam theory. For a circular pipe, Cowper [30] solved the three-dimensional elasticity equations and concluded

$$K_s = \frac{6(1+\upsilon)(1+s)^2}{(7+6\upsilon)(1+s)^2 + (20+12\upsilon)s^2} \quad s = \frac{r_i}{r_o} \tag{3.14}$$

where r_i is the inner radius and r_o is the outer radius. Assuming constant fluid and beam mass densities along with constant cross-sectional areas, one obtains

$$m_p = \int_{A_p} \rho_p A_p dA = \rho_p A_p \tag{3.15}$$

$$m_f = \int_{A_f} \rho_f A_f dA = \rho_f A_f \tag{3.16}$$

$$\hat{I}_p = \int_{A_p} \rho_p z^2 dA = \rho_p I_p \tag{3.17}$$

$$\hat{I}_f = \int_{A_f} \rho_f z^2 dA = \rho_f I_f \tag{3.18}$$

where I_p and I_f are the rotary inertias of the beam and fluid respectively. Substituting (3.8)- (3.10) into (3.7) and using (3.11)-(3.18) and (3.3)-(3.4) yields

$$\begin{aligned} 0 = \int_0^T \int_0^L \Bigg\{ & N_{xx} \frac{\partial \delta u_o}{\partial x} + M_{xx} \frac{\partial \delta \phi}{\partial x} + Q_x \left(\frac{\partial \delta w_0}{\partial x} + \delta \phi \right) - m_p (\dot{u}_0 \delta \dot{u}_o + \dot{w}_0 \delta \dot{w}_0) \\ & + m_f v^2 \frac{\partial^2 w_0}{\partial x^2} \left(\sin\theta \delta u_0 + \cos\theta \delta w_0 \right) - m_f [(v\cos\theta + \dot{u}_0)\delta(v\cos\theta + \dot{u}_0) \\ & + (v\sin\theta - \dot{w}_0)\delta(v\sin\theta - \dot{w}_0)] \Bigg\} dx dt \end{aligned} \tag{3.19}$$

In order to derive the equations of motion and the accompanying boundary terms, all terms that involve differentiation of the variational operator δ must be integrated by parts (spatial and time); this procedure must be used in order to use the fundamental lemma of calculus. After integrating by parts, and gathering terms that involve δu_o, δw_0, and $\delta \phi$, (3.19) yields

$$\begin{aligned} 0 = & \int_0^T \int_0^L \left[-\frac{\partial N_{xx}}{\partial x} + (m_p + m_f) \frac{\partial^2 u_0}{\partial x^2} + m_f v \sin\theta \left(\frac{\partial^2 w_0}{\partial x \partial t} + v \frac{\partial^2 w_0}{\partial x^2} \right) \right] \delta u_0 \\ & + \int_0^T \int_0^L \left[-\frac{\partial M_{xx}}{\partial x} + Q_x + (\hat{I}_f + \hat{I}_p) \frac{\partial^2 \phi}{\partial t^2} \right] \delta \phi \\ & + \int_0^T \int_0^L \Bigg\{ -\frac{\partial Q_x}{\partial x} - \frac{\partial}{\partial x} \left(\frac{\partial w_0}{\partial x} N_{xx} \right) + (m_p + m_f) \frac{\partial^2 w_0}{\partial t^2} + m_f v^2 \cos\theta \frac{\partial^2 w_0}{\partial x^2} \\ & + m_f \left[\cos\theta \left(2 \frac{\partial^2 w_0}{\partial x \partial t} - \frac{\partial u_0}{\partial t} \frac{\partial^2 w_0}{\partial x^2} \right) + \sin\theta \left(\frac{\partial^2 u_0}{\partial x \partial t} + \frac{\partial w_0}{\partial t} \frac{\partial^2 w_0}{\partial x^2} \right) \right] \Bigg\} \delta w_0 \\ & + \int_0^T [N_{xx} \delta u_0 + M_{xx} \delta \phi \\ & + \left(Q_x + \frac{\partial w_0}{\partial x} N_{xx} - m_f v (\sin\theta \dot{u}_0 + \cos\theta \dot{w}_0) \right) \delta w_0 \Bigg]_o^L dt \end{aligned} \tag{3.20}$$

where all boundary terms evaluated at the time limits are assumed to vanish, $[\bullet]_0^T = 0$. If the reader so chooses to verify steps involved in arriving at (3.20), the following relations will be helpful

$$\delta\cos\theta = \sin\theta\frac{\partial w_0}{\partial x},\ \delta\sin\theta = -\cos\theta\frac{\partial \delta w_0}{\partial x} \tag{3.21}$$

$$\frac{\partial}{\partial t}(v\cos\theta) = v\sin\theta\frac{\partial^2 w_0}{\partial x\partial t},\ \frac{\partial}{\partial t}(v\sin\theta) = -v\cos\theta\frac{\partial^2 w_0}{\partial t\partial x} \tag{3.22}$$

$$\frac{\partial}{\partial x}\left(\frac{\partial u_0}{\partial t}\sin\theta\right) = \frac{\partial^2 u_0}{\partial t\partial x}\sin\theta - \cos\theta\frac{\partial u_0}{\partial t}\frac{\partial^2 w_0}{\partial x^2} \tag{3.23}$$

Since $\delta u_0, \delta w_0$, and $\delta\phi$ are all arbitrary, the quantities inside the brackets and braces vanish independently (i.e. use of the fundamental lemma of calculus). Assuming that the beam is made of linear isotropic homogeneous material, the constitutive equations can be written as

$$N_{xx} = E_p A_p\frac{\partial u_0}{\partial x} \tag{3.24}$$

$$M_{xx} = E_p I_p\frac{\partial \phi}{\partial x} \tag{3.25}$$

$$Q_x = G_p A_p K_s\left(\frac{\partial w_0}{\partial x} + \phi\right) \tag{3.26}$$

where E_p is the modulus of elasticity, I_p is the area moment of inertia (not to be confused with the mass moment of inertia appearing before), and G_p is the shear modulus. Although the same symbol is used for the mass and area moments of inertia, the presence $\hat{I}_p$ and $\hat{I}_f$ will distinguish the two. Substituting (3.24)-(3.26) in (3.20),

using the approximation $\sin\theta \approx \theta$ and $\cos\theta \approx 1$, and dropping all non-linear terms yield the three linear equations of motion:

$$\delta u_0 : \ (m_p + m_f)\ddot{u}_0 - E_p A_p u_0'' = 0 \tag{3.27}$$

$$\delta w_0 : \ (m_p + m_f)\ddot{w}_0 + 2m_f v\dot{w}_0' + m_f v^2 w_0'' - G_p A_p K_s(\phi' + w_0'') = 0 \tag{3.28}$$

$$\delta \phi : \ (\hat{I}_p + \hat{I}_f)\ddot{\phi} - E_p I_p \phi'' + G_p A_p K_s(\phi + w_0') = 0 \tag{3.29}$$

where the prime denotes partial differentiation with respect to x. These equations are also found in [14, 22]. There are some new terms (accelerations) multiplied by m_f appearing in (3.28) that should be clarified: (i) $\ddot{w}_0$ represents the transverse acceleration of the fluid, (ii) $2v\dot{w}_0'$ represents the Coriolis acceleration associated with the axial velocity *v* which will cause negative or positive damping, and (iii) $v^2 w_0''$ represents the centripetal acceleration of the fluid which is similar to a compressive follower force (buckling load) on a column as stated by Laithier [4]. The boundary terms will be examined more closely when we study the specific problem at hand. Depending solely on which boundary conditions are studied, the dominance of the centripetal force or the Coriolis force will dictate which type of instability is present. If the right-hand side of the beam is simply-supported, it will be subject to buckling. If the right-hand side is free, it will be subject to flutter (oscillatory instability).

It is evident that (3.27) is completely uncoupled from (3.28) and (3.29), thus the axial deformation problem (bar problem) is treated independent of the transverse deformation problem (beam problem). Only the beam problem will be considered in this

work. If there were no fluid present in the beam ($m_f = v = \hat{I}_f = 0$), (3.27)-(3.29) simplify to the well known equations for the transient vibration of a bar and Timoshenko beam:

$$m_p \ddot{u}_0 - E_p A_p u_0'' = 0 \tag{3.30}$$

$$m_p \ddot{w}_0 - G_p A_p K_s (\phi' + w_0'') = 0 \tag{3.31}$$

$$\hat{I}_p \ddot{\phi} - E_p I_p \phi'' + G_p A_p K_s (\phi + w_0') = 0 \tag{3.32}$$

C. Non-Dimensional Equations of Motion

Consider only the transverse equations of motion for a Timoshenko beam:

$$(m_p + m_f)\frac{\partial^2 w_0}{\partial t^2} + 2m_f v \frac{\partial^2 w_0}{\partial t \partial x} + m_f v^2 \frac{\partial^2 w_0}{\partial x^2} - G_p A_p K_s \left(\frac{\partial \phi}{\partial x} + \frac{\partial^2 w_0}{\partial x^2} \right) = 0 \tag{3.33}$$

$$(\hat{I}_p + \hat{I}_f)\frac{\partial^2 \phi}{\partial t^2} - E_p I_p \frac{\partial^2 \phi}{\partial x^2} + G_p A_p K_s \left(\phi + \frac{\partial w_0}{\partial x} \right) = 0 \tag{3.34}$$

Letting $\xi = \frac{x}{L}$ and $\eta = \frac{w_0}{L}$ yields

$$(m_p + m_f)\frac{\partial^2 \eta}{\partial t^2} + \left(\frac{2m_f v}{L} \right)\frac{\partial^2 \eta}{\partial \xi \partial t} + \left(\frac{m_f v^2}{L^2} \right)\frac{\partial^2 \eta}{\partial \xi^2} - G_p A_p K_s \left(\frac{1}{L^2}\frac{\partial^2 \eta}{\partial \xi^2} + \frac{1}{L^2}\frac{\partial \phi}{\partial \xi} \right) \tag{3.35}$$

$$\left(\frac{\hat{I}_p + \hat{I}_f}{L} \right)\frac{\partial^2 \phi}{\partial t^2} - \frac{E_p I_p}{L^3}\frac{\partial^2 \phi}{\partial \xi^2} + G_p A_p K_s \left(\frac{1}{L}\frac{\partial \eta}{\partial \xi} + \frac{1}{L}\phi \right) = 0 \tag{3.36}$$

Letting $\tau = \sqrt{\frac{E_p I_p}{m_f + m_p}} \left(\frac{t}{L^2} \right)$ and doing some algebraic manipulations, (3.35) and (3.36) respectively become

$$\frac{\partial^2\eta}{\partial\tau^2}+\frac{2m_f vL}{E_pI_p}\sqrt{\frac{E_pI_p}{(m_p+m_f)}}\frac{\partial^2\eta}{\partial\xi\partial\tau}+\frac{m_f v^2L^2}{E_pI_p}\frac{\partial^2\eta}{\partial\xi^2}-\frac{L^2G_pA_pK_s}{E_pI_p}\left(\frac{\partial^2\eta}{\partial\xi^2}+\frac{\partial\phi}{\partial\xi}\right)=0 \tag{3.37}$$

$$\left(\frac{\hat{I}_p+\hat{I}_f}{L^2(m_p+m_f)}\right)\frac{\partial^2\phi}{\partial\tau^2}-\frac{\partial^2\phi}{\partial\xi^2}+\left(\frac{G_pA_pK_sL^2}{E_pI_p}\right)\left(\frac{\partial\eta}{\partial\xi}+\phi\right)=0 \tag{3.38}$$

The dimensionless quantities are defined as

$$\Lambda=\frac{G_pA_pK_sL^2}{E_pI_p} \tag{3.39}$$

$$\sigma=\frac{\hat{I}_p+\hat{I}_f}{L^2(m_p+m_f)} \tag{3.40}$$

$$\beta=\frac{m_f}{m_{f+}m_p} \tag{3.41}$$

$$u=\sqrt{\frac{m_f}{E_pI_p}}vL \tag{3.42}$$

where Λ is the "slenderness" of the beam, σ is the rotary inertia constant (not to be confused with stress), β is the mass ratio, and *u* is the non-dimensional velocity. Hence, (3.37) and (3.38) become

$$\frac{\partial^2\eta}{\partial\tau^2}+2\sqrt{\beta}u\frac{\partial^2\eta}{\partial\xi\partial\tau}-(\Lambda-u^2)\frac{\partial^2\eta}{\partial\xi^2}-\Lambda\frac{\partial\phi}{\partial\xi}=0 \tag{3.43}$$

$$\sigma\frac{\partial^2\phi}{\partial\tau^2}-\frac{\partial^2\phi}{\partial\xi^2}+\Lambda\left(\frac{\partial\eta}{\partial\xi}+\phi\right)=0 \tag{3.44}$$

Equations (3.43) and (3.44) will serve as the main equations throughout the rest of this study.

In addition to non-dimensionalizing the equations of motion, the moment and shear force expressions should also be non-dimensionalized. Letting

$$\bar{M}_{xx} = \frac{L}{E_p I_p} M_{xx} \tag{3.45}$$

$$\bar{Q}_x = \frac{L^2}{E_p I_p} Q_x \tag{3.46}$$

yields the non-dimensional bending moment and shear force as

$$\bar{M}_{xx} = \frac{\partial \phi}{\partial \xi} \tag{3.47}$$

$$\bar{Q}_x = \Lambda \left(\frac{\partial \eta}{\partial \xi} + \phi \right) \tag{3.48}$$

The previous non-dimensional quantities and equations of motion are borrowed from Paidoussis [14].

CHAPTER IV

EIGENVALUE PROBLEM AND APPROXIMATE SOLUTION

In the previous chapter we formulated the equations of motion for the transverse vibration of a Timoshenko beam and non-dimensionalized these equations ((3.43) and (3.44)). It is the intent of this chapter to separate the variables, combine the two equations (in the spatial coordinate), and seek an approximate solution to the single spatial equation via the Bubnov-Galerkin weighted residual method. Cantilevered boundary conditions will now be imposed in order to derive the appropriate (and approximate) basis functions.

A. Eigenvalue Problem

Noting that (3.43) and (3.44) involve a single time derivative, a solution of the form

$$\eta = H(\xi)e^{\Omega\tau}\ ,\ \phi = \Phi(\xi)e^{\Omega\tau} \tag{4.1}$$

is needed instead of a solution of the form $[\bullet]e^{i\Omega\tau}$ because introducing the imaginary constant is unnecessary. Substituting (4.1) into (3.43) and (3.44) and dividing throughout by $e^{\Omega\tau}$ yields

$$\Omega^2 H + 2\sqrt{\beta}u\Omega\frac{dH}{d\xi} - (\Lambda - u^2)\frac{d^2H}{d\xi^2} - \Lambda\frac{d\Phi}{d\xi} = 0 \tag{4.2}$$

$$\sigma\Omega^2\Phi - \frac{d^2\Phi}{d\xi^2} + \Lambda\left(\frac{dH}{d\xi} + \Phi\right) = 0 \tag{4.3}$$

where $\Omega = \sqrt{\frac{m_f + m_p}{E_p I_p}}\left(\frac{L^2}{t}\right)$. Equations (4.2) and (4.3) now represent two coupled ordinary differential equations (instead of two partial differential equations) which represent the natural vibration of the Timoshenko beam conveying fluid. Through a few differentiation steps and much algebraic manipulation, (4.2) and (4.3) can be combined through elimination of $\Phi(\xi)$. Thus

$$\begin{aligned}&(\Lambda - u^2)\frac{d^4H}{d\xi^4} - 2\sqrt{\beta}u\Omega\frac{d^3H}{d\xi^3} + (u^2(\Omega^2\sigma + \Lambda) - \Omega^2(\Lambda\sigma + 1))\frac{d^2H}{d\xi^2} \\ &+2\Omega u\sqrt{\beta}(\Omega^2\sigma + \Lambda)\frac{dH}{d\xi} + (\Omega^2\sigma + \Lambda)\Omega^2 H = 0\end{aligned} \tag{4.4}$$

or

$$\begin{aligned}&(\sigma H)\Omega^4 + \left(2u\sqrt{\beta}\sigma\frac{dH}{d\xi}\right)\Omega^3 + \left((u^2\sigma - 1)\frac{d^2H}{d\xi^2} + \Lambda H\right)\Omega^2 \\ &\left(-2\sqrt{\beta}u\frac{d^3H}{d\xi^3} + 2u\sqrt{\beta}\Lambda\frac{dH}{d\xi}\right)\Omega + \left((\Lambda - u^2)\frac{d^4H}{d\xi^4} + u^2\Lambda\frac{d^2H}{d\xi^2}\right) = 0\end{aligned} \tag{4.5}$$

B. Boundary Conditions

Since (4.4) and (4.5) are fourth-order ordinary differential equations in $H(\xi)$, there must be four boundary conditions. At each end of the beam one element of each of the following pairs

$$(\phi, \bar{M}_{xx}) \tag{4.6}$$

$$(\eta, \bar{Q}_x) \tag{4.7}$$

must be specified. The quantities ϕ and η are the essential (or primary) variables, so the specification of either constitutes an essential (geometric) boundary condition (EBC).

The quantities $\bar{M}_{xx}$ and $\bar{Q}_x$ are the force (or secondary) variables, so any specification of either constitutes a natural (force) boundary condition (NBC).

For the problem of a cantilevered beam (left end clamped and right end free),

$$\phi(\xi,\tau)=\eta(\xi,\tau)=0 \text{ at } \xi=0 \tag{4.8}$$

$$\bar{M}_{xx}(\xi,\tau)=\bar{Q}_x(\xi,\tau)=0 \text{ at } \xi=1 \tag{4.9}$$

and thus the first element of the pairs (4.6) and (4.7) is specified at $\xi=0$ and second element of the pairs (4.6) and (4.7) is specified at $\xi=1$. Since (4.8) and (4.9) only involve specification of a spatial variable, the separated spatial variables can also be used, hence

$$H(0)=\Phi(0)=0 \tag{4.10}$$

$$\frac{dH}{d\xi}(1)+\Phi(1)=\frac{d\Phi}{d\xi}(1)=0 \tag{4.11}$$

where (3.47) and (3.48) have been used for the expressions for $\bar{M}_{xx}$ and $\bar{Q}_x$. Since (4.4) involves only $H(\xi)$, (4.10) and (4.11) must be re-written in terms of $H(\xi)$ only. The new four boundary conditions are

$$H(0)=0 \tag{4.12}$$

$$(\Lambda-u^2)\frac{d^3H}{d\xi^3}(0)-2\sqrt{\beta}u\Omega\frac{d^2H}{d\xi^2}(0)+(\Lambda-\Omega^2)\frac{dH}{d\xi}(0)=0 \tag{4.13}$$

$$(\Lambda-u^2)\frac{d^3H}{d\xi^3}(1)-2\sqrt{\beta}u\Omega\frac{d^2H}{d\xi^2}(1)-\Omega^2(\sigma+1)\frac{dH}{d\xi}(1)=0 \tag{4.14}$$

$$(\Lambda-u^2)\frac{d^2H}{d\xi^2}(1)-2\sqrt{\beta}u\Omega\frac{dH}{d\xi}(1)-\Omega^2H(1)=0 \tag{4.15}$$

which are very complicated and will not be satisfied exactly. Instead, the boundary conditions for the single equation of a cantilevered Timoshenko beam without fluid will be satisfied. The single equation (non-dimensionalized) for the natural vibration of a Timoshenko beam without fluid (retaining the rotary inertia term) is

$$\frac{d^4H}{d\xi^4}+\omega^2(S+1)\frac{d^2H}{d\xi^2}+\omega^2\left(\omega^2S-\frac{I}{A}\right)H=0 \tag{4.16}$$

Equation (4.16) can also be found in [4, 31].

The new boundary conditions to be satisfied are

$$H(0)=0 \tag{4.17}$$

$$\frac{1}{S}\frac{d^3H}{d\xi^3}(0)+\left(\omega^2+\frac{T^2}{S^2}\right)\frac{dH}{d\xi}(0)=0 \tag{4.18}$$

$$\frac{1}{S}\frac{d^2H}{d\xi^2}(1)+\omega^2H(1)=0 \tag{4.19}$$

$$\frac{d^3H}{d\xi^3}(1)+\omega^2(1+S)\frac{dH}{d\xi}(1)=0 \tag{4.20}$$

where $S=\frac{E_p}{K_sG_p}$, $T^2=\frac{A_p}{I_p}$, and $\omega^2=\frac{\left(\frac{1}{t^2}\right)\rho L^2}{E_p}$ (square of the non-dimensional frequency of the beam without fluid). See [4] for explicit derivation of (4.17)-(4.20) Therefore, for known values of E_p, A_p, K_s, I_p, and ω^2, one can solve (4.4) subject to boundary conditions (4.17)-(4.20).

C. The Bubnov-Galerkin Weighted Residual Method

The Bubnov-Galerkin weighted residual method is an approximation technique for solutions of differential equations; it is also the approximate solution witch minimizes the potential energy. Unlike the Raleigh-Ritz method, the Bubnov-Galerkin method requires basis functions that satisfy all boundary conditions (essential as well as natural).

We seek a solution of the form

$$H_N = \sum_{j=1}^{N} c_j \psi_j \tag{4.21}$$

to (4.4) where the ψ_j's are the basis functions and the c_j's are the non-zero constants to be determined. The only situation which some of the constants can be zero is if the basis functions, ψ_j's, are of the same form as the exact (closed form) solution and the number of functions taken is greater than the number terms in the exact solution; i.e. $c_j = 0$ for all terms of higher order than the exact solution. This situation will not occur in the present work. The number of basis functions taken (*N*) will dictate the degree of the accuracy of the solution obtained. The basis functions, ψ_j's, must: (1) satisfy all the boundary conditions, (2) be linearly independent, and (3) must form a complete set (i.e. all lower order terms must be included). See Reddy [12] for a more detailed description of the Bubnov-Galerkin approximation along other weighted residual approximations. Since (4.21) is only an approximation, (4.4) will not be satisfied exactly.

The residual is defined as

$$R_N = (\Lambda - u^2)\frac{d^4 H_N}{d\xi^4} - 2\sqrt{\beta}u\Omega\frac{d^3 H_N}{d\xi^3} + (u^2(\Omega^2\sigma + \Lambda) - \Omega^2(\Lambda\sigma + 1))\frac{d^2 H_N}{d\xi^2}$$
$$+2\Omega u\sqrt{\beta}(\Omega^2\sigma + \Lambda)\frac{dH_N}{d\xi} + (\Omega^2\sigma + \Lambda)\Omega^2 H_N \tag{4.22}$$

which does not vanish. Instead, the Bubnov-Galerkin method forces each basis function, ψ_j , to be orthogonal to R_N in the weighted integral sense. Define $R_N = R_{N1} + R_{N2} + R_{N3} + R_{N4} + R_{N5}$, where

$$R_{N1} = (\Lambda - u^2)\frac{d^4 H_N}{d\xi^4} \tag{4.23}$$

$$R_{N2} = -2\sqrt{\beta}u\Omega\frac{d^3 H_N}{d\xi^3} \tag{4.24}$$

$$R_{N3} = (u^2(\Omega^2\sigma + \Lambda) - \Omega^2(\Lambda\sigma + 1))\frac{d^2 H_N}{d\xi^2} \tag{4.25}$$

$$R_{N4} = 2\Omega u\sqrt{\beta}(\Omega^2\sigma + \Lambda)\frac{dH_N}{d\xi} \tag{4.26}$$

$$R_{N5} = (\Omega^2\sigma + \Lambda)\Omega^2 H_N \tag{4.27}$$

Therefore, the orthogonality condition yields

$$\begin{aligned} 0 &= \int_0^1 \psi_1 (R_{N1} + R_{N2} + R_{N3} + R_{N4} + R_{N5}) d\xi \\ &\vdots \\ 0 &= \int_0^1 \psi_i (R_{N1} + R_{N2} + R_{N3} + R_{N4} + R_{N5}) d\xi \\ &\vdots \\ 0 &= \int_0^1 \psi_N (R_{N1} + R_{N2} + R_{N3} + R_{N4} + R_{N5}) d\xi \end{aligned} \tag{4.28}$$

After substituting (4.21) into (4.28), one obtains

$$
\begin{aligned}
0 &= \int_0^1 \psi_1 \left[\begin{array}{l} (\Lambda - u^2)\sum_{j=1}^{N} \frac{d^4\psi_j}{d\xi^4} - 2\sqrt{\beta}u\Omega \sum_{j=1}^{N} \frac{d^3\psi_j}{d\xi^3} \\ +(u^2(\Omega^2\sigma+\Lambda) - \Omega^2(\Lambda\sigma+1))\sum_{j=1}^{N} \frac{d^2\psi_j}{d\xi^2} \\ +2\Omega u\sqrt{\beta}(\Omega^2\sigma+\Lambda)\sum_{j=1}^{N} \frac{d\psi_j}{d\xi} + (\Omega^2\sigma+\Lambda)\Omega^2 \sum_{j=1}^{N} \psi_j \end{array} \right] c_j d\xi \\
&\vdots \\
0 &= \int_0^1 \psi_i \left[\begin{array}{l} (\Lambda - u^2)\sum_{j=1}^{N} \frac{d^4\psi_j}{d\xi^4} - 2\sqrt{\beta}u\Omega \sum_{j=1}^{N} \frac{d^3\psi_j}{d\xi^3} \\ +(u^2(\Omega^2\sigma+\Lambda) - \Omega^2(\Lambda\sigma+1))\sum_{j=1}^{N} \frac{d^2\psi_j}{d\xi^2} \\ +2\Omega u\sqrt{\beta}(\Omega^2\sigma+\Lambda)\sum_{j=1}^{N} \frac{d\psi_j}{d\xi} + (\Omega^2\sigma+\Lambda)\Omega^2 \sum_{j=1}^{N} \psi_j \end{array} \right] c_j d\xi \\
&\vdots \\
0 &= \int_0^1 \psi_N \left[\begin{array}{l} (\Lambda - u^2)\sum_{j=1}^{N} \frac{d^4\psi_j}{d\xi^4} - 2\sqrt{\beta}u\Omega \sum_{j=1}^{N} \frac{d^3\psi_j}{d\xi^3} \\ +(u^2(\Omega^2\sigma+\Lambda) - \Omega^2(\Lambda\sigma+1))\sum_{j=1}^{N} \frac{d^2\psi_j}{d\xi^2} \\ +2\Omega u\sqrt{\beta}(\Omega^2\sigma+\Lambda)\sum_{j=1}^{N} \frac{d\psi_j}{d\xi} + (\Omega^2\sigma+\Lambda)\Omega^2 \sum_{j=1}^{N} \psi_j \end{array} \right] c_j d\xi
\end{aligned}
\tag{4.29}
$$

or after factoring out the summation symbol,

$$0=\int_0^1 \psi_1 \sum_{j=1}^{N} \left[\begin{array}{l} (\Lambda-u^2)\dfrac{d^4\psi_j}{d\xi^4}-2\sqrt{\beta}u\Omega\dfrac{d^3\psi_j}{d\xi^3} \\ +(u^2(\Omega^2\sigma+\Lambda)-\Omega^2(\Lambda\sigma+1))\dfrac{d^2\psi_j}{d\xi^2} \\ +2\Omega u\sqrt{\beta}(\Omega^2\sigma+\Lambda)\dfrac{d\psi_j}{d\xi}+(\Omega^2\sigma+\Lambda)\Omega^2\psi_j \end{array} \right] c_j d\xi$$

$$\vdots$$

$$0=\int_0^1 \psi_i \sum_{j=1}^{N} \left[\begin{array}{l} (\Lambda-u^2)\dfrac{d^4\psi_j}{d\xi^4}-2\sqrt{\beta}u\Omega\dfrac{d^3\psi_j}{d\xi^3} \\ +(u^2(\Omega^2\sigma+\Lambda)-\Omega^2(\Lambda\sigma+1))\dfrac{d^2\psi_j}{d\xi^2} \\ +2\Omega u\sqrt{\beta}(\Omega^2\sigma+\Lambda)\dfrac{d\psi_j}{d\xi}+(\Omega^2\sigma+\Lambda)\Omega^2\psi_j \end{array} \right] c_j d\xi$$

$$\vdots$$

$$0=\int_0^1 \psi_N \sum_{j=1}^{N} \left[\begin{array}{l} (\Lambda-u^2)\dfrac{d^4\psi_j}{d\xi^4}-2\sqrt{\beta}u\Omega\dfrac{d^3\psi_j}{d\xi^3} \\ +(u^2(\Omega^2\sigma+\Lambda)-\Omega^2(\Lambda\sigma+1))\dfrac{d^2\psi_j}{d\xi^2} \\ +2\Omega u\sqrt{\beta}(\Omega^2\sigma+\Lambda)\dfrac{d\psi_j}{d\xi}+(\Omega^2\sigma+\Lambda)\Omega^2\psi_j \end{array} \right] c_j d\xi \qquad (4.30)$$

The matrix form of (4.30) is

$$\left(\left[R_1\right]+\left[R_2\right]+\left[R_3\right]+\left[R_4\right]+\left[R_5\right]\right)\{c\}=0 \qquad (4.31)$$

where

$$R_{1ij}=(\Lambda-u^2)\int_0^1\left(\psi_i\frac{d^4\psi_j}{d\xi^4}\right)d\xi \qquad (4.32)$$

$$R_{2ij}=-2\sqrt{\beta}u\Omega\int_0^1\left(\psi_i\frac{d^3\psi_j}{d\xi^3}\right)d\xi \qquad (4.33)$$

$$R_{3ij} = (u^2(\Omega^2\sigma + \Lambda) - \Omega^2(\Lambda\sigma + 1))\int_0^1 \left(\psi_i \frac{d^2\psi_j}{d\xi^2}\right) d\xi \tag{4.34}$$

$$R_{4ij} = 2\Omega u\sqrt{\beta}(\Omega^2\sigma + \Lambda)\int_0^1 \left(\psi_i \frac{d\psi_j}{d\xi}\right) d\xi \tag{4.35}$$

$$R_{5ij} = (\Omega^2\sigma + \Lambda)\Omega^2 \int_0^1 \left(\psi_i\psi_j\right) d\xi \tag{4.36}$$

and $\{c\}$ is the column vector of constants. The simplest form of (4.31) is

$$[K]\{c\} = 0 \tag{4.37}$$

where

$$K_{ij} = R_{1ij} + R_{2ij} + R_{3ij} + R_{4ij} + R_{5ij} \quad i, j = 1..N \tag{4.38}$$

It should be noted that (4.31), a *NxN* matrix, is not a symmetric matrix. The reasoning behind breaking up (4.38) into smaller terms is to make the numerical program easier to write.

D. Basis Functions

Two families of basis functions will be considered in this work: trigonometric\hyperbolic functions and polynomial functions. The trigonometric\hyperbolic functions are exact solutions to (4.16) subject to cantilevered boundary conditions (4.17)-(4.20). The n^{th} non dimensional natural frequency of the non-fluid beam is given by

$$2 + \left(\frac{\alpha}{\beta} - \frac{\beta}{\alpha}\right)\sinh\alpha\sin\beta - \left(\frac{C}{D} + \frac{D}{C}\right)\cosh\alpha\cos\beta = 0 \tag{4.39}$$

and the n^{th} mode shape is given by

$$\psi_n = \cosh\alpha\xi - \cos\beta\xi - \hat{H}\left(\frac{\alpha}{C}\sinh\alpha\xi + \frac{\beta}{D}\sin\beta\xi\right) \tag{4.40}$$

where

$$C = S + \left(\frac{\alpha}{\omega_n}\right)^2 \tag{4.41}$$

$$D = S - \left(\frac{\beta}{\omega_n}\right)^2 \tag{4.42}$$

$$\hat{H} = \frac{C\cosh\alpha - D\cos\beta}{\alpha\sinh\alpha + \beta\sin\beta} \tag{4.43}$$

$$\alpha = \frac{\omega_n}{\sqrt{2}}\sqrt{\sqrt{(s^2 + r^2)} - (s + r)} \tag{4.44}$$

$$\beta = \frac{\omega_n}{\sqrt{2}}\sqrt{\sqrt{(s^2 + r^2)} + (s + r)} \tag{4.45}$$

$$s = S - 1 \tag{4.46}$$

$$r = \frac{2T}{\omega_n} \tag{4.47}$$

and T, ω_n, and S were defined earlier. Equations (4.39)-(4.47) can be found in [31]. It is clear that functions (mode shapes) in (4.40) are linearly independent and all lower order frequencies are included; therefore, the family of functions is complete. Since the pipe will be taken to be circular $A = \pi(r_o^2 - r_i^2)$ and $I = \frac{\pi}{4}(r_0^4 - r_i^4)$, therefore

$$\frac{A}{I} = \frac{4}{(r_0^2 + r_i^2)} \tag{4.48}$$

As for deriving polynomial functions that satisfy (4.17)-(4.20) , it is evident that they should at least be of order three to avoid a zero value after differentiating. Noticing

that (4.17)-(4.20) represent four homogeneous boundary conditions, a fourth order polynomial (five constants) should be considered while taking the highest order term's coefficient to be 1. Since (4.17) says each approximation function cannot contain any constant terms, the linear term will be the lowest order term (for the first polynomial) and there will now be only three boundary conditions to satisfy ((4.18)-(4.20)). The first polynomial function is

$$\psi_1 = a_1\xi + b_1\xi^2 + c_1\xi^2 + \xi^4 \tag{4.49}$$

where a_1, b_1, c_1 are to be determined by (4.18)-(4.20). Choosing successive polynomials of lowest order higher than the highest order of the previous one (e.g. $\psi_2 = \xi^5 + \cdots$), the boundary condition (4.18) will always be satisfied (not matter what the values of the constants are), therefore only two constants will be needed to satisfy (4.19) and (4.20). Again, (4.19) and (4.20) represent homogeneous boundary conditions so a three term polynomial should be chosen with its highest order term's coefficient set arbitrarily equal to 1. Hence

$$\psi_2 = a_2\xi^5 + b_2\xi^6 + \xi^7 \tag{4.50}$$

$$\psi_i = a_i\xi^{3i-1} + b_i\xi^{3i} + \xi^{3i+1}\ ,\ i = 2\ldots N \tag{4.51}$$

where the $a_i's, b_i's$ are determined from (4.19) and (4.20). It should be noted that the polynomials in (4.51) are linearly independent from one another and form a complete set since no lower order terms were omitted. To author's knowledge, this is the first time the polynomial functions have been used as basis functions (for this particular problem) and are explicitly given.

CHAPTER V

DETERMINATION OF THE CRITICAL VELOCITIES

The aim of this chapter is to ascertain the non-dimensional critical velocities at which the beam flutters (goes unstable) for a particular value of β. In order to determine these critical velocities, the Routh-Hurwitz stability criteria will be employed. Once each of these critical velocities are found, a $U_{critical}$ vs. β graph will be produced.

In order to proceed any further, some material parameters and numerical values must first be given. Considering a steel circular pipe, $E_p = 30x10^6\ psi$, $\upsilon = 0.3$, $G_p = \frac{E}{2(1+\upsilon)} = 11.5x10^6\ psi$, and $L = 1.0in$. Also, the non-dimensional transverse frequencies for the non-fluid beam must be given for each slenderness ratio (Λ). Three orders of thickness will be considered: thin (Euler-Bernoulli) ($\Lambda \sim 10^5$), moderately thick ($\Lambda \sim 10^3$), and thick ($\Lambda \sim 10^2$). For very thick beams ($\Lambda \sim 10$), the non-dimensional frequencies (without fluid) are close to the longitudinal frequencies of a bar. In addition to having higher frequencies, Laithier [4] proved the problem of buckling (along with flutter) also exists when $\Lambda \sim 10$ depending on which mode is studied. To avoid this complication, this very thick case will not be studied. The frequencies for all three thicknesses and the bar are in Table 5.1. The foregoing results were obtained through MAPLE 9.5 using an INTEL P4 system.

Table 5.1
Natural frequencies (without fluid) for various beam thicknesses

	ω_{bar}	$\Lambda \sim 10^5$	$\Lambda \sim 10^3$	$\Lambda \sim 10^2$	$\Lambda \sim 10$
ω_1	1.570796327	$2.362372626 \times 10^{-3}$	$2.337654720 \times 10^{-2}$	$7.212260362 \times 10^{-2}$	$2.122360546 \times 10^{-1}$
ω_2	4.712388981	$1.477368423 \times 10^{-2}$	$1.435269561 \times 10^{-1}$	$4.247818785 \times 10^{-1}$	1.104139140
ω_3	7.853981635	$4.130946503 \times 10^{-2}$	$3.966633082 \times 10^{-1}$	1.144960166	2.782898680
ω_4	10.99557429	$8.082982514 \times 10^{-2}$	$7.665781524 \times 10^{-1}$	2.152082224	4.798831388
ω_5	14.13716694	$1.334205190 \times 10^{-1}$	1.250066803	3.411857169	6.885963501

A. Rotary Inertia

Assuming the fluid is an infinitely long and infinitely flexible rod (plug-flow model) moving inside the tube, this rod has rotary inertia ([4, 11, 14]). Paidoussis [14] calculated σ (3.40) to be on the order of 10^{-3} or10^{-4}. He also concluded that the presence of the rotary inertia coefficient destabilized the system; the critical velocity would be lower. Moreover, he showed the lower value of the critical velocity is uniform for all values of β and the value is very close to the value obtained when $\sigma = 0$. Therefore, we will take $\sigma = 0$ in the foregoing discussion.

B. Routh-Hurwitz Stability Criteria

Noticing that (4.37) represents *N* homogeneous equations (assuming $[K]$ is invertible), the only solution that for $\{c\}$ that exists is the trivial one

$$c_1 = c_2 = \cdots = c_N = 0 \tag{5.1}$$

This contradicts the Bubnov-Galerkin criterion that not all of the determined constants must be non-zero. Therefore, one must conclude that the coefficient matrix must be singular (non-invertible); hence

$$\det([K]) = 0 \tag{5.2}$$

Once (5.2) is evaluated, an equation of the form

$$f(\Omega) = a_0\Omega^n + a_1\Omega^{n-1} + \cdots + a_{n-1}\Omega + a_n = 0 \tag{5.3}$$

results where the coefficients, a_i'*s* ,are functions of β and u. Taking $\sigma = 0$, the order of Ω in (5.3) is *2N* , where *N* is the number of basis functions (terms) taken.

Once (5.3) is established, a Hurwitz determinant is formed with its elements being the coefficients in (5.3) (see Appendix A or [3] for the derivation). For $N = 2$ $(n = 4)$

$$T_4 = \begin{vmatrix} a_1 & a_0 & 0 & 0 \\ a_3 & a_2 & a_1 & 0 \\ 0 & a_4 & a_3 & a_2 \\ 0 & 0 & 0 & a_4 \end{vmatrix} = 0 \tag{5.4}$$

and for $n > 4$

$$T_n = \begin{vmatrix} a_1 & a_3 & a_5 & a_7 & \cdots & a_{2n-1} \\ a_0 & a_2 & a_4 & a_6 & \cdots & a_{2n-2} \\ 0 & a_1 & a_3 & a_5 & \cdots & a_{2n-3} \\ 0 & a_0 & a_2 & a_4 & \cdots & a_{2n-4} \\ \vdots & \vdots & \vdots & \vdots & \ddots & \vdots \\ 0 & 0 & 0 & 0 & 0 & a_n \end{vmatrix} \tag{5.5}$$

which yields an equation involving just 2 unknowns, β and u. Because the stability of a system is solely dependent on whether the real part of at least one eigenvalue changes from negative to positive, the purpose of formulating these determinants is to create an expression (involving u and β) for where $\mathrm{Re}(\Omega) = 0$ (for any Ω). In progressing from (5.3) to (5.5) notice that the number of unknowns are cut down from three to two. In order to determine the critical value of *u*, a value for the mass ratio β is substituted into (5.5) and the equation is solved for *u*. Once the roots of *u* are obtained, the smallest positive real value is chosen as the critical velocity.

C. Determination of the Critical Velocities by Trigonometric\Hyperbolic Basis Functions for a Thin Beam

1. Two-Term Approximation

For a very thin beam ($\Lambda \sim 10^5$), the beam is essentially an Euler-Bernoulli beam. For all the calculations in this section, we will take $s = \frac{r_i}{r_o} = 0.9$, thus $K_s = 0.553$ and $\Lambda = 4.703581016 \times 10^5$. Because of the aforementioned statement, the rotary inertia term will be neglected ($\sigma = 0$). The two trigonometric\hyperbolic functions are calculated (N=2) from (4.40)-(4.47) and Table 5.1

$$\begin{aligned}
&\psi_1 = \cosh(1.873164451\xi) - \cos(1.874834902\xi) \\
&-.7335200160\sinh(1.873164451\xi) + .7328783684\sin(1.874834902\xi) \\
&\psi_2 = \cosh(4.681178124\xi) - \cos(4.691624810\xi) \\
&-1.018707870\sinh(4.681178124\xi) + 1.016542838\sin(4.691624810\xi)
\end{aligned} \tag{5.6}$$

Substituting (5.6) and into (4.37) and using (5.2) one arises at

$$\begin{aligned}
&f(\Omega) = (1.860538410x10^{11})\Omega^4 + (1.489684018x10^{12}\sqrt{\beta}u)\Omega^3 + \\
&(5.673131814x10^{12}\sqrt{\beta}u - 2.311558504x10^{12}u^2 + 9.227477883x10^{13})\Omega^2 + \\
&(-2.600938751x10^{12}\sqrt{\beta}u^3 + 3.686558328x10^{14}\sqrt{\beta}u)\Omega + \\
&+(1.109282486x10^{15} + 4.621547898x10^{13}u^2 + 1.979282128x10^{12}u^4) = 0
\end{aligned} \tag{5.7}$$

and hence (5.4) can be used. After selecting the appropriate coefficients and evaluating the Hurwitz determinant, (5.4) yields a 10^{th} order equation in u

$$\begin{aligned}
&(6.542196630x10^{48}\beta - 4.350657158x10^{49}\beta^2)u^{10} \\
&+(-2.564306915x10^{51}\beta + 5.150739183x10^{51}\beta^2)u^8 \\
&+(-1.439525714x10^{52}\beta + 1.196046463x10^{53}\beta^2)u^6 \\
&+(3.456052241x10^{54}\beta^2 - 4.631506116x10^{53}\beta)u^4 \\
&+(2.543342023x10^{55}\beta)u^2 = 0
\end{aligned} \tag{5.8}$$

For each value of β $(0 \le \beta \le 0.99)$, equation (5.8) can be solved and the smallest positive real value of *u* gives the value for the critical velocity. For example, when $\beta = 0.1$,

$$
\begin{aligned}
u_1 &= 0.0 \\
u_2 &= 0.0 \\
u_3 &= -2.449382666 + 4.204079422i \\
u_4 &= 2.449382666 - 4.204079422i \\
u_5 &= -2.449382666 - 4.204079422i \\
u_6 &= 2.449382666 + 4.204079422i \\
u_7 &= -4.702764105 \\
u_8 &= 4.702764105 \\
u_9 &= -30.59900565 \\
u_{10} &= 30.59900565
\end{aligned}
\tag{5.9}
$$

hence, $U_{critical} = 4.702764105$. Table 5.2 gives the critical velocities for all values of β. Figure 5.1 shows the plot of $U_{critical}$ vs. β.

Table 5.2
Dimensionless critical velocities for the two-term trigonometric\hyperbolic approximation ($\Lambda \sim 10^5$)

β	U_{crit}	β	U_{crit}	β	U_{crit}	β	U_{crit}
0.01	4.221410035	0.26	5.948455211	0.51	8.320991370	0.76	9.628788291
0.02	4.268771126	0.27	6.044169059	0.52	8.395337364	0.77	9.663124514
0.03	4.317529487	0.28	6.141547449	0.53	8.467444262	0.78	9.696502965
0.04	4.367740138	0.29	6.240411904	0.54	8.537348310	0.79	9.728959665
0.05	4.419459729	0.30	6.340560148	0.55	8.605092803	0.80	9.760529104
0.06	4.472746378	0.31	6.441768121	0.56	8.670726635	0.81	9.791244310
0.07	4.527659472	0.32	6.543792900	0.57	8.734303028	0.82	9.821136892
0.08	4.584259397	0.33	6.646376457	0.58	8.795878424	0.83	9.850237104
0.09	4.642607188	0.34	6.749250117	0.59	8.855511527	0.84	9.878573901
0.10	4.702764105	0.35	6.852139522	0.60	8.913262473	0.85	9.906174991
0.11	4.764791094	0.36	6.954769880	0.61	8.969192158	0.86	9.933066884
0.12	4.828748140	0.37	7.056871200	0.62	9.023361655	0.87	9.959274954
0.13	4.894693487	0.38	7.158183276	0.63	9.075831746	0.88	9.984823481
0.14	4.962682710	0.39	7.258460165	0.64	9.126662519	0.89	10.00973571
0.15	5.032767630	0.40	7.357473988	0.65	9.175913095	0.90	10.03403388
0.16	5.104995051	0.41	7.455017896	0.66	9.223641338	0.91	10.05773930
0.17	5.179405323	0.42	7.550908173	0.67	9.269903704	0.92	10.08087236
0.18	5.256030722	0.43	7.644985446	0.68	9.314755086	0.93	10.10345260
0.19	5.334893654	0.44	7.737115086	0.69	9.358248708	0.94	10.12549872
0.20	5.416004699	0.45	7.827186894	0.70	9.400436071	0.95	10.14702867
0.21	5.499360544	0.46	7.915114137	0.71	9.441366892	0.96	10.16805960
0.22	5.584941825	0.47	8.000832196	0.72	9.481089108	0.97	10.18860801
0.23	5.672710978	0.48	8.084296802	0.73	9.519648868	0.98	10.20868968
0.24	5.762610176	0.49	8.165482117	0.74	9.557090527	0.99	10.22831975
0.25	5.854559462	0.50	8.244378683	0.75	9.593456701	1.00	10.24751276

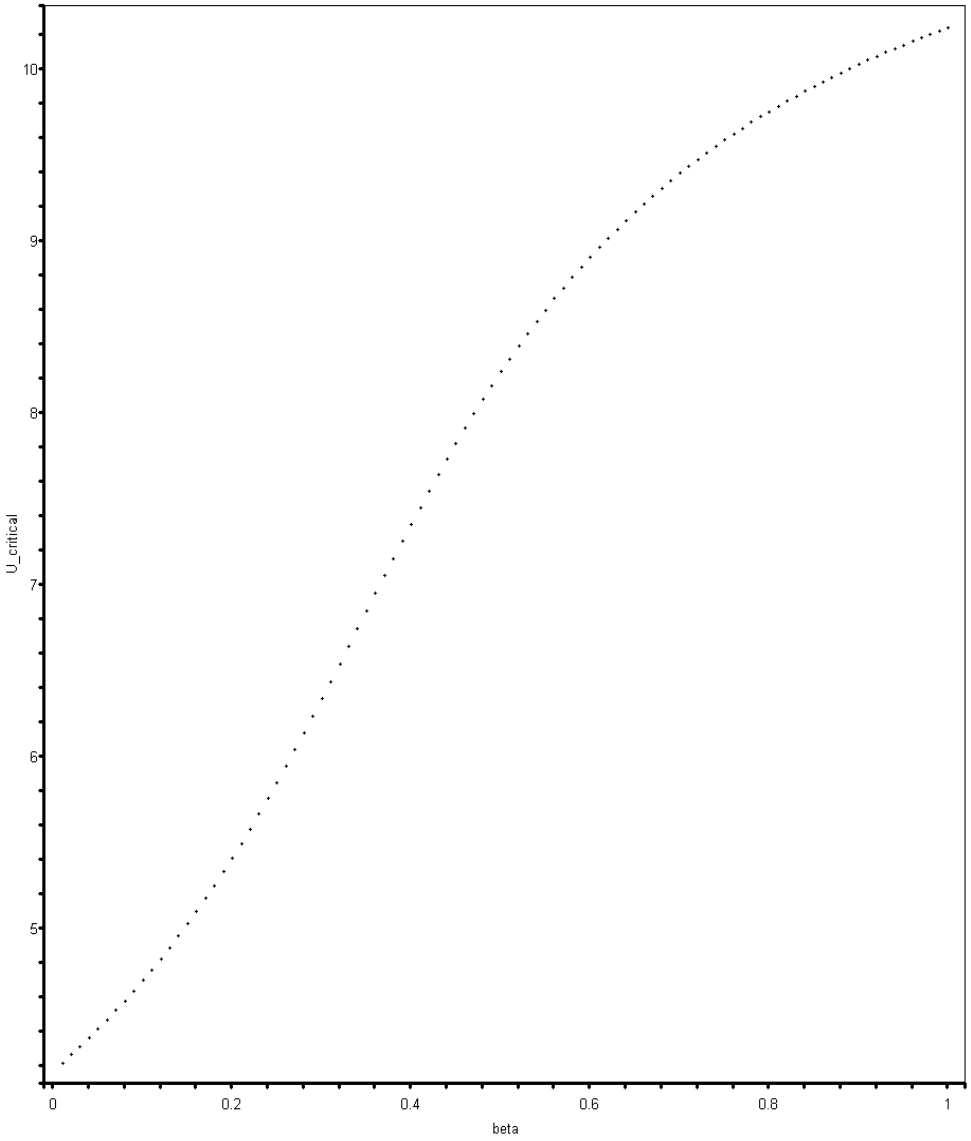

Fig. 5.1. Critical velocity vs. β for the two-term trigonometric\hyperbolic approximation ($\Lambda \sim 10^5$)

2. Four-Term Approximation

For the *N=4* $(n = 8, \sigma = 0)$ case, the basis functions are once again calculated from (4.40)-(4.47)

$$\begin{aligned}
&\psi_1 = \cosh(1.873164451\xi) - \cos(1.874834902\xi) \\
&- 0.7335200160 \sinh(1.873164451\xi) + 0.7328783684 \sin(1.874834902\xi) \\
&\psi_2 = \cosh(4.681178124\xi) - \cos(4.691624810\xi) \\
&- 1.018707870 \sinh(4.681178124\xi) + 1.016542838 \sin(4.691624810\xi) \\
&\psi_3 = \cosh(7.821844789\xi) - \cos(7.851055879\xi) \\
&- 0.9991985754 \sinh(7.821844789\xi) + 0.9957637917 \sin(7.851055879\xi) \\
&\psi_4 = \cosh(10.93316575\xi) - \cos(10.99032445\xi) \\
&- 1.000035711 \sinh(10.93316575\xi) + 0.9953879581 \sin(10.99032445\xi)
\end{aligned} \tag{5.10}$$

Substituting (5.10) into (5.2) yields an 8^{th} order equation in Ω. After collecting the appropriate coefficients and substituting them into (5.5) yields a 36^{th} order equation in *u*. For $\beta = 0.1$ the 36 roots are given in Table 5.3 and the critical velocity is $U_{critical} = 4.746540677$. The critical velocities for each value of β are given in Table 5.4 and the plot of $U_{critical}$ vs. β is given in Figure 5.2. One should notice the "jumps" around $\beta = 0.3, 0.8$.

$$f(\Omega) = (3.443344741\text{x}10^{22})\Omega^8 + (5.523318652\text{x}10^{23}\sqrt{\beta}\text{u})\Omega^7$$
$$+(6.489481487\text{x}10^{26} - 5.411008641\text{x}10^{24}\text{u}^2 + 1.008227739\text{x}10^{25}\beta\text{u}^2)\Omega^6$$
$$+(7.786825486\text{x}10^{27}\sqrt{\beta}\text{u} + 8.074998852\text{x}10^{25}\beta^{\frac{3}{2}}\text{u}^3 - 5.898127290\text{x}10^{25}\sqrt{\beta}\text{u}^3)\Omega^5$$
$$+(-4.172277419\text{x}10^{26}\beta\text{u}^4 + 6.777574523\text{x}10^{28}\beta\text{u}^2 + 4.621439498\text{x}10^{28}\text{u}^2 2.147868959\text{x}10^{26}\text{u}^4 +$$
$$3.050278695\text{x}10^{26}\beta^2\text{u}^4 + 2.214426501\text{x}10^{30})\Omega^4$$
$$+(2.341714523\text{x}10^{29}\beta^{\frac{3}{2}}\text{u}^3 + 1.436842443\text{x}10^{27}\sqrt{\beta}\text{u}^5 - 3.240227522\text{x}10^{29}\sqrt{\beta}\text{u}^3 -$$
$$-7.050412717\text{x}10^{26}\text{u}^5\beta^{\frac{3}{2}} + 1.770572859\text{x}10^{31}\sqrt{\beta}\text{u})\Omega^3$$
$$+(-1.766344991\text{x}10^{27}\text{u}^6 + 5.056966847\text{x}10^{29}\text{u}^4 - 9.465015344\text{x}10^{32}$$
$$+6.253028853\text{x}10^{31}\beta\text{u}^2 - 7.955888196\text{x}10^{29}\beta\text{u}^4 - 4.127538098\text{x}10^{31}\text{u}^2$$
$$+4.334146950\text{x}10^{27}\text{u}^6\beta)\Omega^2$$
$$+(-2.036010697\text{x}10^{27}\sqrt{\beta}\text{u}^7 + -1.014158015\text{x}10^{32}\sqrt{\beta}\text{u}^3 + 3.781881737\text{x}10^{33}\sqrt{\beta}\text{u} +$$
$$1.179212620\text{x}10^{30}\sqrt{\beta}\text{u}^5)\Omega$$
$$+(1.399483970\text{x}10^{27}\text{u}^8 + 4.29405850\text{x}10^{30}\text{u}^4 + 1.133308150\text{x}10^{34} - 3.73127493\text{x}10^{28}\text{u}^6$$
$$+2.600115578\text{x}10^{32}\text{u}^2) = 0 \qquad (5.11)$$

Table 5.3
Roots of equation (5.11) for $\beta = 0.1$

u_1 =0.0	u_{13} =-7.580242862-4.266506421i	u_{25} =-10.48349485+5.821908346i
u_2 =0.0	u_{14} =7.580242862+4.266506421i	u_{26} =10.48349485-5.821908346i
u_3 =0.0	u_{15} =-7.580242862+4.266506419i	u_{27} =-10.48349485-5.821908347i
u_4 =0.0	u_{16} =7.580242862-4.266506419i	u_{28} =10.48349485+5.821908347i
u_5 =-2.253832431x10^{-8} +21.78561692i	u_{17} =-7.479523848-3.139185011i	u_{29} =-11.82218069
u_6 =2.253832431x10^{-8} -21.78561692i	u_{18} =7.479523848+3.139185011i	u_{30} =11.82218069
u_7 =-2.417020505-5.636323862i	u_{19} =-7.479523848+3.139185010i	u_{31} =-12.07179829+1.094525628i
u_8 =2.417020505+5.636323862i	u_{20} =7.479523848-3.139185010i	u_{32} =12.07179829-1.094525628i
u_9 =-2.417020505+5.636323862i	u_{21} =-8.680900169-.6969853683i	u_{33} =-12.07179829-1.094525622i
u_{10} =2.417020505-5.636323862i	u_{22} =8.680900169+.6969853683i	u_{34} =12.07179829+1.094525622i
u_{11} =-4.746540677	u_{23} =-8.680900169+.6969853676i	u_{35} =-58.85580076
u_{12} =4.746540677	u_{24} =8.680900169-.6969853676i	u_{36} =58.85580076

Table 5.4
Dimensionless critical velocities for the four-term trigonometric\hyperbolic approximation ($\Lambda \sim 10^5$)

β	U_{crit}	β	U_{crit}	β	U_{crit}	β	U_{crit}
0.01	4.233753436	0.26	6.393321613	0.51	9.507870285	0.76	11.95055796
0.02	4.282902171	0.27	6.577303699	0.52	9.574943843	0.77	11.94997497
0.03	4.333753365	0.28	6.797366526	0.53	9.643376725	0.78	11.94992809
0.04	4.386403648	0.29	7.099303067	0.54	9.713192982	0.79	14.40550130
0.05	4.440957081	0.30	7.590605972	0.55	9.784454107	0.80	14.49439919
0.06	4.497526001	0.31	7.565615774	0.56	9.857119408	0.81	14.58094515
0.07	4.556231754	0.32	7.559441609	0.57	9.931333445	0.82	14.66510011
0.08	4.617205796	0.33	8.513104096	0.58	10.00707237	0.83	14.74686020
0.09	4.680590643	0.34	8.563850657	0.59	10.08454971	0.84	14.82627975
0.10	4.746541264	0.35	8.612716538	0.60	10.16380287	0.85	14.90329731
0.11	4.815226581	0.36	8.661062163	0.61	10.24507503	0.86	14.97784472
0.12	4.886831354	0.37	8.709568588	0.62	10.32855175	0.87	15.04997621
0.13	4.961558403	0.38	8.758688238	0.63	10.41456833	0.88	15.11955427
0.14	5.039631595	0.39	8.808717620	0.64	10.50350092	0.89	15.18657966
0.15	5.121299601	0.40	8.859799044	0.65	10.59586255	0.90	15.25100500
0.16	5.206840968	0.41	8.912070706	0.66	10.69248223	0.91	15.31283906
0.17	5.296571111	0.42	8.965586719	0.67	10.79428825	0.92	15.37203884
0.18	5.390852264	0.43	9.020417628	0.68	10.90284070	0.93	15.42863601
0.19	5.490108129	0.44	9.076583800	0.69	11.02047132	0.94	15.48261564
0.20	5.594845880	0.45	9.134099488	0.70	11.15124317	0.95	15.53401959
0.21	5.705689922	0.46	9.192986907	0.71	11.30305407	0.96	15.58284099
0.22	5.823437974	0.47	9.253229098	0.72	11.49649060	0.97	15.62916369
0.23	5.949152114	0.48	9.314848048	0.73	11.90530020	0.98	15.67307761
0.24	6.084322242	0.49	9.377833309	0.74	11.95511797	0.99	15.71458231
0.25	6.231175824	0.50	9.442172727	0.75	11.95207843	1.00	15.75375386

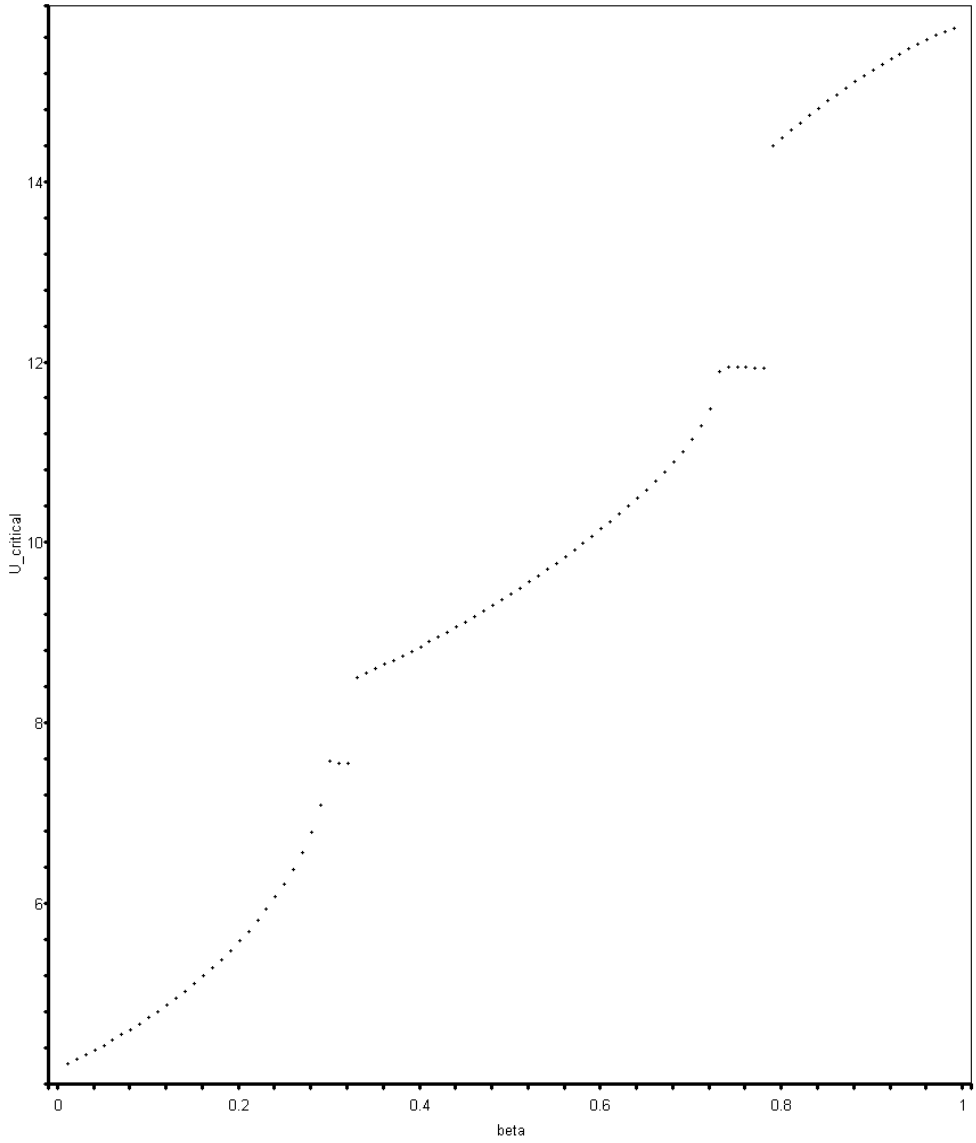

Fig. 5.2. Critical velocity vs. β for the four-term trigonometric\hyperbolic approximation ($\Lambda \sim 10^5$)

3. Five-Term Approximation

The five approximation functions (N=5, $\sigma = 0$), for a very thin beam are

$$
\begin{aligned}
&\psi_1 = \cosh(1.873164451\xi) - \cos(1.874834902\xi) \\
&- 0.7335200160 \sinh(1.873164451\xi) + 0.7328783684 \sin(1.874834902\xi) \\
&\psi_2 = \cosh(4.681178124\xi) - \cos(4.691624810\xi) \\
&- 1.018707870 \sinh(4.681178124\xi) + 1.016542838 \sin(4.691624810\xi) \\
&\psi_3 = \cosh(7.821844789\xi) - \cos(7.851055879\xi) \\
&- 0.9991985754 \sinh(7.821844789\xi) + 0.9957637917 \sin(7.851055879\xi) \\
&\psi_4 = \cosh(10.93316575\xi) - \cos(10.99032445\xi) \\
&- 1.000035711 \sinh(10.93316575\xi) + 0.9953879581 \sin(10.99032445\xi) \\
&\psi_5 = \cosh(14.03611773\xi) - \cos(14.13046951\xi) \\
&- 0.9999983960 \sinh(14.03611773\xi) + 0.9942332301 \sin(14.13046951\xi)
\end{aligned}
\tag{5.12}
$$

Substituting (5.12) into (5.2) yields a 10^{th} order equation in Ω. After selecting the appropriate coefficients and constructing (5.5), one gets a 55^{th} order equation in u. For the $\beta = 0.1$ example, there are 55 roots for u (due to brevity, these roots will be omitted) and $U_{critical} = 4.740665864$. Table 5.5 gives the critical velocities for all values of β and Figure 5.3 gives the graph of $U_{critical}$ vs. β.

$$f(\Omega) = (1.476444719\text{x}10^{28})\Omega^{10} + (3.006878853\text{x}10^{29}\sqrt{\beta}\text{u})\Omega^{9}$$
$$+(8.655652471\text{x}10^{32} + 8.546362881\text{x}10^{30}\beta\text{u}^{2} +$$
$$8.546362881\text{x}10^{30}\beta\text{u}^{2} - 4.866226949\text{x}10^{30}\text{u}^{2})\Omega^{8} +$$
$$(1.378611379\text{x}10^{34}\sqrt{\beta}\text{u} + 1.040623618\text{x}10^{32}\beta^{\frac{3}{2}}\text{u}^{3} - 7.425941872\text{x}10^{31}\sqrt{\beta}\text{u}^{3})\Omega^{7} +$$
$$(1.114332876\text{x}10^{33}\beta\text{u}^{4} - 1.602526085\text{e}36\text{u}^{2} + 2.262090810\text{x}10^{35}\beta\text{u}^{2} +$$
$$8.678793662\text{x}10^{32}\beta^{2}\text{u}^{4} + 1.201833522\text{x}10^{37} + 4.861585509\text{x}10^{32}\text{u}^{4})\Omega^{6} +$$
$$(5.255342693\text{x}10^{33}\sqrt{\beta}\text{u}^{5} + 3.250266455\text{x}10^{33}\beta^{\frac{5}{2}}\text{u}^{5} + 1.438327550\text{x}10^{38}\sqrt{\beta}\text{u} -$$
$$1.804718601\text{x}10^{36}\sqrt{\beta}\text{u}^{3} + 1.655909996\text{x}10^{36}\beta^{\frac{3}{2}}\text{u}^{3} - 6.593102213\text{x}10^{33}\text{u}^{5}\beta^{\frac{3}{2}})\Omega^{5} +$$
$$(-1.243216321\text{x}10^{34}\text{u}^{6}\beta^{2} - 9.698098881\text{x}10^{38}\text{u}^{2} - 7.224951137\text{x}10^{36}\text{u}^{4} +$$
$$3.833884227\text{x}10^{34}\text{u}^{6}\beta + 5.638407733\text{x}10^{36}\beta^{2}\text{u}^{4} - 1.603335468\text{x}10^{34}\text{u}^{6} -$$
$$-1.364783541\text{x}10^{37}\beta\text{u}^{4} + 3.817547309\text{x}10^{40} + 1.222139595\text{x}10^{39}\beta\text{u}^{2})\Omega^{4} +$$
$$(4.164039730\text{x}10^{39}\beta^{\frac{3}{2}}\text{u}^{3} - 3.551420849\text{x}10^{37}\text{u}^{5}\beta^{\frac{3}{2}} + 1.134249143\text{x}10^{35}\text{u}^{7}\beta^{\frac{3}{2}} -$$
$$6.908362541\text{x}10^{39}\sqrt{\beta}\text{u}^{3} - 1.003736082\text{x}10^{35}\sqrt{\beta}\text{u}^{7} + 3.050027469\text{x}10^{41}\sqrt{\beta}\text{u} +$$
$$4.808238874\text{x}10^{37}\sqrt{\beta}\text{u}^{5})\Omega^{3} + (1.124751848\text{x}10^{38}\text{u}^{6}\beta - 7.741038514\text{x}10^{41}\text{u}^{2} -$$
$$1.573388001\text{x}10^{35}\text{u}^{8}\beta + 1.614851895\text{x}10^{43} + 1.261700713\text{x}10^{35}\text{u}^{8} + 1.071405037\text{x}10^{42}\beta\text{u}^{2} -$$
$$1.788089093\text{x}10^{40}\beta\text{u}^{4} - 6.705818264\text{x}10^{37}\text{u}^{6} + 1.169845076\text{x}10^{40}\text{u}^{4})\Omega^{2} +$$
$$(2.902572439\text{x}10^{40}\sqrt{\beta}\text{u}^{5} - 6.452896592\text{x}10^{43}\sqrt{\beta}\text{u} - 2.018219429\text{x}10^{42}\sqrt{\beta}\text{u}^{3} -$$
$$1.607830404\text{x}10^{38}\sqrt{\beta}\text{u}^{7} + 3.852634776\text{x}10^{35}\sqrt{\beta}\text{u}^{9})\Omega + (3.647965296\text{x}10^{42}\text{u}^{2} -$$
$$2.939036828\text{x}10\text{e}41\text{u}^{4} - 1.359381528\text{x}10^{37}\text{u}^{8} + 9.74271902\text{x}10^{38}\text{u}^{6}$$
$$+9.81376717\text{x}10^{34}\text{u}^{10} + 1.932981949\text{x}10^{44}) \tag{5.13}$$

When examining Figure 5.3, there is another jump around $\beta = 0.5$ and some non-monotonic behavior in the highest ranges of β. This non-monotonic behavior is some sort of numerical artifact and will soon be explained as insignificant for the present study.

Figures 5.1-5.2 agree very well with the results obtained by Vittori. It is apparent from these figures, the discontinuities (or "jumps") appear when higher order approximations are used. Vittori also showed that more jumps are present in the higher range of β when a higher order approximation is used. Also, from Tables 5.2-5.5, the critical velocities are increasing for $\beta > 0.3$. Because the Bubnov-Galerkin approximation should improve with more terms taken, the linear model taken in this work is apparently poor for the higher ranges of β; hence the reasoning behind stopping the approximation after five terms. Figure 5.4 shows that the four-term and five-term approximation are very close for $0.0 \le \beta \le 0.3$, i.e. the solution has converged after five terms.

Table 5.5
Dimensionless critical velocities for the five-term trigonometric\hyperbolic. approximation ($\Lambda \sim 10^5$)

β	U_{crit}	β	U_{crit}	β	U_{crit}	β	U_{crit}
0.01	4.234313959	0.26	6.359729755	0.51	10.04078283	0.76	15.30040970
0.02	4.283433961	0.27	6.534628773	0.52	10.08841994	0.77	14.85730731
0.03	4.334242398	0.28	6.740417198	0.53	10.12032508	0.78	15.34106700
0.04	4.386832684	0.29	7.010801409	0.54	10.18670899	0.79	15.12089161
0.05	4.441305325	0.30	7.556994054	0.55	10.21724326	0.80	15.20968556
0.06	4.497768321	0.31	7.522608854	0.56	10.25122905	0.81	15.16159818
0.07	4.556337766	0.32	7.520383384	0.57	10.31217194	0.82	15.60012850
0.08	4.617139020	0.33	7.526262715	0.58	10.34832167	0.83	15.26196981
0.09	4.680307207	0.34	8.438313091	0.59	10.43333671	0.84	15.71547219
0.10	4.745988635	0.35	8.487518566	0.60	10.45269840	0.85	15.28334048
0.11	4.814341938	0.36	8.535363518	0.61	10.48509478	0.86	15.98923795
0.12	4.885539463	0.37	8.583432475	0.62	10.53646935	0.87	15.52182265
0.13	4.959769362	0.38	8.630259462	0.63	10.57897434	0.88	15.49649859
0.14	5.037238562	0.39	8.679586736	0.64	10.61565241	0.89	16.50340298
0.15	5.118174709	0.40	8.726325393	0.65	10.64083982	0.90	15.89904034
0.16	5.202832202	0.41	8.776124150	0.66	10.69142307	0.91	16.72307991
0.17	5.291497111	0.42	8.828183216	0.67	10.73269878	0.92	16.01295964
0.18	5.384496735	0.43	8.880048327	0.68	10.76645935	0.93	16.61701709
0.19	5.482212371	0.44	8.932333717	0.69	10.79230362	0.94	16.75232227
0.20	5.585098184	0.45	8.987985203	0.70	10.83632709	0.95	16.59510512
0.21	5.693713724	0.46	9.044288119	0.71	10.88137672	0.96	16.80310760
0.22	5.808770397	0.47	9.100599744	0.72	14.82437355	0.97	17.88277356
0.23	5.931211380	0.48	9.159058969	0.73	14.63004337	0.98	17.69950809
0.24	6.062353689	0.49	9.219371744	0.74	14.75443785	0.99	18.47784571
0.25	6.204154330	0.50	9.279984033	0.75	15.04971420	1.00	18.44501344

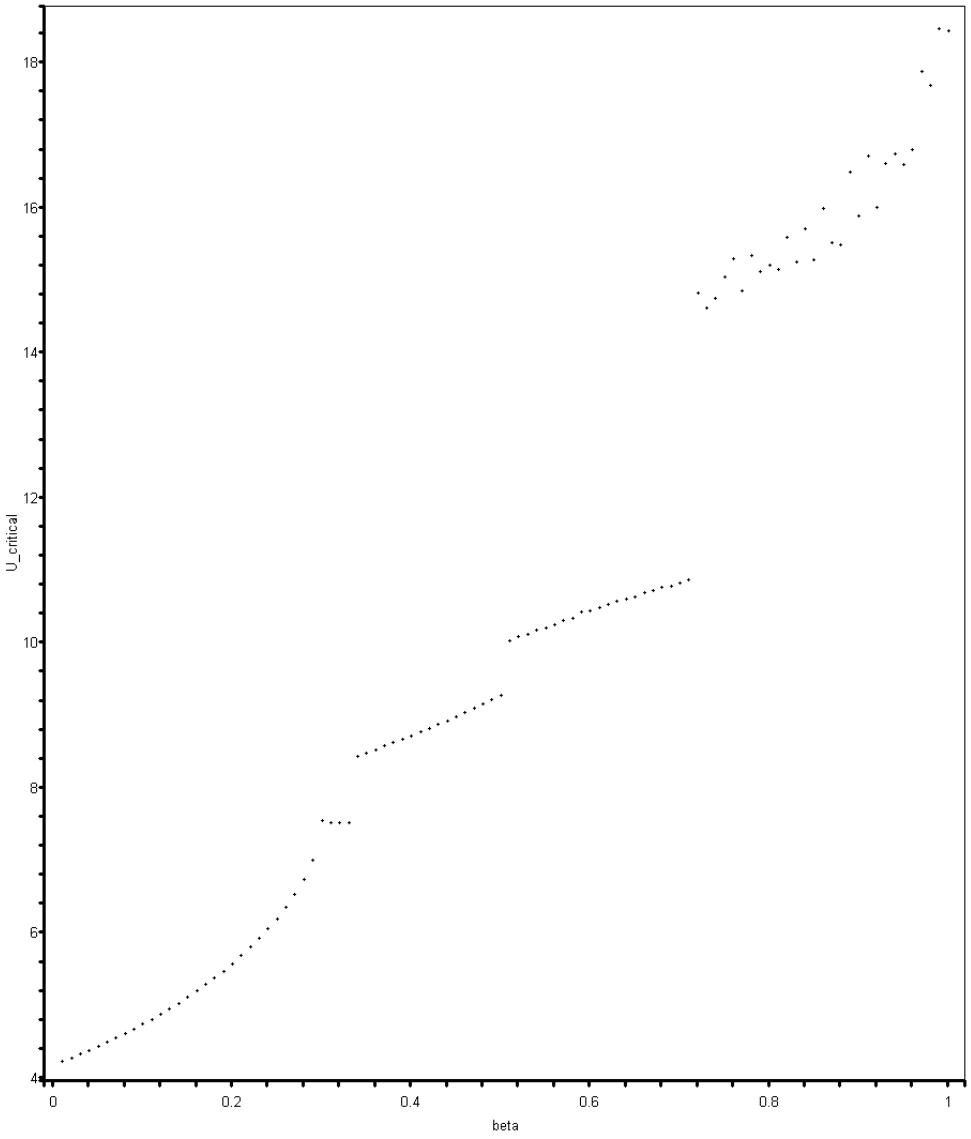

Fig. 5.3. Critical velocity vs. β for the five-term trigonometric\hyperbolic approximation ($\Lambda \sim 10^5$)

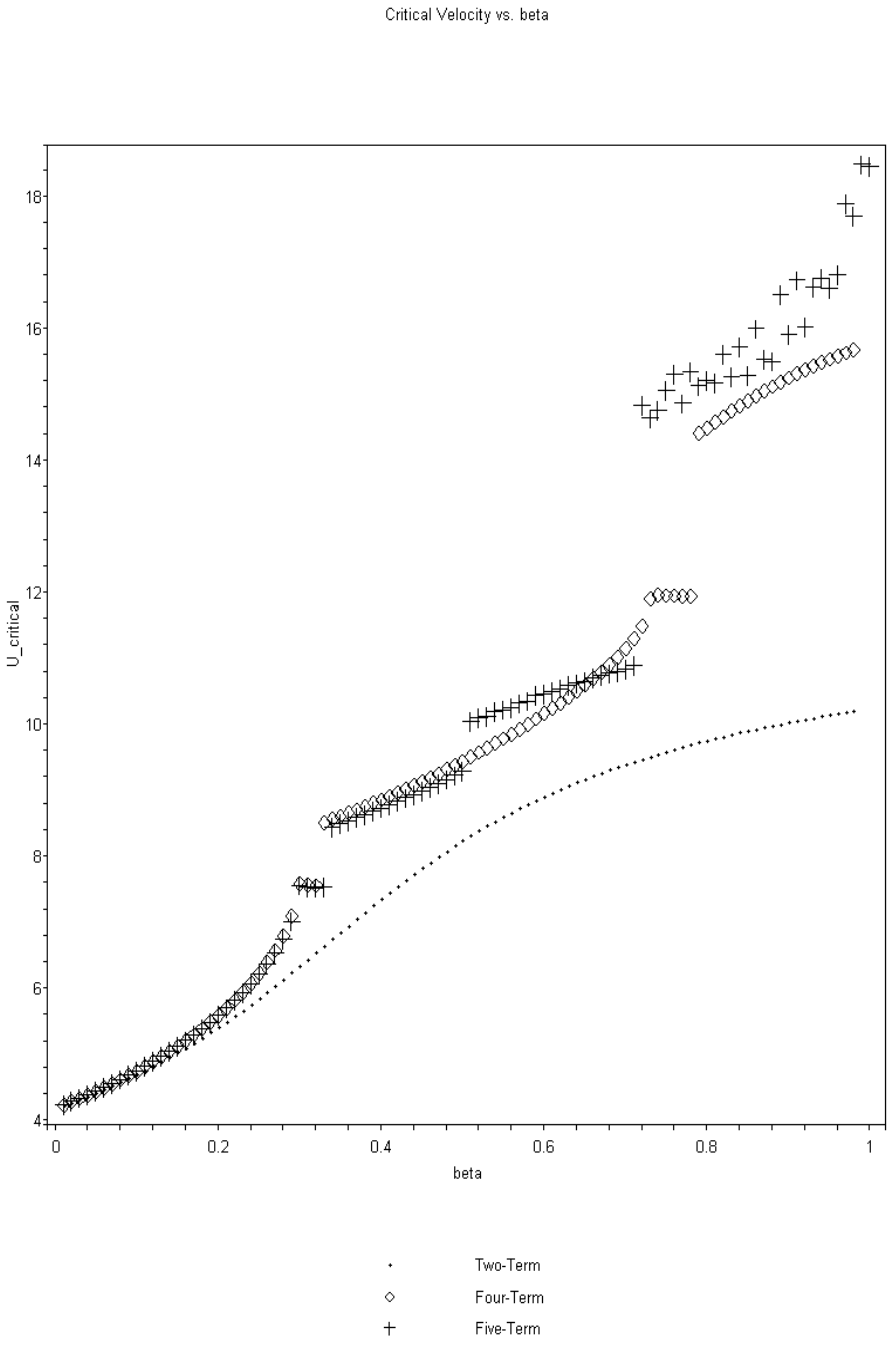

Fig. 5.4. Critical velocity vs. β for the two, four, and five-term trigonometric\hyperbolic approximation ($\Lambda \sim 10^5$)

D. Determination of the Critical Velocities by Polynomial Basis Functions for a Thin Beam

For a thin beam, the first five polynomial basis functions are derived from (4.50) and (4.51) where the $a_i's$ and $b_i's$ are calculated from (4.17)-(4.20).

$$\begin{aligned}
\psi_1 &= 5.570738179\text{x}10^{-5}\xi + 6.000025474\xi^2 - 4.000022805\xi^3 + 1.0\xi^4 \\
\psi_2 &= 2.099979645\xi^5 - 2.799997625\xi^6 + 1.0\xi^7 \\
\psi_3 &= 1.607092325\xi^8 - 2.499973720\xi^9 + 1.0\xi^{10} \\
\psi_4 &= 1.418101674\xi^{11} - 2.363583419\xi^{12} + 1.0\xi^{13} \\
\psi_5 &= 1.318571698\xi^{14} - 2.285633603\xi^{15} + 1.0\xi^{16}
\end{aligned} \tag{5.14}$$

The procedure and the orders of Ω and u for the respective order of approximation (N) are identical to the trigonometric\hyperbolic functions in the previous section; the foregoing results will only include the values and graphs of $U_{critical}$ vs. β for each order of approximation N. The values of the critical velocities for each order of approximation are in Tables 5.6-5.8 and their respective graphs are in Figures 5.5-5.7.

1. Two-Term Approximation

Table 5.6
Dimensionless critical velocities for the two-term polynomial approximation ($\Lambda \sim 10^5$)

β	U_{crit}	β	U_{crit}	β	U_{crit}	β	U_{crit}
0.01	4.574317086	0.26	6.608556520	0.51	9.633946056	0.76	11.60830548
0.02	4.628811949	0.27	6.723964212	0.52	9.737947147	0.77	11.66498976
0.03	4.684998985	0.28	6.841700029	0.53	9.839622317	0.78	11.72037064
0.04	4.742948348	0.29	6.961582846	0.54	9.938973490	0.79	11.77448772
0.05	4.802732510	0.30	7.083405445	0.55	10.03601227	0.80	11.82737941
0.06	4.864426090	0.31	7.206936531	0.56	10.13075854	0.81	11.87908287
0.07	4.928105637	0.32	7.331923614	0.57	10.22323915	0.82	11.92963410
0.08	4.993849329	0.33	7.458096682	0.58	10.31348682	0.83	11.97906791
0.09	5.061736575	0.34	7.585172520	0.59	10.40153903	0.84	12.02741794
0.10	5.131847534	0.35	7.712859497	0.60	10.48743714	0.85	12.07471673
0.11	5.204262490	0.36	7.840862597	0.61	10.57122555	0.86	12.12099572
0.12	5.279061107	0.37	7.968888475	0.62	10.65295102	0.87	12.16628525
0.13	5.356321524	0.38	8.096650283	0.63	10.73266203	0.88	12.21061466
0.14	5.436119280	0.39	8.223872089	0.64	10.81040825	0.89	12.25401225
0.15	5.518526057	0.40	8.350292716	0.65	10.88624011	0.90	12.29650536
0.16	5.603608225	0.41	8.475668869	0.66	10.96020838	0.91	12.33812038
0.17	5.691425187	0.42	8.599777544	0.67	11.03236386	0.92	12.37888279
0.18	5.782027527	0.43	8.722417627	0.68	11.10275713	0.93	12.41881718
0.19	5.875454966	0.44	8.843410820	0.69	11.17143826	0.94	12.45794729
0.20	5.971734164	0.45	8.962601869	0.70	11.23845672	0.95	12.49629603
0.21	6.070876392	0.46	9.079858243	0.71	11.30386114	0.96	12.53388554
0.22	6.172875163	0.47	9.195069354	0.72	11.36769923	0.97	12.57073717
0.23	6.277703863	0.48	9.308145384	0.73	11.43001768	0.98	12.60687155
0.24	6.385313528	0.49	9.419015909	0.74	11.49086210	0.99	12.64230858
0.25	6.495630840	0.50	9.527628296	0.75	11.55027695	1.00	12.67706752

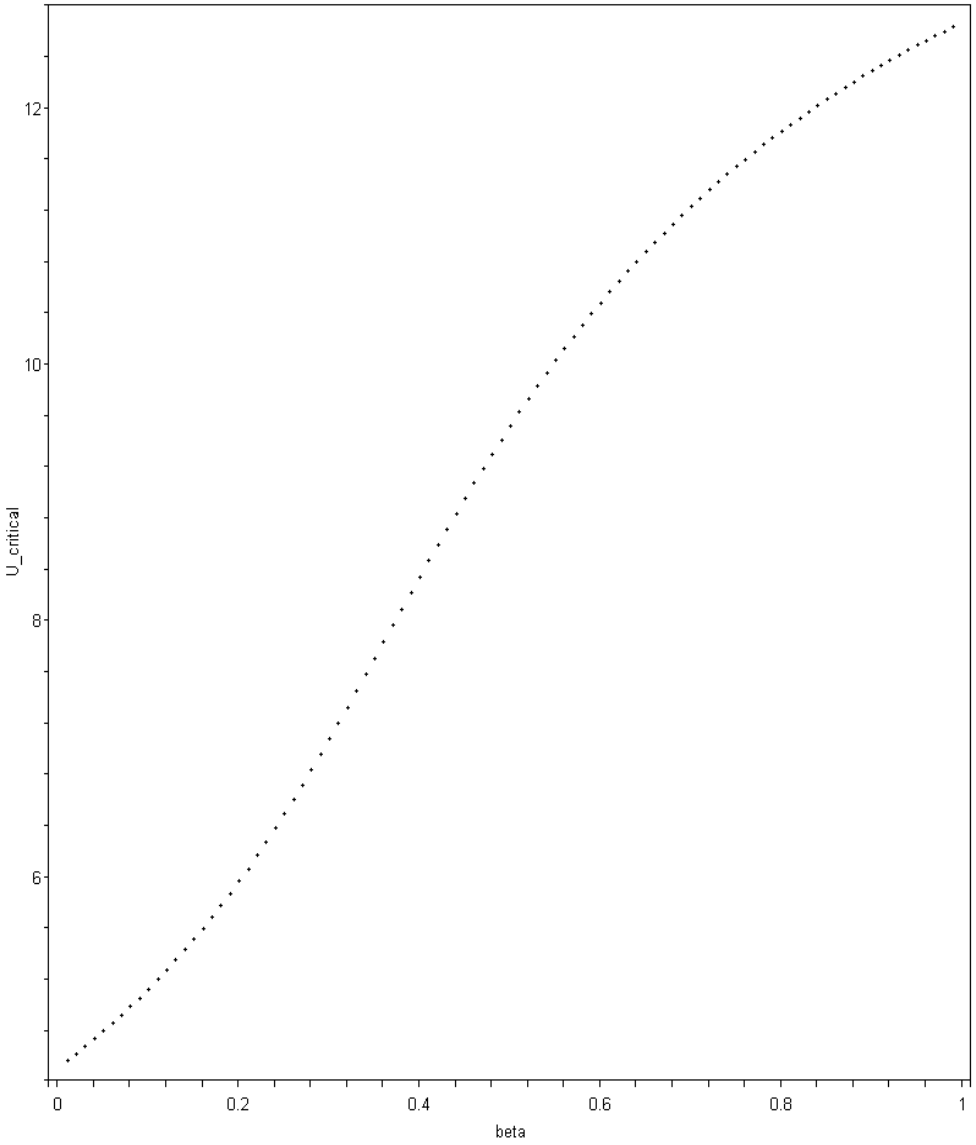

Fig. 5.5. Critical velocity vs. β for the two-term polynomial approximation ($\Lambda \sim 10^5$)

2. Four-Term Approximation

Table 5.7
Dimensionless critical velocities for the four-term polynomial approximation ($\Lambda \sim 10^5$)

β	U_{crit}	β	U_{crit}	β	U_{crit}	β	U_{crit}
0.01	4.300848070	0.26	6.337738515	0.51	9.712134272	0.76	11.22555628
0.02	4.349924264	0.27	6.484947893	0.52	9.771064185	0.77	11.28722394
0.03	4.400630703	0.28	6.645528566	0.53	9.830290868	0.78	11.34918293
0.04	4.453053422	0.29	6.824523868	0.54	9.889785696	0.79	11.41150279
0.05	4.507284329	0.30	7.031857713	0.55	9.949527397	0.80	11.47425998
0.06	4.563421741	0.31	7.292195738	0.56	10.00948780	0.81	11.53754711
0.07	4.621570818	0.32	7.717634013	0.57	10.06964316	0.82	11.60146862
0.08	4.681844208	0.33	8.465092121	0.58	10.12995867	0.83	11.66615070
0.09	4.744362590	0.34	8.638313234	0.59	10.19040986	0.84	11.73173630
0.10	4.809255417	0.35	8.742102736	0.60	10.25097708	0.85	11.79839337
0.11	4.876661693	0.36	8.823279679	0.61	10.31162976	0.86	11.86632792
0.12	4.946730863	0.37	8.893773218	0.62	10.37234756	0.87	11.93578043
0.13	5.019623855	0.38	8.958437125	0.63	10.43311241	0.88	12.00705077
0.14	5.095514415	0.39	9.019693791	0.64	10.49390634	0.89	12.08051093
0.15	5.174590698	0.40	9.078906580	0.65	10.55472268	0.90	12.15662044
0.16	5.257057404	0.41	9.136908209	0.66	10.61554908	0.91	12.23599263
0.17	5.343138539	0.42	9.194223656	0.67	10.67637622	0.92	12.31943774
0.18	5.433081420	0.43	9.251208392	0.68	10.73720886	0.93	12.40809018
0.19	5.527162297	0.44	9.308096653	0.69	10.79805354	0.94	12.50359475
0.20	5.625694542	0.45	9.365053885	0.70	10.85891288	0.95	12.60854408
0.21	5.729041088	0.46	9.422186202	0.71	10.91980154	0.96	12.72740805
0.22	5.837633236	0.47	9.479561799	0.72	10.98074190	0.97	12.86932698
0.23	5.952000188	0.48	9.537228604	0.73	11.04175365	0.98	13.06021890
0.24	6.072816194	0.49	9.595210038	0.74	11.10286776	0.99	13.16035854
0.25	6.200977987	0.50	9.653511020	0.75	11.16412094	1.00	13.24542632

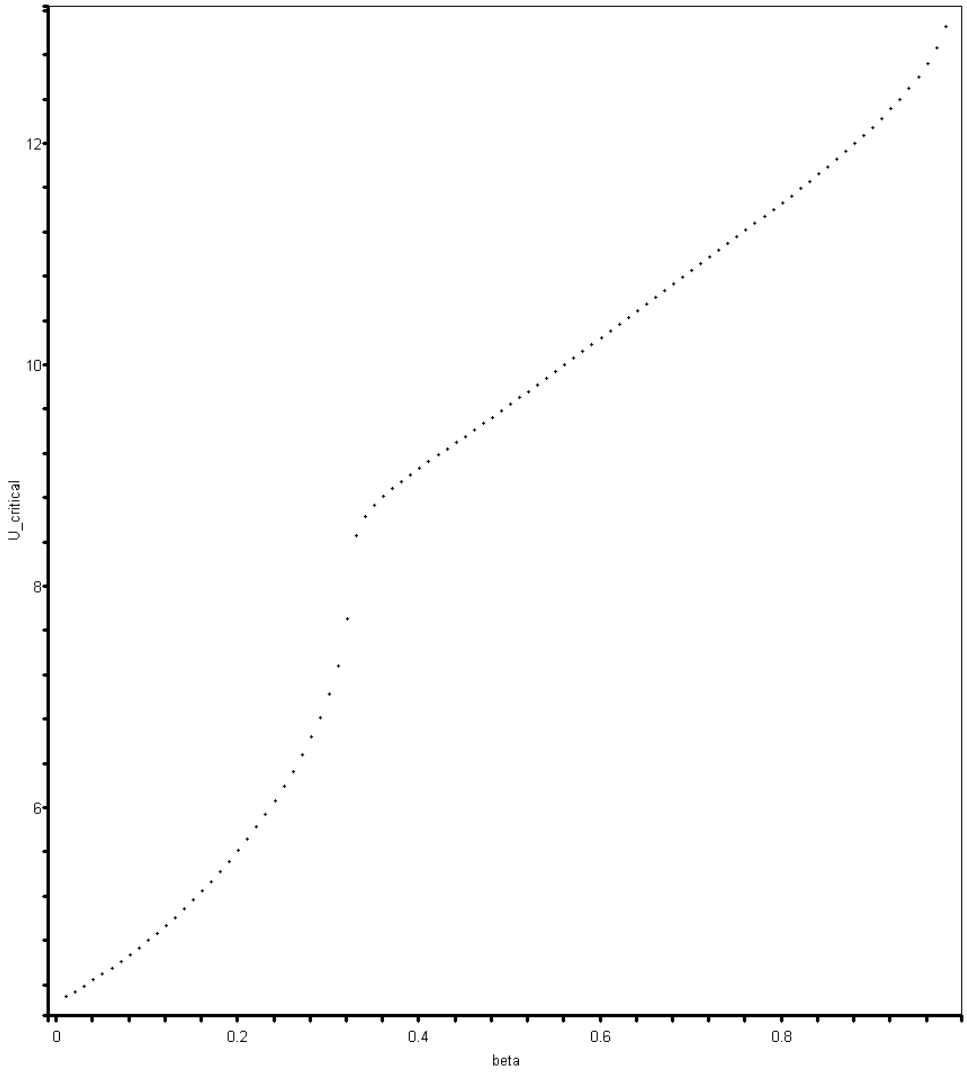

Fig. 5.6. Critical velocity vs. β for the four-term polynomial approximation ($\Lambda \sim 10^5$)

3. Five-Term Approximation

Table 5.8
Dimensionless critical velocities for the five-term polynomial approximation ($\Lambda \sim 10^5$)

β	U_{crit}	β	U_{crit}	β	U_{crit}	β	U_{crit}
0.01	4.271521963	0.26	6.320057929	0.51	9.565431586	0.76	11.10705690
0.02	4.320571894	0.27	6.471125261	0.52	9.620968871	0.77	11.18135545
0.03	4.371274280	0.28	6.638238271	0.53	9.677184642	0.78	11.25833900
0.04	4.423716736	0.29	6.829417025	0.54	9.733837521	0.79	11.33899169
0.05	4.477992715	0.30	7.063953311	0.55	9.791362986	0.80	11.42464513
0.06	4.534201984	0.31	7.428003149	0.56	9.849206436	0.81	11.52116096
0.07	4.592451081	0.32	8.607362654	0.57	9.907515323	0.82	11.62634001
0.08	4.652853812	0.33	8.673398782	0.58	9.966907232	0.83	11.75006168
0.09	4.715531843	0.34	8.727448808	0.59	10.02520343	0.84	11.91153272
0.10	4.780615325	0.35	8.776198409	0.60	10.08536986	0.85	14.48149226
0.11	4.848243594	0.36	8.822741519	0.61	10.14497551	0.86	14.61468903
0.12	4.918566045	0.37	8.868218153	0.62	10.20522975	0.87	14.72288146
0.13	4.991743322	0.38	8.913718600	0.63	10.26580615	0.88	14.84405494
0.14	5.067948400	0.39	8.959243439	0.64	10.32703314	0.89	14.94783790
0.15	5.147368621	0.40	9.005473009	0.65	10.38748861	0.90	15.04076591
0.16	5.230208021	0.41	9.052122018	0.66	10.44984335	0.91	15.14214303
0.17	5.316690668	0.42	9.099863854	0.67	10.51242997	0.92	15.23817527
0.18	5.407065911	0.43	9.148213406	0.68	10.57446077	0.93	15.32770988
0.19	5.501615224	0.44	9.197326533	0.69	10.63753914	0.94	15.41645156
0.20	5.600663403	0.45	9.247435289	0.70	10.70147086	0.95	15.50673281
0.21	5.704594898	0.46	9.298412519	0.71	10.76655409	0.96	15.58592144
0.22	5.813879267	0.47	9.350102216	0.72	10.83235213	0.97	15.66912091
0.23	5.929111524	0.48	9.402980369	0.73	10.89837270	0.98	15.74998666
0.24	6.051077881	0.49	9.456191885	0.74	10.96614429	0.99	15.83278824
0.25	6.180864362	0.50	9.510309468	0.75	11.03577974	1.00	15.90522339

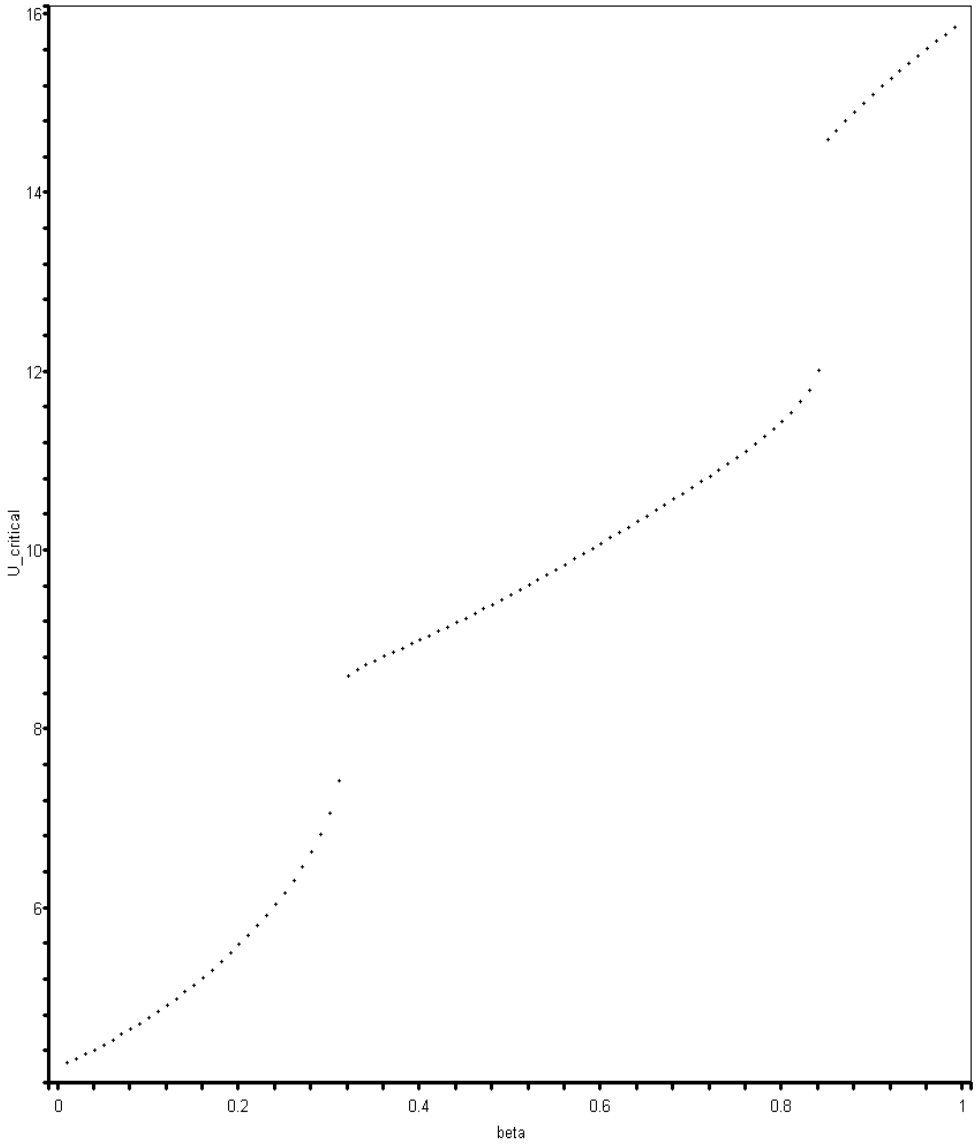

Fig. 5.7. Critical velocity vs. β for the five-term polynomial approximation($\Lambda \sim 10^5$)

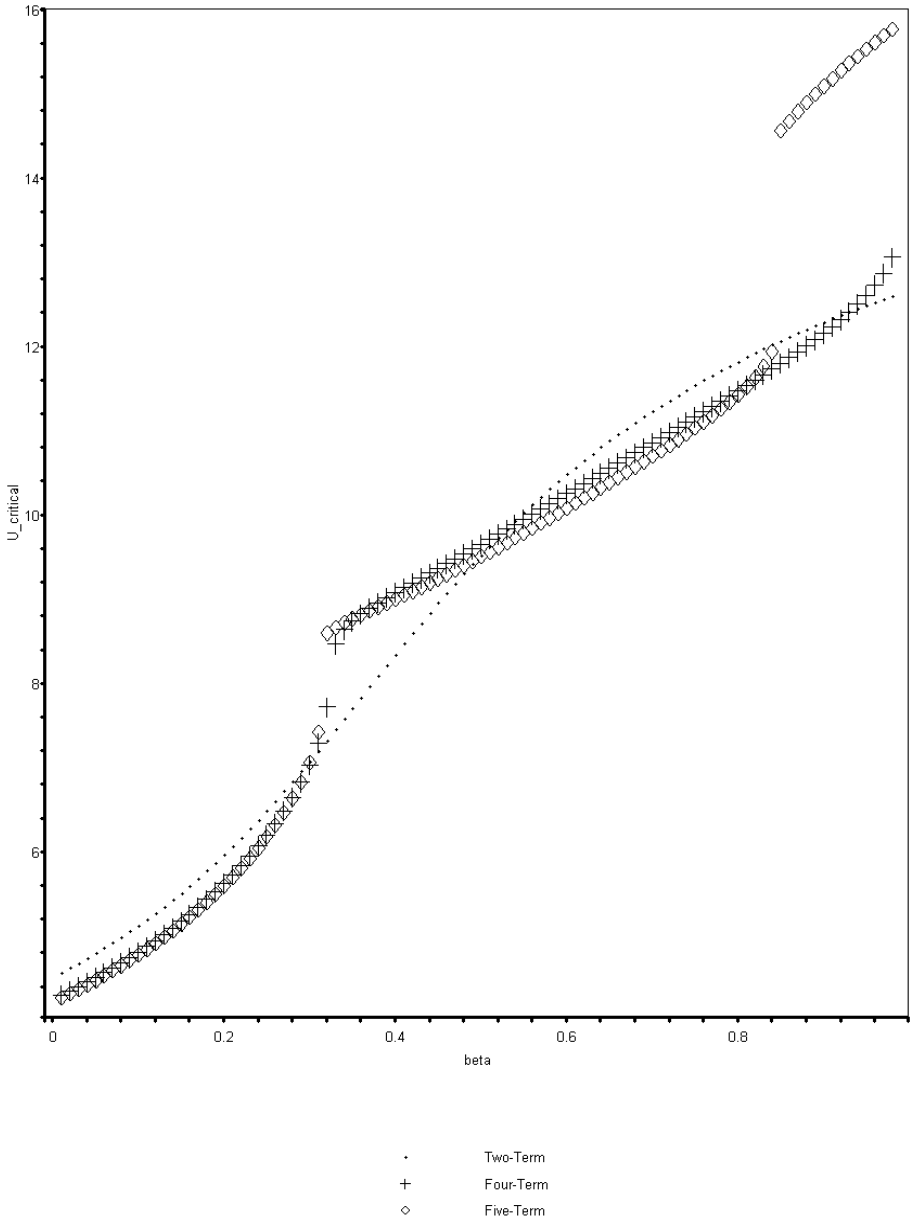

Fig. 5.8. Critical velocity vs. β for the two, four, and five-term polynomial approximation ($\Lambda \sim 10^5$)

From examining Figures 5.5-5.8, it is clear that jumps are still present with the polynomial approximation. The jump around $\beta = 0.3$ is present for the four-term approximation and the jumps around $\beta = 0.3$ and $\beta = 0.8$ exist for the five-term approximation. For low values of β (β <0.3), the values for the critical velocities are close with the trigonometric\hyperbolic approximation. As shown by Vittori, a large number of polynomial functions (about 30) are needed to mimic the trigonometric\hyperbolic functions for large values of β. Since the linear model has been shown to be poor for the higher values of β, the fact that polynomial results give a poor representation is not of concern. In fact, as will be seen in the final chapter, the polynomial basis functions will actually be closer to the exact (numerically integrated) critical velocities. The cause for the non-monotonic behavior of $U_{criitical}$ vs. β for the higher-order approximations is not yet determined and should be studied closer in future work.

E. Determination of the Critical Velocities by Trigonometric\Hyperbolic Basis Functions for a Moderately Thick and Thick Beam

For a moderately thick beam, $\Lambda \sim 10^3$, and for a thick beam, $\Lambda \sim 10^2$. The proceeding material parameters will stay the same: $s = \frac{r_i}{r_o} = 0.9$ (K_s=0.553), $\upsilon = 0.3$, $E_p = 30x10^6\ psi$, $G_p = \frac{E}{2(1+\upsilon)} = 11.5x10^6\ psi$, and $L = 1.0in$; the only parameter that will change will be the slenderness ratio Λ. Again, the process for finding the critical velocity is the same as before. We will find *N* trigonometric\hyperbolic and polynomial basis functions, substitute these functions into(4.38) in order to obtain a coefficient matrix, take the determinant of this coefficient matrix which results into a polynomial equation in Ω, collect coefficients of Ω to be substituted into (5.5), substitute a value of β into the resulting equation, solve for the roots of this equation, and pick out the smallest positive root which is the critical velocity.

Tables 5.9 and 5.10 give the critical velocities for each value of β for $\Lambda \sim 10^3$ and $\Lambda \sim 10^2$ respectively for the two-term trigonometric/hyperbolic approximation. Figures 5.9 and 5.10 show the plots of $U_{critical}$ vs. β for $\Lambda \sim 10^3$ and $\Lambda \sim 10^2$ respectively superposed on a plot where $\Lambda \sim 10^5$ (*N=2*). Figure 5.11 shows plots of $U_{critical}$ vs. β for all three slenderness ratios. It is seen that the $\Lambda \sim 10^3$ and $\Lambda \sim 10^2$ graphs are similar in behavior to the $\Lambda \sim 10^5$ graph but give lower critical velocities; thicker beams always gives lower critical velocities for all values of β.

1. Two-Term Approximation

Table 5.9
Dimensionless critical velocities for the two-term trigonometric\hyperbolic approximation ($\Lambda \sim 10^3$)

β	U_{crit}	β	U_{crit}	β	U_{crit}	β	U_{crit}
0.01	4.180703542	0.26	5.900452455	0.51	8.220123411	0.76	9.493390142
0.02	4.227969685	0.27	5.995139015	0.52	8.292313091	0.77	9.526973563
0.03	4.276633161	0.28	6.091365584	0.53	8.362336452	0.78	9.559630077
0.04	4.326748445	0.29	6.188947336	0.54	8.430230898	0.79	9.591394217
0.05	4.378371494	0.30	6.287677400	0.55	8.496040110	0.80	9.622299062
0.06	4.431559572	0.31	6.387329249	0.56	8.559812704	0.81	9.652376291
0.07	4.486371016	0.32	6.487659909	0.57	8.621601088	0.82	9.681656245
0.08	4.542864929	0.33	6.588413910	0.58	8.681460456	0.83	9.710167965
0.09	4.601100803	0.34	6.689327829	0.59	8.739447902	0.84	9.737939258
0.10	4.661138043	0.35	6.790135196	0.60	8.795621700	0.85	9.764996743
0.11	4.723035392	0.36	6.890571531	0.61	8.850040672	0.86	9.791365902
0.12	4.786850226	0.37	6.990379282	0.62	8.902763677	0.87	9.817071129
0.13	4.852637730	0.38	7.089312382	0.63	8.953849183	0.88	9.842135779
0.14	4.920449909	0.39	7.187140244	0.64	9.003354916	0.89	9.866582218
0.15	4.990334456	0.40	7.283651036	0.65	9.051337600	0.90	9.890431858
0.16	5.062333434	0.41	7.378654151	0.66	9.097852723	0.91	9.913705212
0.17	5.136481799	0.42	7.471981823	0.67	9.142954374	0.92	9.936421929
0.18	5.212805742	0.43	7.563489952	0.68	9.186695130	0.93	9.958600833
0.19	5.291320879	0.44	7.653058140	0.69	9.229125955	0.94	9.980259965
0.20	5.372030308	0.45	7.740589149	0.70	9.270296150	0.95	10.00141661
0.21	5.454922567	0.46	7.826007796	0.71	9.310253313	0.96	10.02208736
0.22	5.539969568	0.47	7.909259477	0.72	9.349043331	0.97	10.04228810
0.23	5.627124563	0.48	7.990308423	0.73	9.386710375	0.98	10.06203408
0.24	5.716320260	0.49	8.069135801	0.74	9.423296927	0.99	10.08133993
0.25	5.807467189	0.50	8.145737745	0.75	9.458843792	1.00	10.10021969

Table 5.10
Dimensionless critical velocities for the two-term trigonometric\hyperbolic approximation ($\Lambda \sim 10^2$)

β	U_{crit}	β	U_{crit}	β	U_{crit}	β	U_{crit}
0.01	4.015034722	0.26	5.655019036	0.51	7.618734498	0.76	8.572470283
0.02	4.060810528	0.27	5.742113125	0.52	7.674573671	0.77	8.596868234
0.03	4.107932151	0.28	5.830081222	0.53	7.728501310	0.78	8.620561341
0.04	4.156449416	0.29	5.918705141	0.54	7.780574051	0.79	8.643577554
0.05	4.206412977	0.30	6.007751864	0.55	7.830850881	0.80	8.665943518
0.06	4.257874019	0.31	6.096977545	0.56	7.879392240	0.81	8.687684633
0.07	4.310883919	0.32	6.186132075	0.57	7.926259260	0.82	8.708825116
0.08	4.365493796	0.33	6.274964043	0.58	7.971513145	0.83	8.729388058
0.09	4.421753980	0.34	6.363225771	0.59	8.015214659	0.84	8.749395478
0.10	4.479713369	0.35	6.450678185	0.60	8.057423706	0.85	8.768868379
0.11	4.539418655	0.36	6.537095311	0.61	8.098199021	0.86	8.787826796
0.12	4.600913423	0.37	6.622268101	0.62	8.137597903	0.87	8.806289848
0.13	4.664237093	0.38	6.706007489	0.63	8.175676044	0.88	8.824275778
0.14	4.729423709	0.39	6.788146587	0.64	8.212487375	0.89	8.841802004
0.15	4.796500562	0.40	6.868541987	0.65	8.248083990	0.90	8.858885157
0.16	4.865486649	0.41	6.947074217	0.66	8.282516080	0.91	8.875541123
0.17	4.936390993	0.42	7.023647449	0.67	8.315831903	0.92	8.891785080
0.18	5.009210812	0.43	7.098188559	0.68	8.348077783	0.93	8.907631532
0.19	5.083929622	0.44	7.170645738	0.69	8.379298129	0.94	8.923094345
0.20	5.160515277	0.45	7.240986712	0.70	8.409535458	0.95	8.938186781
0.21	5.238918061	0.46	7.309196743	0.71	8.438830430	0.96	8.952921523
0.22	5.319068903	0.47	7.375276567	0.72	8.467221910	0.97	8.967310710
0.23	5.400877832	0.48	7.439240291	0.73	8.494747013	0.98	8.981365961
0.24	5.484232814	0.49	7.501113346	0.74	8.521441169	0.99	8.995098402
0.25	5.568999065	0.50	7.560930580	0.75	8.547338177	1.00	9.008518686

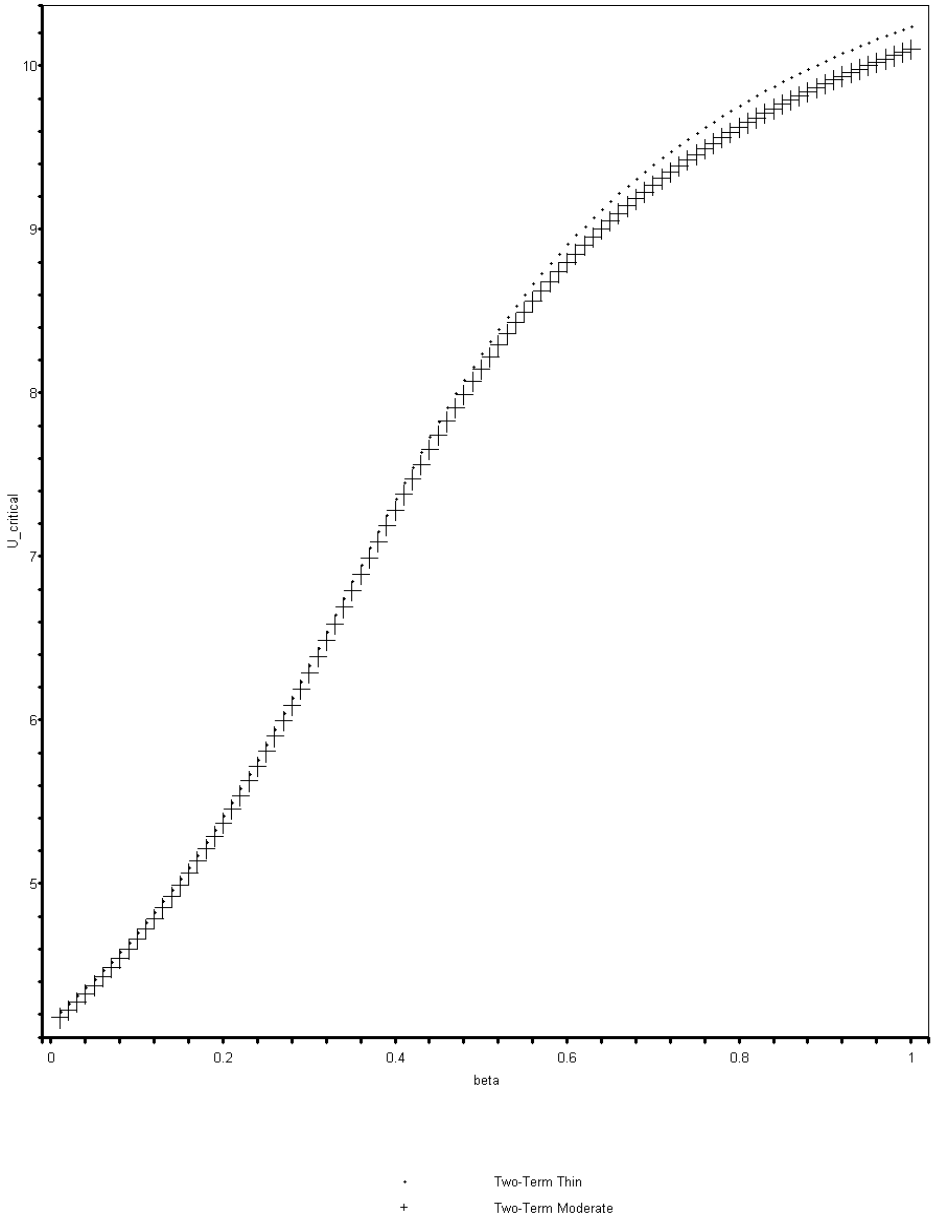

Fig. 5.9. Critical velocity vs. β for the two-term trigonometric\hyperbolic approximation for $\Lambda \sim 10^3$ and $\Lambda \sim 10^5$

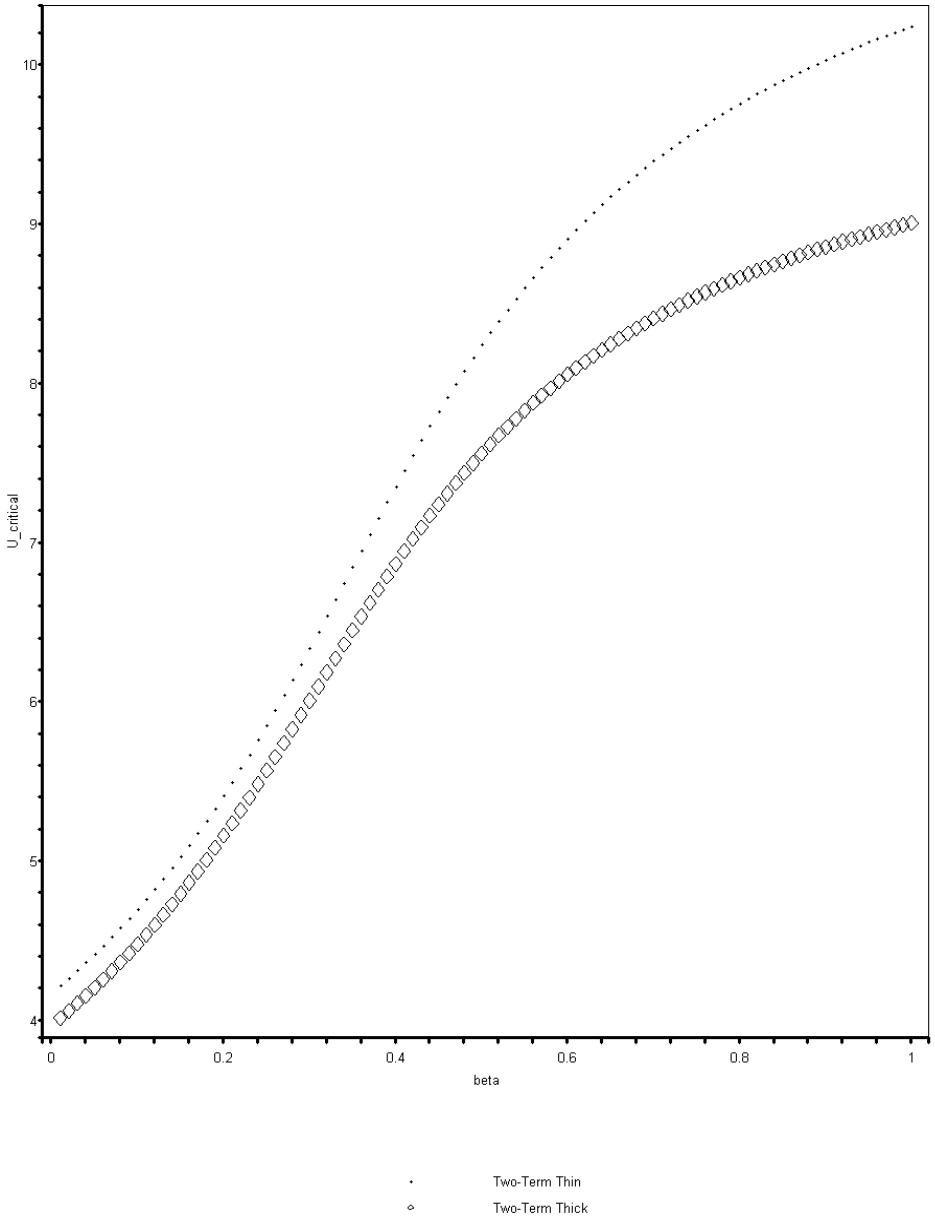

Fig. 5.10. Critical velocity vs. β for the two-term trigonometric\hyperbolic approximation for $\Lambda \sim 10^2$ and $\Lambda \sim 10^5$

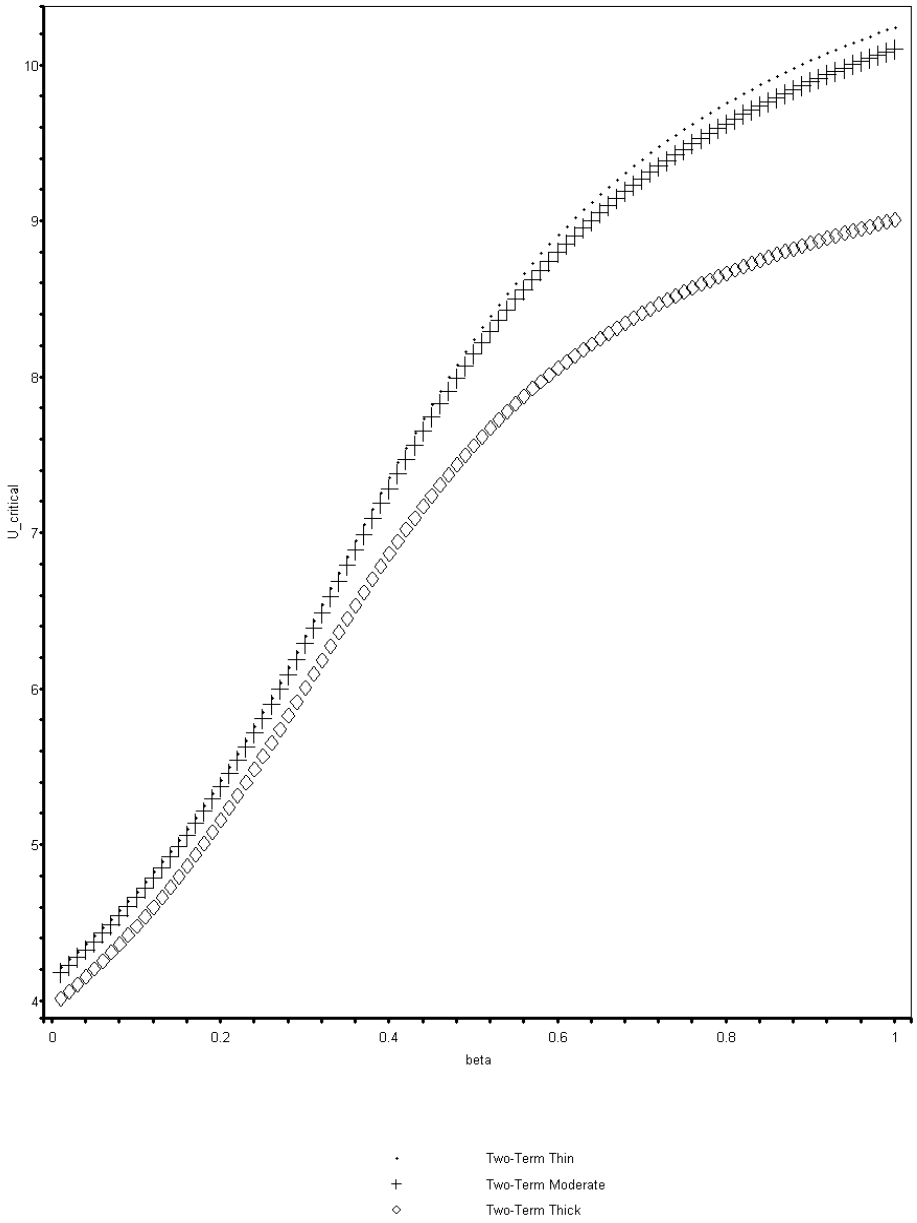

Fig. 5.11. Critical velocity vs. β for the two-term trigonometric\hyperbolic approximation for $\Lambda \sim 10^2$, $\Lambda \sim 10^3$, and $\Lambda \sim 10^5$

Tables 5.11 and 5.12 give the critical velocities for each value of β for $\Lambda \sim 10^3$ and $\Lambda \sim 10^2$ respectively for the four-term trigonometric\hyperbolic approximation. Figures 5.12 and 5.13 show the plots of $U_{critical}$ vs. β for $\Lambda \sim 10^3$ and $\Lambda \sim 10^2$ respectively superposed on a plot where $\Lambda \sim 10^5$ for the four-term approximation. Figure 5.14 shows plots of $U_{critical}$ vs. β for all three slenderness ratios. It is clear from Figures 5.12-5.14 that jumps are present for all three slenderness ratios approximately when $\beta = 0.3$ and $\beta = 0.8$. Once again, thickening the beam consistently lowers the critical velocity. When going from the two-term to four-term approximation, the changes in critical velocities for $\Lambda \sim 10^5 \rightarrow \Lambda \sim 10^3$ and $\Lambda \sim 10^5 \rightarrow \Lambda \sim 10^2$ in the higher ranges of β ($\beta > 0.3$) is more profound (especially when $\Lambda \sim 10^5 \rightarrow \Lambda \sim 10^2$). Since we are only concerned with $\beta \leq 0.3$, these large changes will not come into play.

2. Four-Term Approximation

Table 5.11
Dimensionless critical velocities for the four-term trigonometric\hyperbolic approximation ($\Lambda \sim 10^3$)

β	U_{crit}	β	U_{crit}	β	U_{crit}	β	U_{crit}
0.01	4.186241842	0.26	6.306084980	0.51	9.310859724	0.76	11.62545188
0.02	4.234699214	0.27	6.487425584	0.52	9.375436476	0.77	11.62166082
0.03	4.284822396	0.28	6.706144891	0.53	9.441260815	0.78	11.61880884
0.04	4.336704921	0.29	7.015651700	0.54	9.508306100	0.79	13.91507451
0.05	4.390447558	0.30	7.438198573	0.55	9.576657359	0.80	13.99937671
0.06	4.446158886	0.31	7.418478945	0.56	9.646306144	0.81	14.08085378
0.07	4.503956273	0.32	7.414525007	0.57	9.717273229	0.82	14.15966696
0.08	4.563966667	0.33	8.343109718	0.58	9.789709033	0.83	14.23589743
0.09	4.626327734	0.34	8.392627926	0.59	9.863612243	0.84	14.30961054
0.10	4.691189088	0.35	8.440439461	0.60	9.939221902	0.85	14.38081265
0.11	4.758713865	0.36	8.487755802	0.61	10.01659863	0.86	14.44944954
0.12	4.829080409	0.37	8.535276549	0.62	10.09602450	0.87	14.51560913
0.13	4.902484781	0.38	8.583362766	0.63	10.17781159	0.88	14.57919027
0.14	4.979143415	0.39	8.632277213	0.64	10.26231551	0.89	14.64036147
0.15	5.059297086	0.40	8.682193943	0.65	10.34995543	0.90	14.69890777
0.16	5.143216021	0.41	8.733206877	0.66	10.44167960	0.91	14.75497216
0.17	5.231206887	0.42	8.785372725	0.67	10.53824971	0.92	14.80854201
0.18	5.323623007	0.43	8.838767242	0.68	10.64116638	0.93	14.85962014
0.19	5.420879040	0.44	8.893394609	0.69	10.75284532	0.94	14.90826046
0.20	5.523473698	0.45	8.949276040	0.70	10.87712610	0.95	14.95445865
0.21	5.632023941	0.46	9.006414686	0.71	11.02177094	0.96	14.99835254
0.22	5.747322108	0.47	9.064819662	0.72	11.20693539	0.97	15.03989211
0.23	5.870429901	0.48	9.124468308	0.73	11.64995989	0.98	15.07919375
0.24	6.002846419	0.49	9.185341635	0.74	11.63832333	0.99	15.11634133
0.25	6.146831729	0.50	9.247488462	0.75	11.63070700	1.00	15.15138343

Table 5.12
Dimensionless critical velocities for the four-term trigonometric\hyperbolic approximation ($\Lambda \sim 10^2$)

β	U_{crit}	β	U_{crit}	β	U_{crit}	β	U_{crit}
0.01	4.013425997	0.26	6.030455147	0.51	8.485581410	0.76	10.08592992
0.02	4.059549504	0.27	6.219622407	0.52	8.539572212	0.77	10.08414349
0.03	4.107238242	0.28	6.487098915	0.53	8.594698409	0.78	10.08267977
0.04	4.156578524	0.29	6.827482505	0.54	8.650167628	0.79	10.08182263
0.05	4.207663079	0.30	6.819536682	0.55	8.706462823	0.80	10.08058306
0.06	4.260591771	0.31	6.823314755	0.56	8.763576175	0.81	10.07985104
0.07	4.315472592	0.32	6.831457472	0.57	8.821788343	0.82	10.07935434
0.08	4.372421847	0.33	6.841608425	0.58	8.881031671	0.83	10.07854202
0.09	4.431565854	0.34	7.688822315	0.59	8.941402612	0.84	10.07779091
0.10	4.493041728	0.35	7.730098876	0.60	9.002644279	0.85	12.22410997
0.11	4.556998948	0.36	7.771596072	0.61	9.065574985	0.86	12.26196547
0.12	4.623601337	0.37	7.813460186	0.62	9.130635678	0.87	12.29735450
0.13	4.693028917	0.38	7.856052825	0.63	9.197577750	0.88	12.33113751
0.14	4.765481378	0.39	7.899111584	0.64	9.267517117	0.89	12.36264565
0.15	4.841182760	0.40	7.943265131	0.65	9.341084531	0.90	12.39281083
0.16	4.920385247	0.41	7.988496115	0.66	9.419123784	0.91	12.42129898
0.17	5.003380375	0.42	8.034220166	0.67	9.504484362	0.92	12.44809188
0.18	5.090508203	0.43	8.080784378	0.68	9.600950777	0.93	12.47326506
0.19	5.182177465	0.44	8.128660101	0.69	9.714813320	0.94	12.49681443
0.20	5.278894572	0.45	8.177182789	0.70	9.874998466	0.95	12.51876346
0.21	5.381308779	0.46	8.226590328	0.71	10.10784893	0.96	12.53965716
0.22	5.490291979	0.47	8.276896662	0.72	10.09985745	0.97	12.55903857
0.23	5.607082613	0.48	8.327747550	0.73	10.09472161	0.98	12.57720019
0.24	5.733545766	0.49	8.379693352	0.74	10.09046769	0.99	12.59407558
0.25	5.872764440	0.50	8.432090045	0.75	10.08796692	1.00	12.60998962

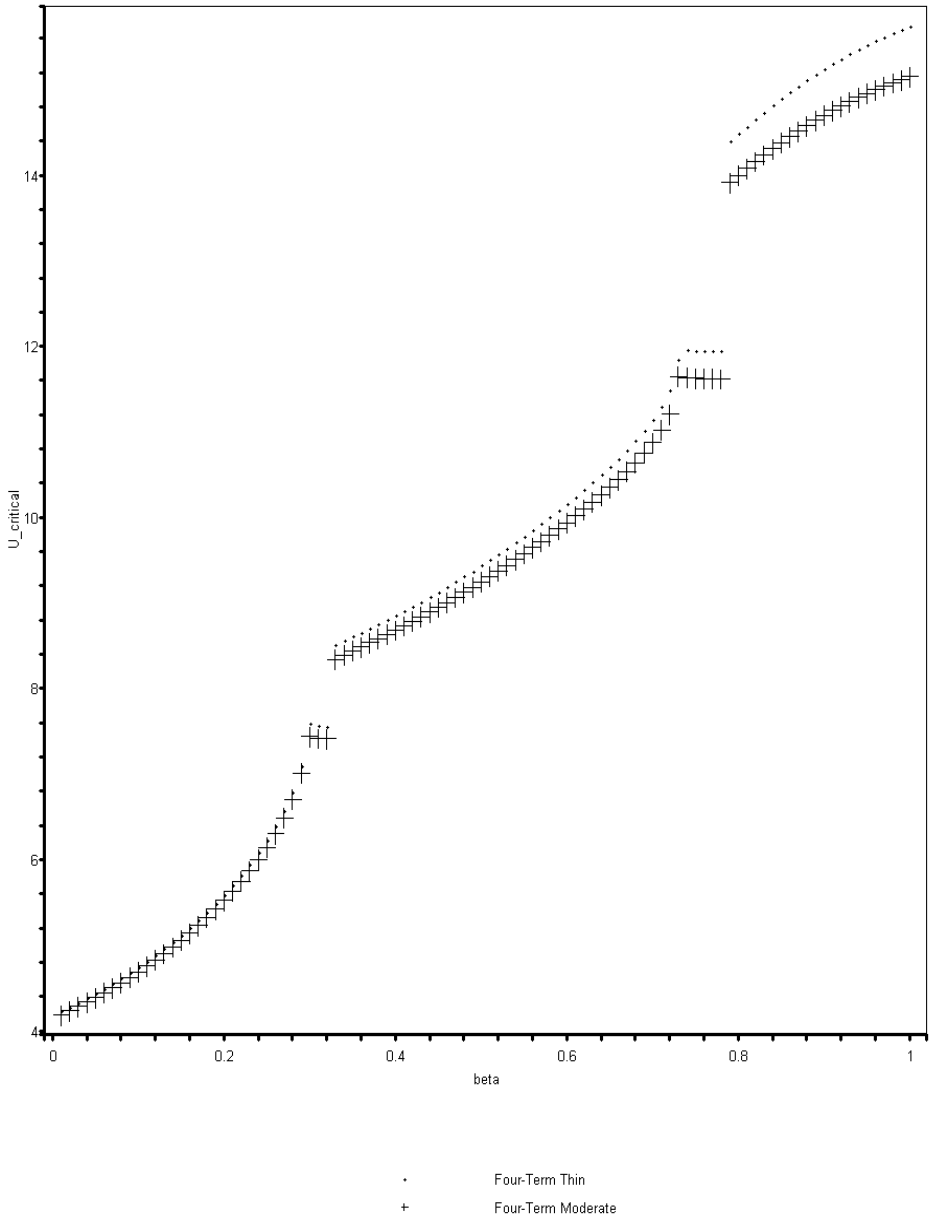

Fig. 5.12. Critical velocity vs. β for the four-term trigonometric\hyperbolic approximation for $\Lambda \sim 10^3$ and $\Lambda \sim 10^5$

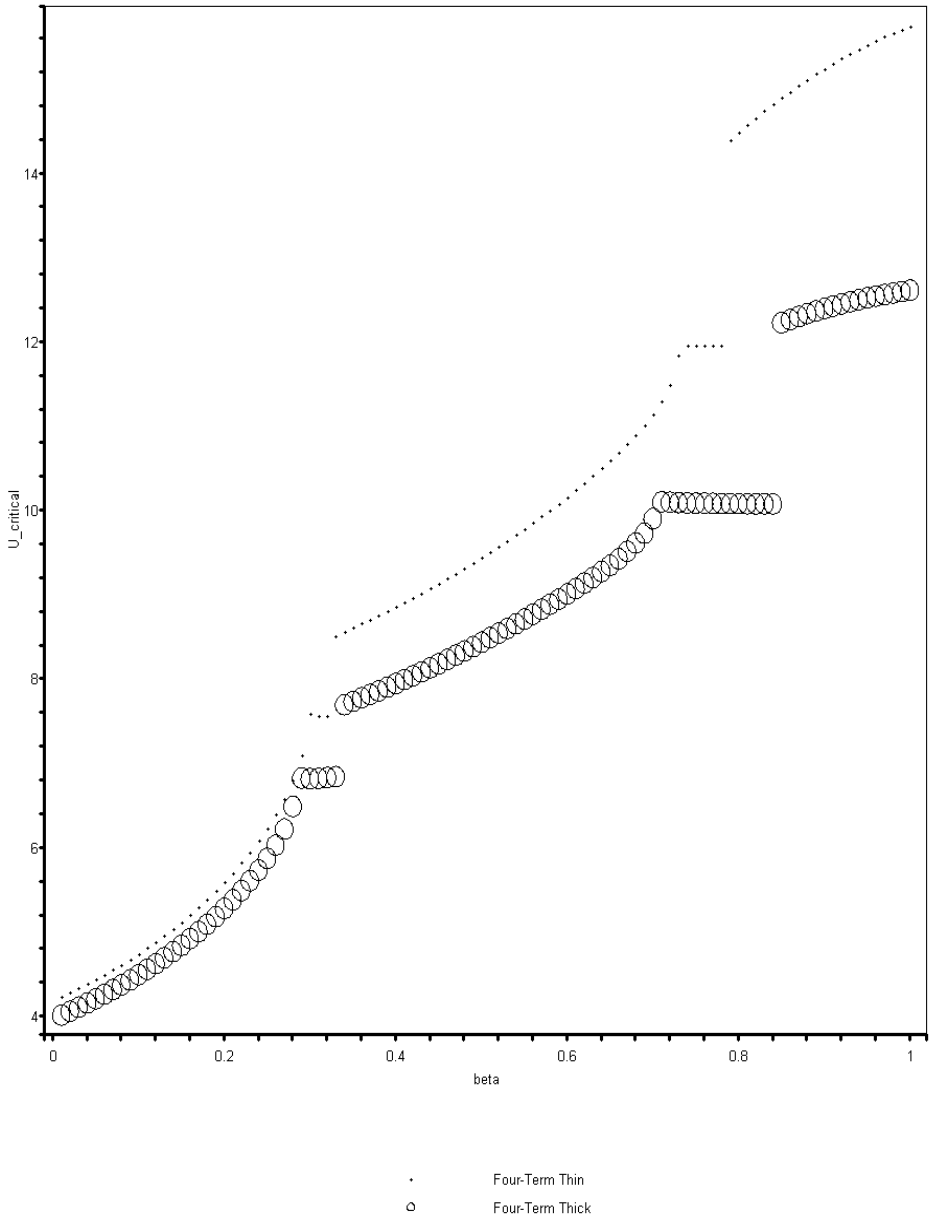

Fig. 5.13. Critical velocity vs. β for the four-term trigonometric\hyperbolic approximation for $\Lambda \sim 10^2$ and $\Lambda \sim 10^5$

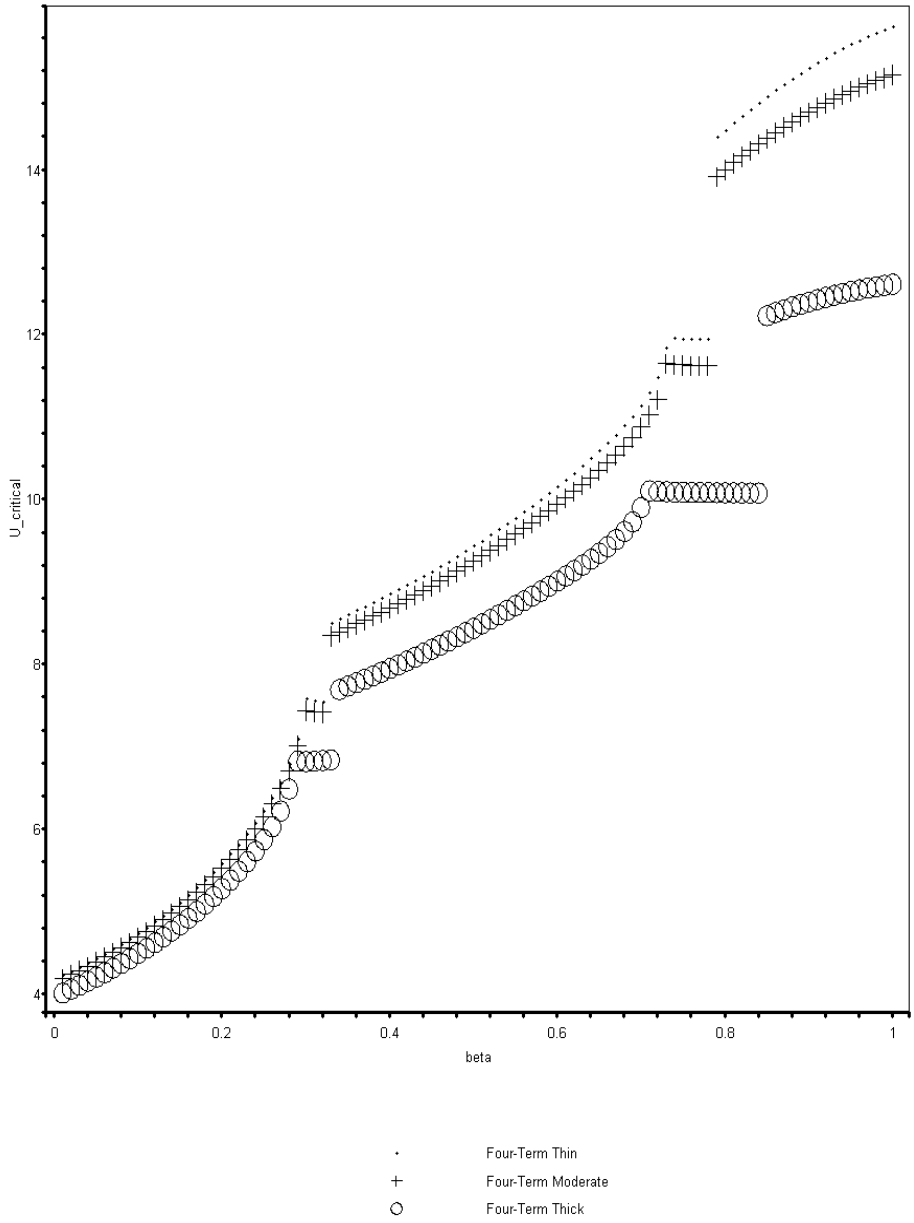

Fig. 5.14. Critical velocity vs. β for the four-term trigonometric\hyperbolic approximation for $\Lambda \sim 10^2$, $\Lambda \sim 10^3$, and $\Lambda \sim 10^5$

Summarizing the results from Figures 5.9-5.14 for the trigonometric\hyperbolic approximation, the critical velocities are consistently lower for thicker beams. The graphs of the thicker beams are very similar to the graphs for the thin beam, i.e. jumps are still present in the four term approximation ($\beta = 0.3$ and $\beta = 0.8$) for all three thicknesses ($\Lambda \sim 10^5, 10^3, 10^2$). Also, for all three thicknesses, the critical velocities increase (for $\beta > 0.3$) in going from the two-term to the four-term approximation, hence, the linear model is again a poor representation for thicker beams. Finally, for the thickest beam being studied ($\Lambda \sim 10^2$), there are profound changes in the critical velocities when compared to the thin beam ($\Lambda \sim 10^5$) for the higher ranges of β . Since the higher ranges of β are not being studied, this outcome is not of interest. As mentioned earlier, the thickest beam of all ($\Lambda \sim 10$) was not studied because of its strange characteristics.

F. Determination of the Critical Velocities by Polynomial Basis Functions for a Moderately Thick and Thick Beam

1. Two-Term Approximation

From Figures 5.15-5.17, it is seen that the plots of the critical velocities versus β for the two-term polynomial approximation mimic the behavior of the two-term trigonometric\hyperbolic approximation (especially in the lower ranges of β), i.e. no jumps are present yet and the thicker beams have consistently lower critical velocities. The values of the critical velocities for each value of β ($\Lambda \sim 10^3$ and $\Lambda \sim 10^2$) for the two-term polynomial approximation are given in Tables 5.13-5.14 respectively. Unlike the two-term trigonometric\hyperbolic. approximation, changes in critical velocities for $\Lambda \sim 10^5 \rightarrow \Lambda \sim 10^3$ and $\Lambda \sim 10^5 \rightarrow \Lambda \sim 10^2$ are greater. When $\Lambda \sim 10^5 \rightarrow \Lambda \sim 10^3$, the differences in critical velocities are slightly more noticeably (in the higher ranges of β) than the trigonometric\hyperbolic approximation. When $\Lambda \sim 10^5 \rightarrow \Lambda \sim 10^2$, the differences in critical velocities are very noticeable (for the entire range of β).

Table 5.13

Dimensionless critical velocities for the two-term polynomial approximation ($\Lambda \sim 10^3$)

β	U_{crit}	β	U_{crit}	β	U_{crit}	β	U_{crit}
0.01	4.567489745	0.26	6.571442158	0.51	9.446299748	0.76	11.22848166
0.02	4.621543467	0.27	6.683915016	0.52	9.542074160	0.77	11.27852732
0.03	4.677260943	0.28	6.798472226	0.53	9.635502270	0.78	11.32736165
0.04	4.734709921	0.29	6.914918853	0.54	9.726599776	0.79	11.37502374
0.05	4.793960216	0.30	7.033035092	0.55	9.815390900	0.80	11.42155129
0.06	4.855083516	0.31	7.152578723	0.56	9.901907002	0.81	11.46698075
0.07	4.918153123	0.32	7.273288410	0.57	9.986185351	0.82	11.51134723
0.08	4.983243625	0.33	7.394887738	0.58	10.06826801	0.83	11.55468464
0.09	5.050430457	0.34	7.517089851	0.59	10.14820083	0.84	11.59702565
0.10	5.119789373	0.35	7.639602462	0.60	10.22603262	0.85	11.63840174
0.11	5.191395779	0.36	7.762132999	0.61	10.30181439	0.86	11.67884327
0.12	5.265323936	0.37	7.884393668	0.62	10.37559867	0.87	11.71837949
0.13	5.341646003	0.38	8.006106176	0.63	10.44743901	0.88	11.75703855
0.14	5.420430905	0.39	8.127005926	0.64	10.51738946	0.89	11.79484759
0.15	5.501743023	0.40	8.246845578	0.65	10.58550421	0.90	11.83183277
0.16	5.585640684	0.41	8.365397800	0.66	10.65183723	0.91	11.86801925
0.17	5.672174455	0.42	8.482457265	0.67	10.71644203	0.92	11.90343131
0.18	5.761385249	0.43	8.597841853	0.68	10.77937141	0.93	11.93809229
0.19	5.853302252	0.44	8.711393116	0.69	10.84067727	0.94	11.97202472
0.20	5.947940703	0.45	8.822976134	0.70	10.90041050	0.95	12.00525028
0.21	6.045299596	0.46	8.932478814	0.71	10.95862086	0.96	12.03778988
0.22	6.145359328	0.47	9.039810788	0.72	11.01535685	0.97	12.06966365
0.23	6.248079430	0.48	9.144901984	0.73	11.07066571	0.98	12.10089100
0.24	6.353396457	0.49	9.247701000	0.74	11.12459333	0.99	12.13149064
0.25	6.461222169	0.50	9.348173369	0.75	11.17718426	1.00	12.16148061

Table 5.14

Dimensionless critical velocities for the two-term polynomial approximation ($\Lambda \sim 10^2$)

β	U_{crit}	β	U_{crit}	β	U_{crit}	β	U_{crit}
0.01	4.505709728	0.26	6.297750420	0.51	8.245418517	0.76	9.101884015
0.02	4.556613188	0.27	6.389832764	0.52	8.296916451	0.77	9.123212652
0.03	4.608986282	0.28	6.482367790	0.53	8.346475857	0.78	9.143900234
0.04	4.662880326	0.29	6.575093502	0.54	8.394169843	0.79	9.163973465
0.05	4.718346936	0.30	6.667738242	0.55	8.440071721	0.80	9.183457714
0.06	4.775437628	0.31	6.760026135	0.56	8.484254295	0.81	9.202377078
0.07	4.834203319	0.32	6.851682878	0.57	8.526789284	0.82	9.220754457
0.08	4.894693719	0.33	6.942441550	0.58	8.567746889	0.83	9.238611621
0.09	4.956956614	0.34	7.032048114	0.59	8.607195454	0.84	9.255969263
0.10	5.021036998	0.35	7.120266322	0.60	8.645201214	0.85	9.272847070
0.11	5.086976072	0.36	7.206881758	0.61	8.681828126	0.86	9.289263762
0.12	5.154810060	0.37	7.291704918	0.62	8.717137746	0.87	9.305237166
0.13	5.224568871	0.38	7.374573166	0.63	8.751189163	0.88	9.320784241
0.14	5.296274575	0.39	7.455351659	0.64	8.784038981	0.89	9.335921147
0.15	5.369939697	0.40	7.533933269	0.65	8.815741319	0.90	9.350663275
0.16	5.445565365	0.41	7.610237674	0.66	8.846347841	0.91	9.365025293
0.17	5.523139306	0.42	7.684209786	0.67	8.875907803	0.92	9.379021189
0.18	5.602633752	0.43	7.755817659	0.68	8.904468124	0.93	9.392664297
0.19	5.684003325	0.44	7.825050102	0.69	8.932073450	0.94	9.405967348
0.20	5.767182966	0.45	7.891914125	0.70	8.958766242	0.95	9.418942481
0.21	5.852086034	0.46	7.956432356	0.71	8.984586862	0.96	9.431601298
0.22	5.938602702	0.47	8.018640520	0.72	9.009573652	0.97	9.443954876
0.23	6.026598798	0.48	8.078585075	0.73	9.033763036	0.98	9.456013802
0.24	6.115915242	0.49	8.136321032	0.74	9.057189605	0.99	9.467788193
0.25	6.206368254	0.50	8.191910010	0.75	9.079886203	1.00	9.479287727

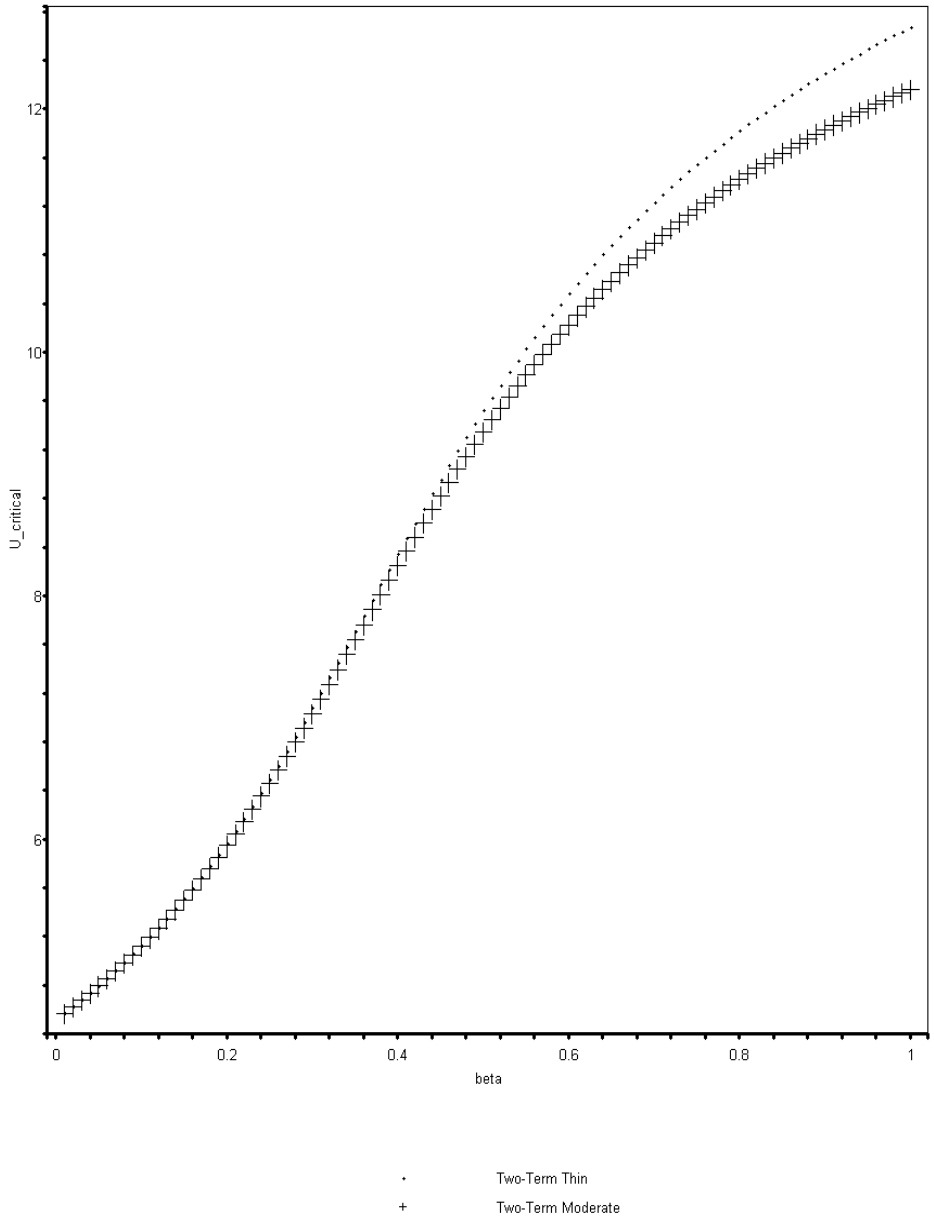

Fig. 5.15. Critical velocity vs. β for the two-term polynomial approximation for $\Lambda \sim 10^3$ and $\Lambda \sim 10^5$

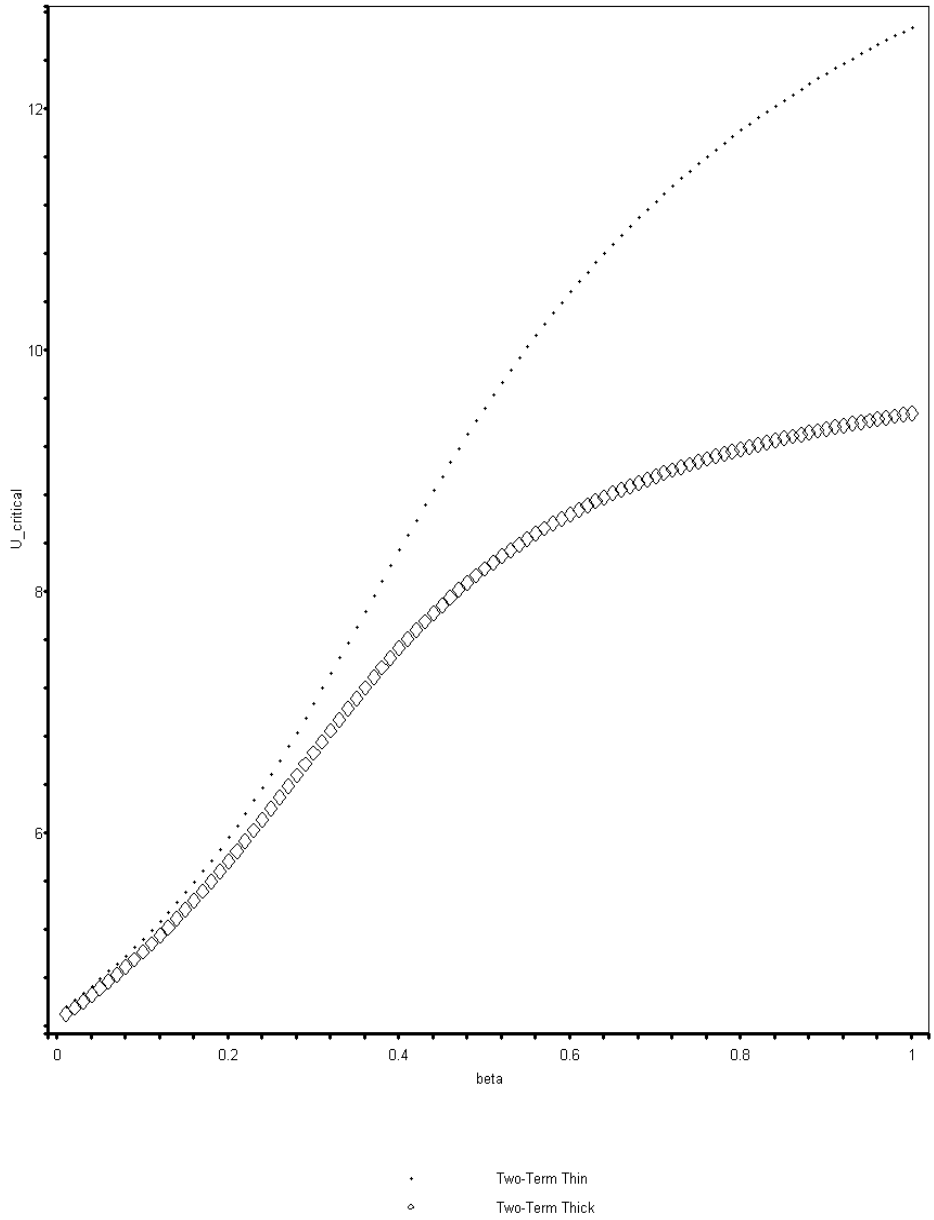

Fig. 5.16. Critical velocity vs. β for the two-term polynomial approximation for $\Lambda \sim 10^2$ and $\Lambda \sim 10^5$

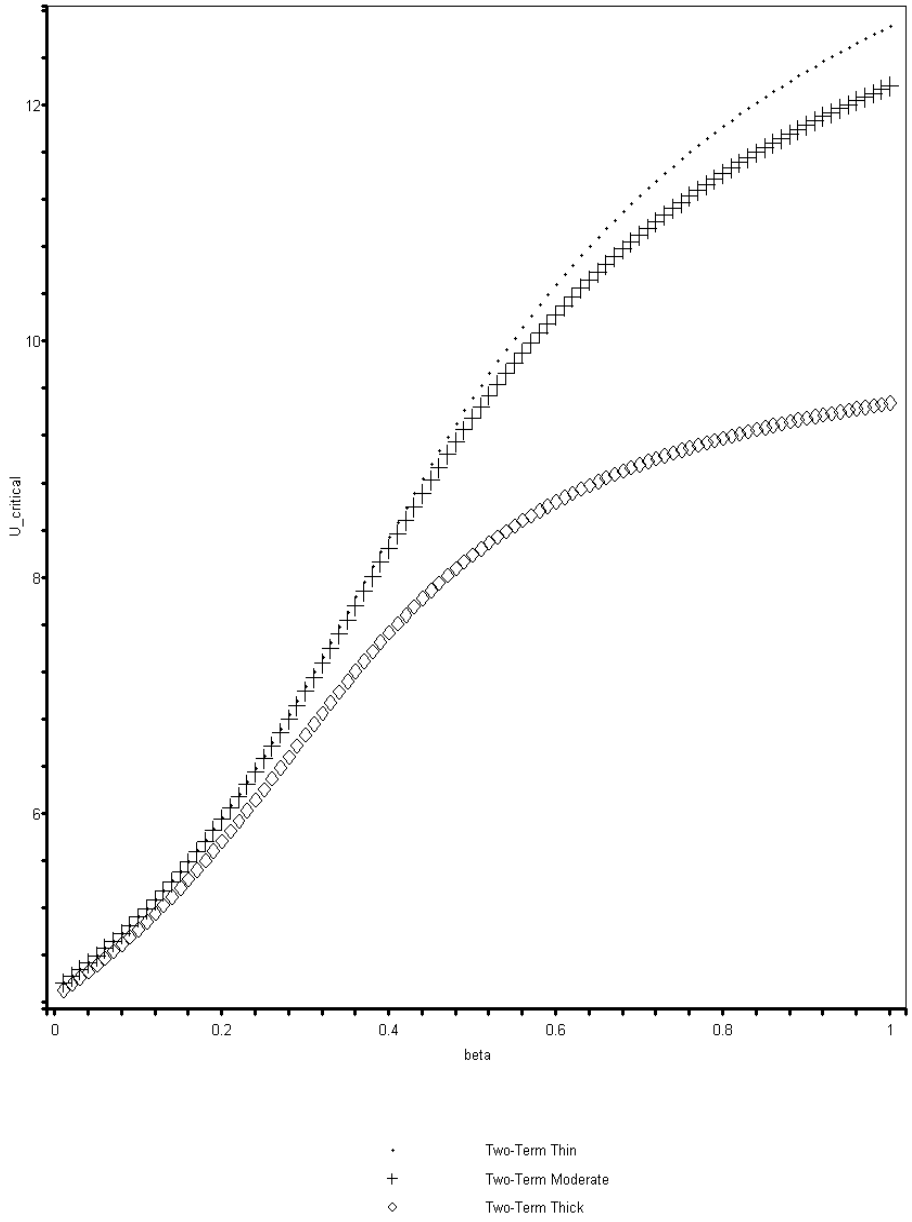

Fig. 5.17. Critical velocity vs. β for the two-term polynomial approximation for $\Lambda \sim 10^2$, $\Lambda \sim 10^3$, and $\Lambda \sim 10^5$

2. Four-Term Approximation

In viewing Figures 5.18-5.20, unlike the two-term polynomial approximation, the plots of the critical velocities versus β for the four-term polynomial approximation do not exactly mimic the behavior of the four-term trigonometric\hyperbolic approximation. The values of the critical velocities for each value of β ($\Lambda \sim 10^3$ and $\Lambda \sim 10^2$) for the four-term polynomial approximation are given in Tables 5.15-5.16 respectively. When $\Lambda \sim 10^3$ (Figures 5.18 and 5.20), there is only one jump (around $\beta = 0.3$) instead of two jumps ($\beta = 0.3$ and $\beta = 0.8$). When $\Lambda \sim 10^2$ (Figures 5.19 and 5.20), there are no jumps present in the graphs. Also, it is seen that the $\Lambda \sim 10^2$ graph has a much more "flatter" shape than the graph obtained by the trigonometric\hyperbolic basis functions (Figures 5.13 and 5.14). Actually, the four-term polynomial basis function critical velocity graph looks closely like the two-term polynomial critical velocity graph (for $\Lambda \sim 10^2$). The reason for this discrepancy has not been studied in this work and further work should address these issues.

Table 5.15
Dimensionless critical velocities for the four-term polynomial approximation ($\Lambda \sim 10^3$)

β	U_{crit}	β	U_{crit}	β	U_{crit}	β	U_{crit}
0.01	4.297837330	0.26	6.283110822	0.51	9.624716456	0.76	11.08041552
0.02	4.346994057	0.27	6.419458638	0.52	9.681709048	0.77	11.13813046
0.03	4.397757504	0.28	6.566381622	0.53	9.739021482	0.78	11.19585692
0.04	4.450207869	0.29	6.727300817	0.54	9.796628705	0.79	11.25364263
0.05	4.504430124	0.30	6.908360582	0.55	9.854502625	0.80	11.31152389
0.06	4.560514332	0.31	7.122463848	0.56	9.912612308	0.81	11.36956034
0.07	4.618555912	0.32	7.406697706	0.57	9.970918292	0.82	11.42781602
0.08	4.678655874	0.33	8.156390254	0.58	10.02939045	0.83	11.48636266
0.09	4.740921283	0.34	8.556189603	0.59	10.08799327	0.84	11.54528091
0.10	4.805465422	0.35	8.677744628	0.60	10.14669201	0.85	11.60466774
0.11	4.872408310	0.36	8.763072170	0.61	10.20545038	0.86	11.66464164
0.12	4.941877074	0.37	8.834012543	0.62	10.26424098	0.87	11.72532641
0.13	5.014006522	0.38	8.897686883	0.63	10.32303811	0.88	11.78688720
0.14	5.088939892	0.39	8.957327916	0.64	10.38181558	0.89	11.84949762
0.15	5.166829760	0.40	9.014609082	0.65	10.44054567	0.90	11.91338863
0.16	5.247839526	0.41	9.070518234	0.66	10.49920553	0.91	11.97883623
0.17	5.332145410	0.42	9.125679808	0.67	10.55778343	0.92	12.04616856
0.18	5.419939418	0.43	9.180481236	0.68	10.61626386	0.93	12.11582952
0.19	5.511433907	0.44	9.235188780	0.69	10.67463557	0.94	12.18839845
0.20	5.606868303	0.45	9.289980367	0.70	10.73290356	0.95	12.26463082
0.21	5.706519023	0.46	9.344973233	0.71	10.79105668	0.96	12.34559744
0.22	5.810715129	0.47	9.400239517	0.72	10.84909559	0.97	12.43293606
0.23	5.919861338	0.48	9.455828391	0.73	10.90704283	0.98	12.52923444
0.24	6.034474525	0.49	9.511768087	0.74	10.96489500	0.99	12.63921698
0.25	6.155241083	0.50	9.568067669	0.75	11.02268259	1.00	12.77332927

Table 5.16
Dimensionless critical velocities for the four-term polynomial approximation ($\Lambda \sim 10^2$)

β	U_{crit}	β	U_{crit}	β	U_{crit}	β	U_{crit}
0.01	4.342691335	0.26	5.989394110	0.51	8.217427918	0.76	9.005737046
0.02	4.388040883	0.27	6.079416802	0.52	8.258754311	0.77	9.028566663
0.03	4.434781950	0.28	6.171737444	0.53	8.299813739	0.78	9.050549278
0.04	4.482970589	0.29	6.266652975	0.54	8.339235116	0.79	9.071897735
0.05	4.532663408	0.30	6.364584391	0.55	8.377561992	0.80	9.092585285
0.06	4.583917176	0.31	6.466096566	0.56	8.415380590	0.81	9.112737160
0.07	4.636787792	0.32	6.571885333	0.57	8.451833313	0.82	9.132100125
0.08	4.691330047	0.33	6.682860534	0.58	8.487935623	0.83	9.151799587
0.09	4.747596357	0.34	6.799975874	0.59	8.522957529	0.84	9.170377246
0.10	4.805635558	0.35	6.924169209	0.60	8.556921666	0.85	9.188239326
0.11	4.865492414	0.36	7.055537732	0.61	8.590455163	0.86	9.205414525
0.12	4.927205192	0.37	7.191831633	0.62	8.623234689	0.87	9.222896313
0.13	4.990805576	0.38	7.327099866	0.63	8.655257656	0.88	9.240249916
0.14	5.056316509	0.39	7.452531611	0.64	8.686336610	0.89	9.255735891
0.15	5.123751663	0.40	7.562630163	0.65	8.716862720	0.90	9.271546582
0.16	5.193115869	0.41	7.656746055	0.66	8.746830554	0.91	9.287515658
0.17	5.264400985	0.42	7.737591261	0.67	8.776102726	0.92	9.302728874
0.18	5.337593007	0.43	7.808313950	0.68	8.804510465	0.93	9.316979840
0.19	5.412668763	0.44	7.871996563	0.69	8.832109100	0.94	9.331271782
0.20	5.489599650	0.45	7.930211162	0.70	8.858958022	0.95	9.345170067
0.21	5.568357358	0.46	7.984474352	0.71	8.885212562	0.96	9.358972082
0.22	5.648920213	0.47	8.035436174	0.72	8.910133185	0.97	9.372310737
0.23	5.731276298	0.48	8.083641031	0.73	8.934988290	0.98	9.385604648
0.24	5.815440675	0.49	8.130089732	0.74	8.959598651	0.99	9.398083539
0.25	5.901449041	0.50	8.174082371	0.75	8.983534306	1.00	9.410667818

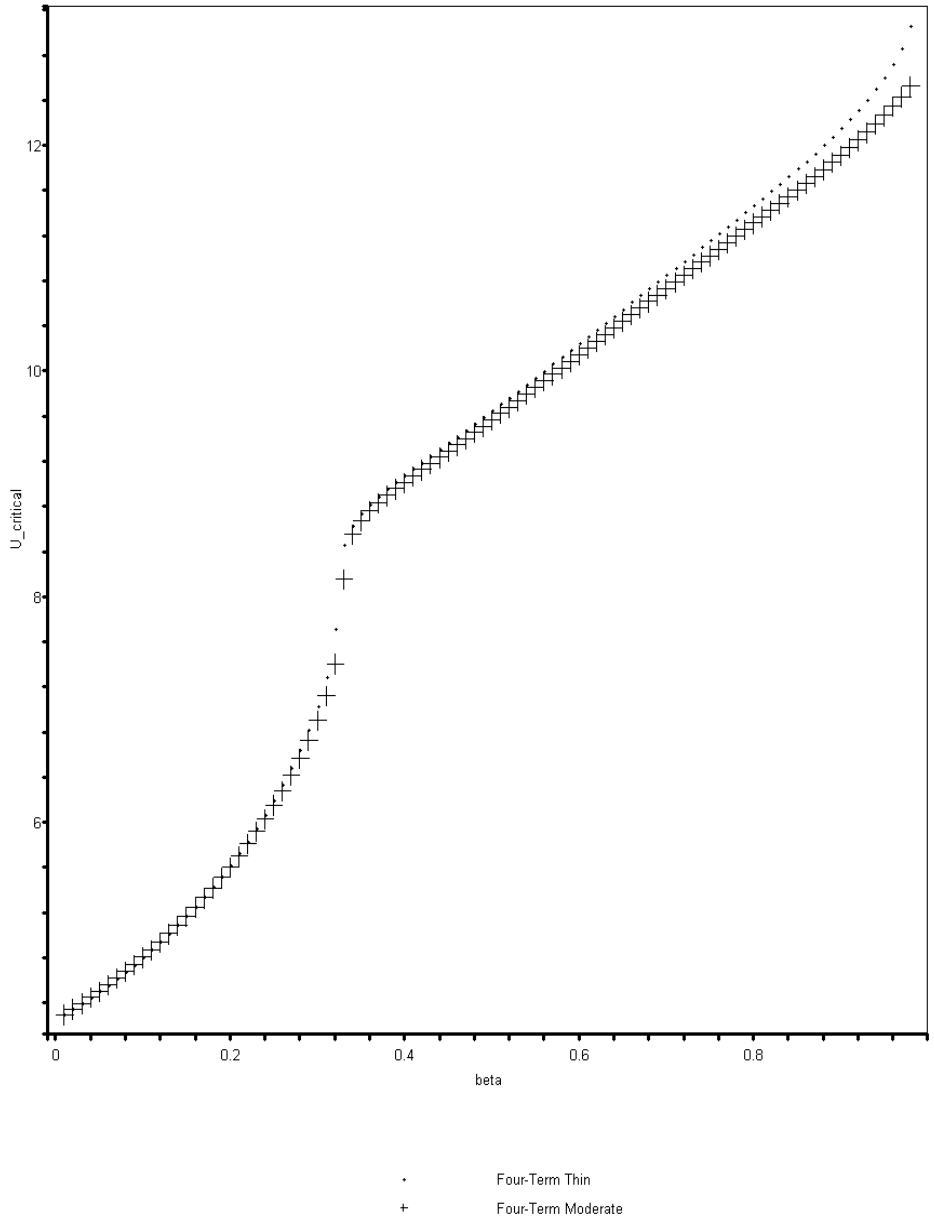

Fig. 5.18. Critical velocity vs. β for the four-term polynomial approximation for $\Lambda \sim 10^3$ and $\Lambda \sim 10^5$

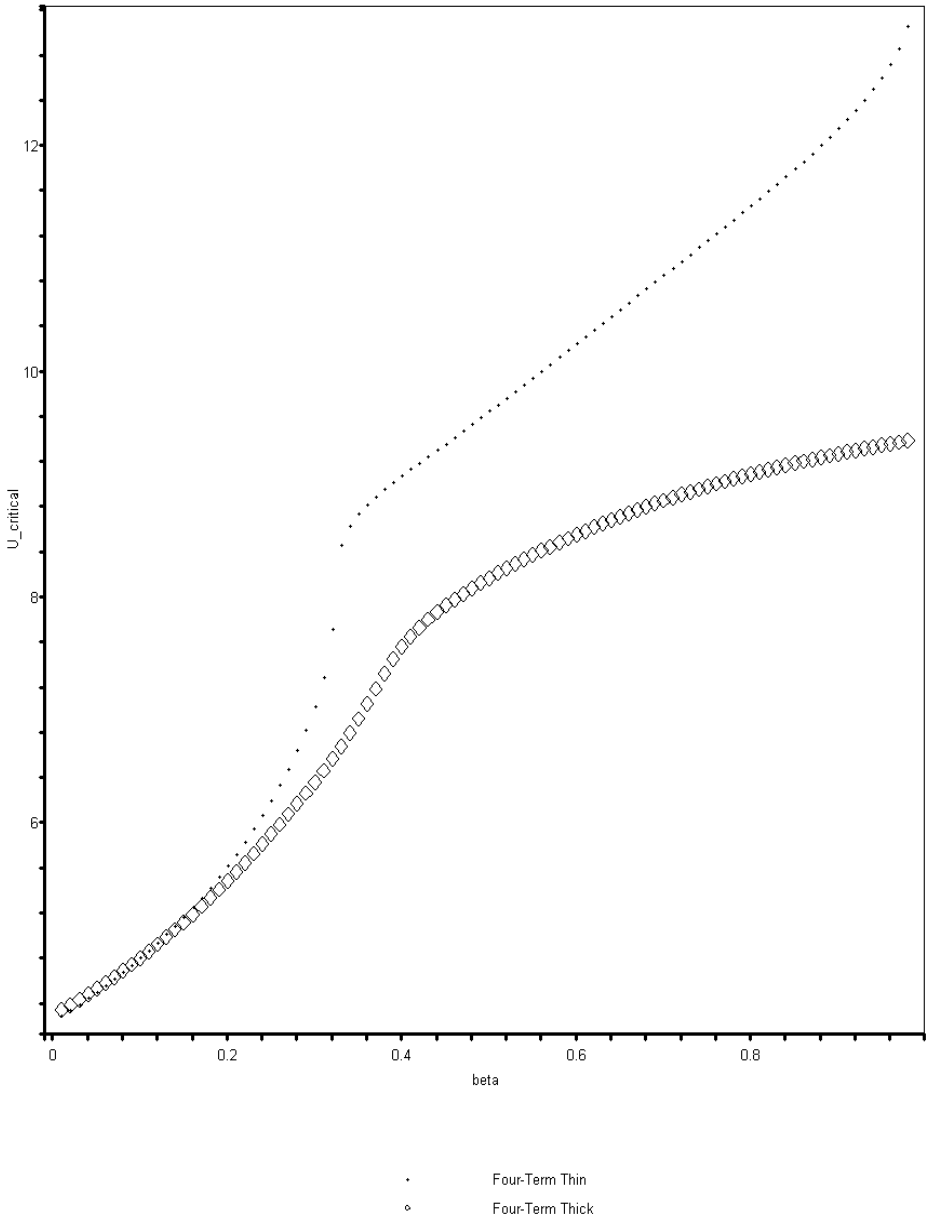

Fig. 5.19. Critical velocity vs. β for the four-term polynomial approximation for $\Lambda \sim 10^2$ and $\Lambda \sim 10^5$

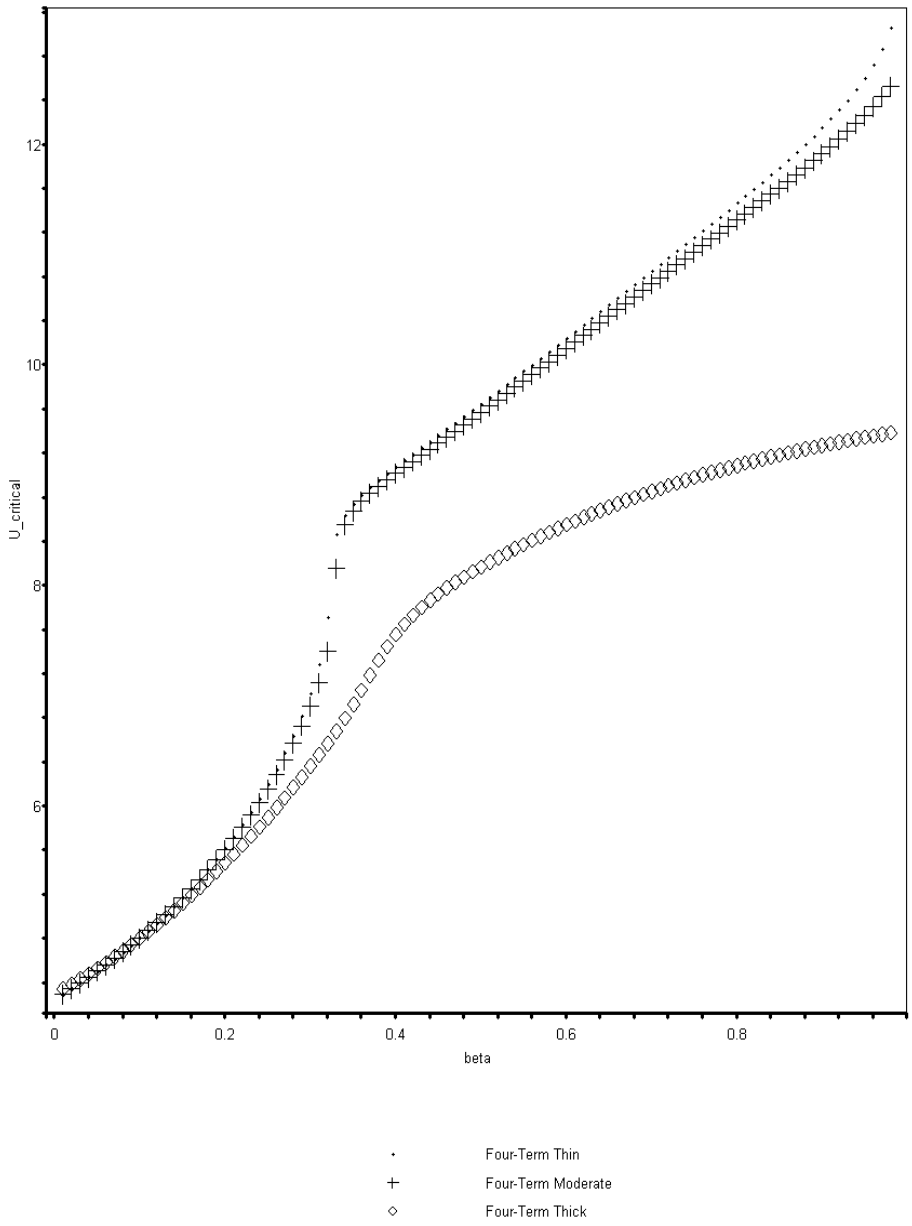

Fig. 5.20. Critical velocity vs. β for the four-term polynomial approximation for $\Lambda \sim 10^2$, $\Lambda \sim 10^3$, and $\Lambda \sim 10^5$

In summary, for the two-term approximations (trigonometric\hyperbolic and polynomial), the differences in critical velocities for ($\Lambda \sim 10^5 \to 10^3$ and $\Lambda \sim 10^5 \to 10^2$) are larger in the trigonometric\hyperbolic approximation compared to the polynomial approximation (for the highest ranges of β). For the four-term approximations, the differences in critical velocities for $\Lambda \sim 10^5 \to 10^3$ over the entire range of β are larger in the trigonometric\hyperbolic approximation compared to the polynomial approximation. However, the differences in critical velocities (for the four-term approximation) for $\Lambda \sim 10^5 \to 10^2$ are larger in the polynomial approximation compared to the trigonometric\hyperbolic approximation for only $\beta \geq 0.3$. Finally, after commenting on all the comparisons of the all the graphs, the first important issue is that the $\Lambda \sim 10^2$ critical velocities are consistently lower than $\Lambda \sim 10^5, 10^2$ (for all β). The second important issue is that only $\beta < 0.3$ critical velocities are relevant, and the differences in critical velocities for higher values of β are not pertinent.

CHAPTER VI

APPROXIMATE SOLUTION OF THE TIME-DEPENDENT EQUATIONS OF MOTION

The goal of this chapter is to solve the two time-dependent non-dimensional equations of motion via the finite element method. A finite element model will be formulated for a typical beam element; four time-dependent coupled ordinary differential equations (because there will be four degrees of freedom per element) will result per element. Once the local matrices (mass, damping, and stiffness) are obtained, assembly procedure for the global mass, damping, and stiffness will be begin. Boundary conditions (essential and force) will be applied to the system to obtain the resulting set (depending on how many elements are taken) of coupled ordinary differential equations (O.D.E.'s). Finally, if *N* elements are taken, the *2(N+1)* coupled O.D.E.'s will be solved numerically and the transverse deflection of the second node of the last element will be plotted versus time.

A. The Weak Form

In order to derive the finite element model, the "weak form" of the two coupled partial differential equations of motion must be formulated. We resort back to these two equations because of simplicity and identification of the boundary terms. From (3.43) and (3.44)

$$\frac{\partial^2 \eta}{\partial \tau^2} + 2\sqrt{\beta} u \frac{\partial^2 \eta}{\partial \xi \partial \tau} - (\Lambda - u^2) \frac{\partial^2 \eta}{\partial \xi^2} - \Lambda \frac{\partial \phi}{\partial \xi} = 0 \tag{6.1}$$

$$\sigma \frac{\partial^2 \phi}{\partial \tau^2} - \frac{\partial^2 \phi}{\partial \xi^2} + \Lambda \left(\frac{\partial \eta}{\partial \xi} + \phi \right) = 0 \tag{6.2}$$

These two equations will be multiplied by two different weighting functions, each will be integrated over a typical element non-dimensional spatial length *h*, and the differentiation of the spatial coordinate ξ will be will be weakened (i.e. integration by parts will be applied); hence the name "weak form." A complete description of the weak form and formulation of a finite element model can be found in Reddy [29]. When integrating by parts, one should be careful on which terms to integrate by parts in order not to create unnecessary forces boundary terms (secondary variables). Definitely, second-order differentiation should be weakened to first order and some first order differentiation should be completely relieved. In order to know which first order (also second, third,…) terms should be relieved, one should already have some foresight of the physicality of the forces that will result. This process will be implemented and explained further in detail. Multiplying by the weighting functions and integrating over an element length gives

$$\int_0^h \left[\frac{\partial^2 \eta}{\partial \tau^2} w_1 + 2\sqrt{\beta} u \frac{\partial^2 \eta}{\partial \xi \partial \tau} w_1 - \Lambda \frac{\partial^2 \eta}{\partial \xi^2} w_1 + u^2 \frac{\partial^2 \eta}{\partial \xi^2} w_1 - \Lambda \frac{\partial \phi}{\partial \xi} w_1 \right] d\xi = 0 \qquad (6.3)$$

$$\int_0^h \left[\sigma \frac{\partial^2 \phi}{\partial \tau^2} w_2 - \frac{\partial^2 \phi}{\partial \xi^2} w_2 + \Lambda \left(\frac{\partial \eta}{\partial \xi} + \phi \right) w_2 \right] d\xi = 0 \qquad (6.4)$$

where $w_1 = \delta\eta$ and $w_2 = \delta\phi$ are the arbitrary variations in the non-dimensional transverse deflection and rotation respectively. Integrating some spatial terms by parts gives

$$\int_0^h \left[\begin{array}{l} \dfrac{\partial^2 \eta}{\partial \tau^2} w_1 + \sqrt{\beta} u \left(\dfrac{\partial^2 \eta}{\partial \xi \partial \tau} w_1 - \dfrac{\partial \eta}{\partial \tau} \dfrac{\partial w_1}{\partial \xi} \dfrac{\partial^2 \eta}{\partial \xi \partial \tau} \right) + \Lambda \dfrac{\partial \eta}{\partial \xi} \dfrac{\partial w_1}{\partial \xi} - u^2 \dfrac{\partial \eta}{\partial \xi} \dfrac{\partial w_1}{\partial \xi} \\ + \Lambda \phi \dfrac{\partial w_1}{\partial \xi} \end{array} \right] d\xi \tag{6.5}$$

$$+ \left[\sqrt{\beta} u \frac{\partial \eta}{\partial \tau} w_1 \right]_0^h + \left[-\Lambda \left(\frac{\partial \eta}{\partial \xi} + \phi \right) w_1 \right]_0^h + \left[u^2 \frac{\partial \eta}{\partial \xi} w_1 \right]_0^h = 0$$

$$\int_0^h \left[\sigma \frac{\partial^2 \phi}{\partial \tau^2} w_2 + \frac{\partial \phi}{\partial \xi} \frac{\partial w_2}{\partial \xi} + \Lambda \left(\frac{\partial \eta}{\partial \xi} + \phi \right) w_2 \right] d\xi + \left[-\frac{\partial \phi}{\partial \xi} w_2 \right]_0^h = 0 \tag{6.6}$$

Remembering the non-dimensional shear force and moment from (3.47) and (3.48), we identify the following boundary terms as

$$\left[-\Lambda \left(\frac{\partial \eta}{\partial \xi} + \phi \right) w_1 \right]_0^h = \left[-Q_x \delta \eta \right]_0^h \tag{6.7}$$

$$\left[-\frac{\partial \phi}{\partial \xi} w_2 \right]_0^h = \left[-M_{xx} \delta \phi \right]_0^h \tag{6.8}$$

The non-dimensional virtual work done by the discharged fluid is

$$\left[\left(\sqrt{\beta} u \frac{\partial \eta}{\partial \tau} + u^2 \frac{\partial \eta}{\partial \xi} \right) w_1 \right]_0^h = \left[\left(\sqrt{\beta} u \frac{\partial \eta}{\partial \tau} + u^2 \frac{\partial \eta}{\partial \xi} \right) \delta \eta \right]_0^h \tag{6.9}$$

which has contributions from the non-dimensional, non-conservative Coriolis and centripetal force. This virtual work contributes energy to the ends of elements and is directly related to instability; the fluid transfers energy to the pipe. The evaluation of these boundary terms will follow.

B. Interpolation Functions

The interpolation (shape) functions used to approximate η and ϕ (taken from Reddy [12]) used in this work are "super-convergent" shape functions (see Appendix B for derivation) which interpolate η and ϕ in terms of all four degrees of freedom (non-dimensional deflections and rotations) per element; there are two nodes per element and two degrees of freedom (one deflection and one rotation) per node. Also, it is conventional to separate the spatial and time dependence between the shape functions and node displacements (rotations); the partial differential equations will now become an O.D.E.'s. This procedure is called the semi-discrete formulation.

$$\eta = \sum_{j=1}^{4} \Delta_j(t)\psi^{(1)}{}_j\left(\xi\right) \tag{6.10}$$

$$\phi = \sum_{j=1}^{4} \Delta_j(t)\psi^{(2)}{}_j(\xi) \tag{6.11}$$

$$\Delta_1 = \eta_1,\ \Delta_2 = \phi_1,\ \Delta_3 = \eta_2,\ \Delta_4 = \phi_2 \tag{6.12}$$

$$\begin{aligned}
\psi^{(1)}{}_1 &= \frac{1}{\mu}\left[\mu - \frac{12\zeta}{\Lambda} - (3-2\zeta)\zeta^2\right] \\
\psi^{(1)}{}_2 &= -\frac{h}{\mu}\left[(1-\zeta)^2\zeta + \frac{6}{\Lambda}(1-\zeta)\zeta\right] \\
\psi^{(1)}{}_3 &= \frac{1}{\mu}\left[\frac{12\zeta}{\Lambda} + (3-2\zeta)\zeta^2\right] \\
\psi^{(1)}{}_4 &= \frac{h}{\mu}\left[(1-\zeta)\zeta^2 + \frac{6}{\Lambda}(1-\zeta)\zeta\right]
\end{aligned} \tag{6.13}$$

$$
\begin{aligned}
\psi^{(2)}{}_1 &= \frac{6}{h\mu}(1-\zeta)\zeta \\
\psi^{(2)}{}_2 &= \frac{1}{\mu}\left(\mu - 4\zeta + 3\zeta^2 - \frac{12\zeta}{\Lambda}\right) \\
\psi^{(2)}{}_3 &= -\frac{6}{h\mu}(1-\zeta)\zeta \\
\psi^{(2)}{}_4 &= \frac{1}{\mu}\left(-2\zeta + 3\zeta^2 + \frac{12\zeta}{\Lambda}\right)
\end{aligned}
\tag{6.14}
$$

where $\mu = 1 + \frac{12}{\Lambda}$ and $\zeta = \frac{\xi}{h}$. Substituting (6.10) and (6.11) into (6.5)and (6.6), using (6.7) and (6.8), and setting $\delta\eta = \psi^{(1)}{}_i$ and $\delta\phi = \psi^{(2)}{}_i$ gives

$$
\begin{aligned}
&\int_0^h \left[\sum_{j=1}^{4}\left(\psi^{(1)}{}_i\psi^{(1)}{}_j\right)\frac{d^2\Delta_j}{d\tau^2} + \sqrt{\beta}u\sum_{j=1}^{4}\left(\psi^{(1)}{}_i\frac{d\psi^{(1)}{}_j}{d\xi} - \frac{d\psi^{(1)}{}_i}{d\xi}\psi^{(1)}{}_j\right)\frac{d\Delta_j}{d\tau} \right. \\
&\left. + \Lambda\sum_{j=1}^{4}\left(\frac{d\psi^{(1)}{}_i}{d\xi}\frac{d\psi^{(1)}{}_j}{d\xi} + \frac{d\psi^{(1)}{}_i}{d\xi}\psi^{(2)}{}_j\right)\Delta_j - u^2\sum_{j=1}^{4}\left(\frac{d\psi^{(1)}{}_i}{d\xi}\frac{d\psi^{(1)}{}_j}{d\xi}\right)\Delta_j \right] d\xi \\
&+ \sqrt{\beta}u\left[\sum_{j=1}^{4}\left(\psi^{(1)}{}_i\psi^{(1)}{}_j\right)\frac{d\Delta_j}{d\tau}\right]_0^h + \left[-Q_x\psi^{(1)}{}_i\right]_0^h + u^2\left[\sum_{j=1}^{4}\left(\psi^{(1)}{}_i\frac{d\psi^{(1)}{}_j}{d\xi}\right)\Delta_j\right]_0^h = 0
\end{aligned}
\tag{6.15}
$$

$$
\begin{aligned}
&\int_0^h \left[\sigma\sum_{j=1}^{4}\left(\psi^{(2)}{}_i\psi^{(2)}{}_j\right)\frac{d^2\Delta_j}{d\tau^2} + \Lambda\sum_{j=1}^{4}\left(\psi^{(2)}{}_i\frac{d\psi^{(1)}{}_j}{d\xi} + \psi^{(2)}{}_i\psi^{(2)}{}_j\right)\Delta_j \right. \\
&\left. + \sum_{j=1}^{4}\left(\frac{d\psi^{(2)}{}_i}{d\xi}\frac{d\psi^{(2)}{}_j}{d\xi}\right)\Delta_j \right] d\xi \\
&+ \left[-M_{xx}\psi^{(2)}{}_i\right]_0^h = 0
\end{aligned}
\tag{6.16}
$$

After factoring out the summation symbol outside the integral, combining (6.15) and (6.16), and gathering terms with respect to the ordinary time derivatives of Δ_j gives

$$\sum_{j=1}^{4}\left\{\int_0^h\left[\begin{array}{l}\left(\psi^{(1)}{}_i\psi^{(1)}{}_j+\sigma\psi^{(2)}{}_i\psi^{(2)}{}_j\right)\dfrac{d^2\Delta_j}{d\tau^2}+\sqrt{\beta}u\left(\psi^{(1)}{}_i\dfrac{d\psi^{(1)}{}_j}{d\xi}-\dfrac{d\psi^{(1)}{}_i}{d\xi}\psi^{(1)}{}_j\right)\dfrac{d\Delta_j}{d\tau}\\ +\left(\Lambda\left(\dfrac{d\psi^{(1)}{}_i}{d\xi}+\psi^{(2)}{}_i\right)\left(\dfrac{d\psi^{(1)}{}_j}{d\xi}+\psi^{(2)}{}_j\right)-u^2\dfrac{d\psi^{(1)}{}_i}{d\xi}\dfrac{d\psi^{(1)}{}_j}{d\xi}+\dfrac{d\psi^{(2)}{}_i}{d\xi}\dfrac{d\psi^{(2)}{}_j}{d\xi}\right)\Delta_j\end{array}\right]d\xi\right\}$$

$$+\sqrt{\beta}u\left[\sum_{j=1}^{4}\left(\psi^{(1)}{}_i\psi^{(1)}{}_j\right)\frac{d\Delta_j}{d\tau}\right]_0^h+u^2\left[\sum_{j=1}^{4}\left(\psi^{(1)}{}_i\frac{d\psi^{(1)}{}_j}{d\xi}\right)\Delta_j\right]_0^h+\left[-M_{xx}\psi^{(2)}{}_i\right]_0^h+\left[-Q_x\psi^{(1)}{}_i\right]_0^h=0 \tag{6.17}$$

or in a simpler form for the e^{th} element

$$\sum_{j=1}^{4}\left(M_{ij}^e\right)\ddot{\Delta}_j^e+\sum_{j=1}^{4}\left(C_{ij}^e+\bar{C}_{ij}^e\right)\dot{\Delta}_j^e+\sum_{j=1}^{4}\left(K_{ij}^e+\bar{K}_{ij}^e\right)\Delta_j^e=F_i^e \tag{6.18}$$

where

$$M_{ij}^e=\int_0^h\left(\psi^{(1)}{}_i\psi^{(1)}{}_j+\sigma\psi^{(2)}{}_i\psi^{(2)}{}_j\right)d\xi \tag{6.19}$$

$$C_{ij}^e=\sqrt{\beta}u\int_0^h\left(\psi^{(1)}{}_i\frac{d\psi^{(1)}{}_j}{d\xi}-\frac{d\psi^{(1)}{}_i}{d\xi}\psi^{(1)}{}_j\right)d\xi \tag{6.20}$$

$$\bar{C}_{ij}^e=\sqrt{\beta}u\left(\psi^{(1)}{}_i(h)\psi^{(1)}{}_j(h)\right) \tag{6.21}$$

$$K_{ij}^e=\int_0^h\left[\begin{array}{l}\Lambda\left(\dfrac{d\psi^{(1)}{}_i}{d\xi}+\psi^{(2)}{}_j\right)\left(\dfrac{d\psi^{(1)}{}_i}{d\xi}+\psi^{(2)}{}_j\right)-u^2\dfrac{d\psi^{(1)}{}_i}{d\xi}\dfrac{d\psi^{(1)}{}_j}{d\xi}\\ +\dfrac{d\psi^{(2)}{}_i}{d\xi}\dfrac{d\psi^{(2)}{}_j}{d\xi}\end{array}\right]d\xi \tag{6.22}$$

$$\bar{K}_{ij}^e=u^2\psi^{(1)}{}_i(h)\frac{d\psi^{(1)}{}_j}{d\xi}(h) \tag{6.23}$$

$$F_1^e=Q_x^e(0)=-Q_{x1}^e \tag{6.24}$$

$$F_2^e=M_{xx}^e(0)=-M_{xx1}^e \tag{6.25}$$

$$F_3^e = Q_x^e(h) = Q_{x2}^e \tag{6.26}$$

$$F_4^e = M_{xx}^e(h) = M_{xx2}^e \tag{6.27}$$

or in matrix form

$$\left[M^e\right]\left\{\ddot{\Delta}^e\right\} + \left[\hat{C}^e\right]\left\{\dot{\Delta}^e\right\} + \left[\hat{K}^e\right]\left\{\Delta^e\right\} = \left\{F^e\right\} \tag{6.28}$$

where

$$\hat{C}_{ij}^e = C_{ij}^e + \bar{C}_{ij}^e\,,\ \hat{K}_{ij}^e = K_{ij}^e + \bar{K}_{ij}^e \tag{6.29}$$

It is seen from (6.19)-(6.22), the local mass matrix $\left(\left[M^e\right]\right)$ is symmetric, the local total damping matrix $\left(\left[\hat{C}^e\right]\right)$ is always skew-symmetric, and the local total stiffness matrix $\left(\left[\hat{K}^e\right]\right)$ is generally not symmetric (because of $\left[\bar{K}^e\right]$). The matrices $\left[\bar{C}^e\right]$ and $\left[\bar{K}^e\right]$ represent force contributions from the non-dimensional Coriolis and centripetal force respectively due to the non-conservative (cantilevered) nature of the system. Normally, force boundary terms appear as vectors on the right-hand side of (6.28), but in this case, the Coriolis and centripetal force cannot be applied externally nor are they reactions. Due these non-traditional forces, the boundary terms must be evaluated in the matrix sense instead of the vector since. The fact that these strange boundary conditions are evaluated at $\xi = h$ only will be explained in the imposition of boundary conditions. The shear force and moment boundary terms can, of course, be evaluated in the vector sense as usual.

Substituting (6.13) and (6.14) into (6.19)-(6.23) yields the matrix elements for the local matrices, thus

$$[M^e] = \frac{1}{420\mathrm{h}(\Lambda+12)^2}\begin{bmatrix} m_{11} & m_{12} & m_{13} & m_{14} \\ & m_{22} & m_{23} & m_{24} \\ & & m_{33} & m_{34} \\ sym & & & m_{44} \end{bmatrix} \tag{6.30}$$

$$[C^e] = \frac{\sqrt{\beta}u}{30(\Lambda+12)}\begin{bmatrix} c_{11} & c_{12} & c_{13} & c_{14} \\ & c_{22} & c_{23} & c_{24} \\ & & c_{33} & c_{34} \\ s-sym & & & c_{44} \end{bmatrix} \tag{6.31}$$

$$\left[\bar{C}^e\right] = \sqrt{\beta}u\begin{bmatrix} 0 & 0 & 0 & 0 \\ 0 & 0 & 0 & 0 \\ 0 & 0 & 1 & 0 \\ 0 & 0 & 0 & 0 \end{bmatrix} \tag{6.32}$$

$$[K^e] = \frac{1}{30\mathrm{h}^3(\Lambda+12)^2}\begin{bmatrix} k_{11} & k_{12} & k_{13} & k_{14} \\ & k_{22} & k_{23} & k_{24} \\ & & k_{33} & k_{34} \\ sym & & & k_{44} \end{bmatrix} \tag{6.33}$$

$$\left[\bar{K}^e\right] = \frac{u^2}{h(12+\Lambda)}\begin{bmatrix} 0 & 0 & 0 & 0 \\ 0 & 0 & 0 & 0 \\ -12 & 6h & 12 & -h(\Lambda+6) \\ 0 & 0 & 0 & 0 \end{bmatrix} \tag{6.34}$$

$$
\begin{aligned}
m_{11} &= (156h^2+504\sigma)\Lambda^2+3528h^2\Lambda+20160h^2 \\
m_{12} &= -2h(21\sigma+11h^2)\Lambda^2-2h(231*h^2-1260\sigma)\Lambda-2520h^3 \\
m_{13} &= (54h^2-504\sigma)\Lambda^2+1512h^2\Lambda+10080h^2 \\
m_{14} &= h(-42\sigma+13h^2)\Lambda^2+h(378h^2+2520\sigma)\Lambda+2520h^3 \\
m_{22} &= 4h^2(14\sigma+h^2)\Lambda^2+4h^2(210\sigma+21h^2)\Lambda+4h^2(5040\sigma+126h^2) \\
m_{23} &= -h(-42\sigma+13h^2)\Lambda^2-h(378h^2+2520\sigma)\Lambda-2520h^3 \\
m_{24} &= -h^2(3h^2+14\sigma)\Lambda-h^2(840\sigma+84h^2)\Lambda-h^2(-10080\sigma+504h^2) \\
m_{33} &= (156h^2+504\sigma)\Lambda^2+3528h^2\Lambda+20160h^2 \\
m_{34} &= 2h(21\sigma+11h^2)\Lambda^2+2h(231h^2-1260\sigma)\Lambda+2520h^3 \\
m_{44} &= 4h^2(14\sigma+h^2)\Lambda^2+4h^2(210\sigma+21h^2)\Lambda+4h^2(5040\sigma+126h^2)
\end{aligned}
\tag{6.35}
$$

$$
\begin{aligned}
c_{11} &= 0 \\
c_{12} &= -6h(\Lambda+10) \\
c_{13} &= 30(\Lambda+12) \\
c_{14} &= 6h(\Lambda+10) \\
c_{22} &= 0 \\
c_{23} &= -6h(\Lambda+10) \\
c_{24} &= -h^2\Lambda \\
c_{33} &= 0 \\
c_{34} &= -6h(\Lambda+10) \\
c_{44} &= 0
\end{aligned}
\tag{6.36}
$$

$$
\begin{aligned}
k_{11} &= (360-36u^2h^2)\Lambda^2+(-720u^2h^2+4320h^2)\Lambda-4320u^2h^2 \\
k_{12} &= 3h(u^2h^2-60)\Lambda^2+(-2160h^3)\Lambda \\
k_{13} &= (-360+36u^2h^2)\Lambda^2+(720u^2h^2-4320h^2)\Lambda+4320u^2h^2 \\
k_{14} &= 3h(u^2h^2-60)\Lambda^2-2160h^2\Lambda \\
k_{22} &= -4h^2(u^2h^2-30)\Lambda^2-4h^2(-180+15u^2h^2-270h^2)\Lambda-4h^2(-1080+90u^2h^2) \\
k_{23} &= -3h(u^2h^2-60)\Lambda^2+2160h^3\Lambda \\
k_{24} &= h^2(u^2h^2+60)\Lambda^2+h^2(1080h^2-720+60u^2h^2)\Lambda+h^2(-4320+360u^2h^2) \\
k_{33} &= (360-36u^2h^2)\Lambda^2+(-720u^2h^2+4320h^2)\Lambda-4320u^2h^2 \\
k_{34} &= -3h(u^2h^2-60)\Lambda^2+2160h^3\Lambda \\
k_{44} &= -4h^2(u^2h^2-30)\Lambda^2-4h^2(-180+15u^2h^2-270h^2)\Lambda-4h^2(-1080+90u^2h^2)
\end{aligned}
\tag{6.37}
$$

C. Assembly of Global Matrices and Imposition of Boundary Conditions

Since the elements are connected in series, the assembled global mass, damping, and stiffness matrices will be a banded. If *N* elements *(N+1* nodes, *2N+2* degrees of freedom) are taken, the general global coefficient matrices for the mass, damping, and stiffness matrices will be of the form

$$[G]_{GLOBAL} = \begin{bmatrix} G_{11}^1 & G_{12}^1 & G_{13}^1 & G_{14}^1 & 0 & \cdots & 0 \\ G_{21}^1 & G_{22}^1 & G_{23}^1 & G_{24}^1 & 0 & \cdots & 0 \\ G_{31}^1 & G_{32}^1 & G_{33}^1 + G_{11}^2 & G_{34}^1 + G_{12}^2 & G_{13}^2 & \cdots & 0 \\ G_{41}^1 & G_{42}^1 & G_{43}^1 + G_{21}^2 & G_{44}^1 + G_{22}^2 & G_{23}^2 & \cdots & 0 \\ 0 & 0 & G_{31}^2 & G_{32}^2 & \ddots & \vdots & \vdots \\ \vdots & \vdots & \vdots & \vdots & \vdots & G_{33}^N & G_{34}^N \\ 0 & 0 & 0 & 0 & \cdots & G_{43}^N & G_{44}^N \end{bmatrix}, \begin{matrix} G = M, \hat{C}, \hat{K} \\ (2(N+1)x2(N+1)) \end{matrix} \tag{6.38}$$

where G_{ij}^e represents the ij^{th} matrix element of the e^{th} finite element.

Since there are no distributed loads applied, the only forces at the nodes will to contributions from the point shear forces and point moments at each node. In assembling the global force vector, one has to add the forces and moments at a node of an element to the forces and moments respectively of an adjacent element sharing that common node. The total force (moment) applied will be equal to the sum of the contributions from each element. The global force vector is of the form

$$\{F\} = \begin{Bmatrix} {Q_{x1}}^{1} \\ {M_{xx1}}^{1} \\ {Q_{x2}}^{1} + {Q_{x1}}^{2} \\ {M_{xx2}}^{1} + {M_{xx1}}^{2} \\ \vdots \\ {Q_{x1}}^{N} + {Q_{x2}}^{N-1} \\ {M_{xx1}}^{N} + {M_{xx2}}^{N-1} \\ {Q_{x1}}^{N} \\ {M_{xx2}}^{N} \end{Bmatrix}, ((2N+2)x1) \tag{6.39}$$

The displacement and rotation of at a node of an element is equal to the displacement and rotation respectively of an adjacent element's node that is common to the two elements, thus $\Delta_1 = \Delta_1^1$, $\Delta_2 = \Delta_2^1$, $\Delta_3 = \Delta_3^1 = \Delta_1^2$, $\Delta_4 = \Delta_4^1 = \Delta_2^2$, …, $\Delta_{2N+1} = \Delta_3^N$, $\Delta_{2N+2} = \Delta_4^N$.

The nodal vector is of the form

$$\{\Delta(t)\} = \begin{Bmatrix} \Delta_1(t) \\ \Delta_2(t) \\ \vdots \\ \Delta_{2N+1}(t) \\ \Delta_{2N+2}(t) \end{Bmatrix}, ((2N+2)x1) \tag{6.40}$$

Due to the fact that no point forces or moments are applied at any node for this problem, all terms in (6.39) except for the top force and moment (reactions) are zero.

$$\{F\} = \begin{Bmatrix} Q_{x1}{}^{1} \\ M_{xx1}{}^{1} \\ 0 \\ 0 \\ \vdots \\ 0 \\ 0 \\ 0 \\ 0 \end{Bmatrix}, ((2N+2)x1) \tag{6.41}$$

These are the force (natural) boundary conditions for this problem. At leftmost node (i.e. node 1 of the first element), the force and moment ($Q_{x1}{}^{1}$ and $M_{xx1}{}^{1}$) cannot be known because the essential variables (η and ϕ) are already known (Refer back to(4.6) and (4.7) for clarification). $Q_{x1}{}^{1}$ and $M_{xx1}{}^{1}$ represent the reaction force and moment which are calculated in the post-computation. Because the beam is cantilevered, the displacement and rotation at node 1 of element 1 are equal to zero, therefore

$$\{\Delta(t)\} = \begin{Bmatrix} 0 \\ 0 \\ \Delta_3(t) \\ \vdots \\ \Delta_{2N+1}(t) \\ \Delta_{2N+2}(t) \end{Bmatrix}, ((2N+2)x1) \tag{6.42}$$

These are the essential boundary conditions of the problem. Because of an argument stated by McIver in [32] in formulating Hamilton's Principle of a closed non-conservative system, the Coriolis and Centripetal force boundary conditions do not contribute at the inlet of an element. Since, the only node in the entire beam that is not an inlet is node 2 of element *N*, hence

$$\left[\bar{C}^1\right]=\left[\bar{C}^2\right]=\cdots=\left[\bar{C}^{N-1}\right]=0 \tag{6.43}$$

$$\left[\bar{K}^1\right]=\left[\bar{K}^2\right]=\cdots=\left[\bar{K}^{N-1}\right]=0 \tag{6.44}$$

This boundary condition comes from (1.6) because the added extra energy (work) is only at the rightmost end of the beam. After imposing (6.41)-(6.44), we can eliminate the first two rows and columns of each of the matrices of (6.38) which results in a *2N* coupled set of second-order O.D.E.'s of the form

$$\left[\tilde{M}\right]\left\{\ddot{\tilde{\Delta}}\right\}+\left[\tilde{C}\right]\left\{\dot{\tilde{\Delta}}\right\}+\left[\tilde{K}\right]\left\{\tilde{\Delta}\right\}=\{0\} \tag{6.45}$$

where

$$\tilde{M}_{ij}=M_{(i+2)(j+2)},\ \tilde{C}_{ij}=\hat{C}_{(i+2)(j+2)},\ \tilde{K}_{ij}=\hat{K}_{(i+2)(j+2)} \tag{6.46}$$

$$\tilde{\Delta}_i(t)=\Delta_{i+2}(t) \tag{6.47}$$

D. The Newmark Method Time Scheme

In order to solve(6.45), one must seek a numerical integration technique. A popular method in structural dynamics in solving a system of O.D.E.'s is the Newmark method time scheme. In this scheme, we fully discretize this system of hyperbolic O.D.E.'s into a set of algebraic equations by using a two parameter "alpha-beta" approximation. The nodal displacements (rotations) and their derivatives are approximated in the form [26]

$$\begin{aligned}\left\{\tilde{\Delta}\right\}_{s+1}&=\left\{\tilde{\Delta}\right\}_s+\Delta t\left\{\dot{\tilde{\Delta}}\right\}_s+\frac{1}{2}(\Delta\tau)^2\left\{\ddot{\tilde{\Delta}}\right\}_{s+\gamma}\\ \left\{\dot{\tilde{\Delta}}\right\}_{s+1}&=\left\{\dot{\tilde{\Delta}}\right\}_s+\left\{\ddot{\tilde{\Delta}}\right\}_{s+\alpha}\Delta\tau\end{aligned} \tag{6.48}$$

where

$$\left\{\ddot{\tilde{\Delta}}\right\}_{s+\theta} = (1-\theta)\left\{\ddot{\tilde{\Delta}}\right\}_{s} + \theta\left\{\ddot{\tilde{\Delta}}\right\}_{s+1},\ \theta = \alpha, \gamma,\ \gamma = 2\beta \tag{6.49}$$

and α, γ are the two stability parameters chosen depending on the problem studied. Since the current problem is linear we will take $\alpha = \gamma = \frac{1}{2}$, which are also stable parameters [29].

Since the right-hand side of (6.45) is equal to zero, for zero initial displacements, velocities, and accelerations (which will be the case for this problem), a trivial zero response will be obtained. Therefore, we will put a "dead load" impact force for the first time step to get the response started. This impact force will be of the form

$$f(\xi, \tau) = \gamma_0 \left(H(\tau) - H(\tau - \tau_0)\right) \tag{6.50}$$

where $H(\tau)$ is the Heaviside function, τ_0 is the interval of the first time step, and γ_0 is a small amplitude. This force belongs on the right-hand side of (6.1) and joins in the assembly similar to (6.39) thereby leading to an assembled force vector of the form $\{F\}$ *((2N+2)x1)* whose first two vector elements are unused exactly like the first two elements in (6.41).

After substituting (6.48) and (6.49) into (6.45) and much algebraic manipulation, we obtain a fully discretized set of algebraic equations [26, 27] of the form

$$\left[\hat{J}\right]\left\{\tilde{\Delta}\right\}_{s+1} = \left\{\hat{F}\right\}_{s+1} \tag{6.51}$$

where

$$\left[\hat{J}\right] = \left[\tilde{K}\right] + a_3\left[\tilde{M}\right] + a_5\left[\tilde{C}\right] \tag{6.52}$$

$$\left\{\hat{F}\right\}_{s+1} = \{F\}_{s+1} + \left[\tilde{M}\right]\left(a_3\left\{\tilde{\Delta}\right\}_s + a_4\left\{\dot{\tilde{\Delta}}\right\}_s + a_5\left\{\ddot{\tilde{\Delta}}\right\}_s\right) + [C]\left(a_5\left\{\tilde{\Delta}\right\}_s + a_6\left\{\dot{\tilde{\Delta}}\right\}_s + a_7\left\{\ddot{\tilde{\Delta}}\right\}_s\right) \tag{6.53}$$

$$\begin{aligned}\left\{\ddot{\tilde{\Delta}}\right\}_{s+1} &= a_3\left(\left\{\tilde{\Delta}\right\}_{s+1} - \left\{\tilde{\Delta}\right\}_s\right) - a_4\left\{\dot{\tilde{\Delta}}\right\}_s - a_5\left\{\ddot{\tilde{\Delta}}\right\}_s \\ \left\{\dot{\tilde{\Delta}}\right\}_{s+1} &= \left\{\dot{\tilde{\Delta}}\right\}_s + a_2\left\{\ddot{\tilde{\Delta}}\right\}_s + a_1\left\{\ddot{\tilde{\Delta}}\right\}_{s+1}\end{aligned} \tag{6.54}$$

and

$$\begin{aligned}&a_1 = \alpha\Delta\tau, a_2 = (1-\alpha)\Delta\tau, a_3 = \frac{2}{\gamma\left(\Delta\tau\right)^2}, a_4 = \frac{2}{\gamma\Delta\tau}, \\ &a_5 = \frac{1}{\gamma} - 1, a_6 = \frac{2\alpha}{\gamma} - 1, a_7 = \frac{\Delta\tau}{2}\left(\frac{2\alpha}{\gamma} - 2\right)\end{aligned} \tag{6.55}$$

Once again, all initial conditions will be taken as zero. Equations (6.51)-(6.54) are repeated (in a loop) for however long desired. For the problem at hand, the system will go unstable or stable in a short amount of time.

E. Numerically Integrated Results

1. Numerically Integrated Results for a Thin Beam

Numerically integrating (6.45) through use of the Newmark time scheme ((6.51)-(6.55)) was done by a program written in MATLAB 7.0.1 (see Appendix C). The non-dimensional fixed parameter values used were $\Lambda \sim 10^5$, $0.01 \le \beta \le 0.20$, $\gamma_0 = 1.0x10^{-4}$, and $\sigma = 0$. The reasoning behind stopping at $\beta = 0.2$ is to steer clear of the "jumps" and divergence present in the higher order approximations (trigonometric\hyperbolic and polynomial). After these values were fixed, the velocity *u* was varied until the onset of instability. The finite element values used in the program were $\Delta\tau = 1.0x10^{-3}$,

$\left\{\tilde{\Delta}\right\}_0 = \{0\}$, $\left\{\dot{\tilde{\Delta}}\right\}_0 = \{0\}$, and $\left\{\ddot{\tilde{\Delta}}\right\}_0 = \{0\}$ with 50 elements integrated over 100 non-dimensional time units. Once $\left\{\tilde{\Delta}\right\}_s \ (s = 1, 2, \ldots)$ was obtained, the value of the deflection $\left(\tilde{\Delta}_{2N-1}\right)_s \ (s = 0, 1, 2 \ldots)$ was plotted versus τ for each time step.

The first example is a thin beam $\left(\Lambda \sim 10^5\right)$ with a very small mass ratio $\beta = 0.01$. When $u = 4.29$, the response was stable as shown in Figure 6.1 and when $u = 4.30$, the response was unstable as shown in Figure 6.2. Therefore, the critical velocity can be approximated as $u = 4.295$. The percent error between this value and the value obtained from the five-term trigonometric\hyperbolic approximation ($u = 4.234$) in Table 5.5 and the five-term polynomial approximation ($u = 4.272$) in Table 5.8 is 1.4% and 0.5% respectively.

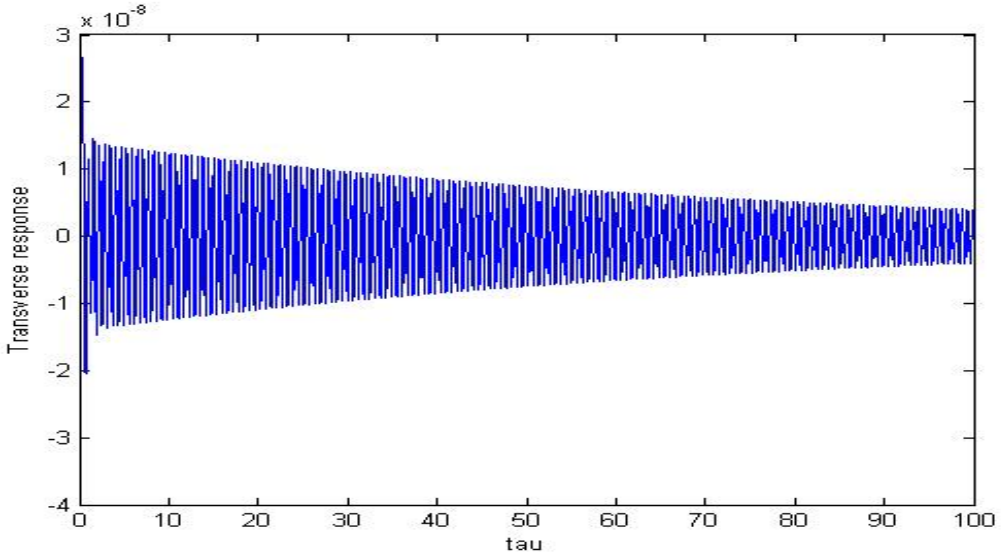

Fig. 6.1. $\tilde{\Delta}_{2N-1}$ vs. τ for $u = 4.29$, $\beta = 0.01$, and $\Lambda \sim 10^5$

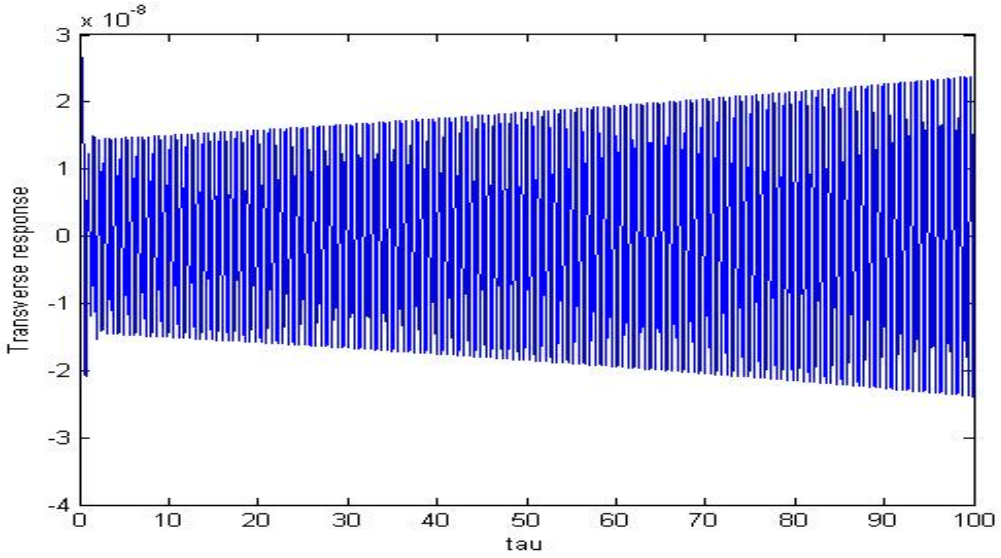

Fig. 6.2. $\tilde{\Delta}_{2N-1}$ vs. τ for $u = 4.30$, $\beta = 0.01$, and $\Lambda \sim 10^5$

When $\beta = 0.05$ Figure 6.3 shows the response to be stable when $u = 4.75$ and Figure 6.4 shows the response to be unstable at $u = 4.76$; therefore, the critical velocity can be approximated as $u = 4.755$. Compared with the value obtained in Table 5.5 ($u = 4.441$) and in Table 5.8 ($u = 4.478$), the percent error is 6.6% and .5.8% respectively.

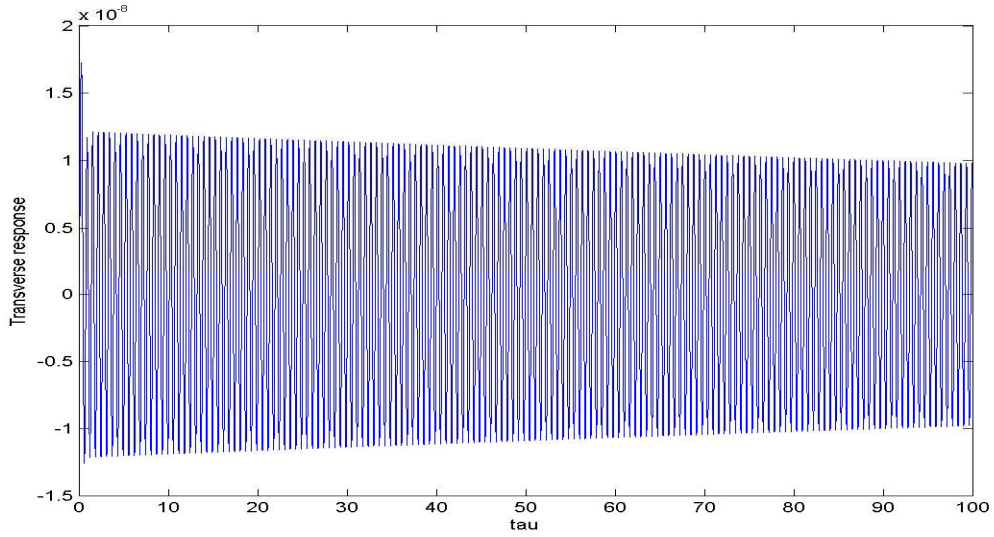

Fig. 6.3. $\tilde{\Delta}_{2N-1}$ vs. τ for $u = 4.75$, $\beta = 0.05$, and $\Lambda \sim 10^5$

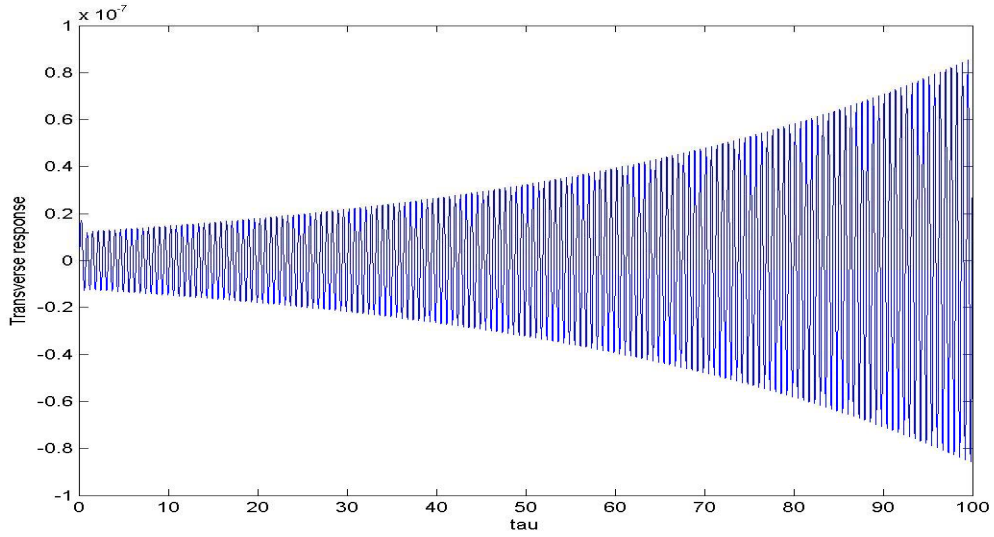

Fig. 6.4. $\tilde{\Delta}_{2N-1}$ vs. τ for $u = 4.76$, $\beta = 0.05$, and $\Lambda \sim 10^5$

When $\beta = 0.10$ Figure 6.5 shows the response to be stable when $u = 5.59$ and Figure 6.6 shows the response to be unstable at $u = 5.60$; therefore, the critical velocity can be approximated as $u = 5.595$. Compared with the value obtained in Table 5.5 ($u = 4.746$) and in Table 5.8 ($u = 4.781$), the percent error is 15.2% and .14.6% respectively.

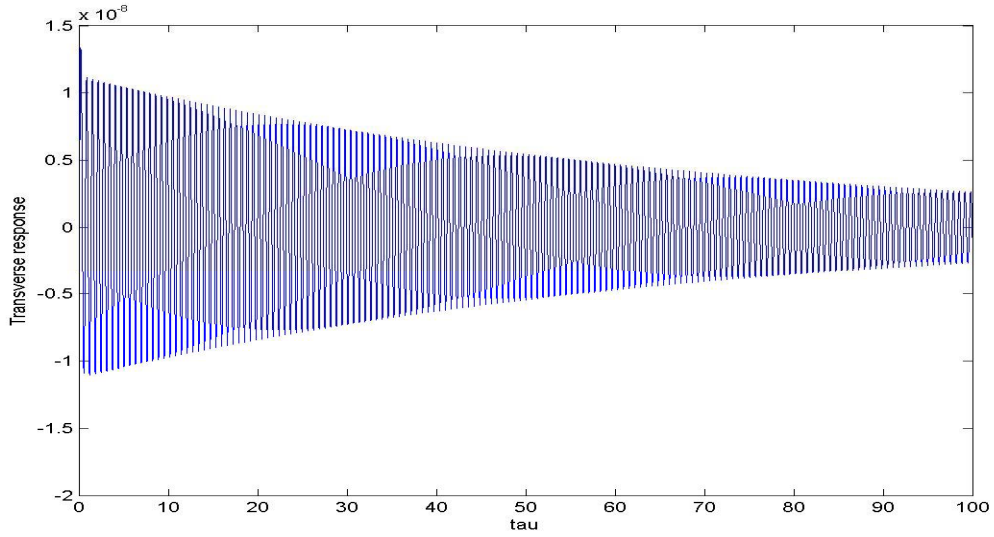

Fig. 6.5. $\tilde{\Delta}_{2N-1}$ vs. τ for $u = 5.59$, $\beta = 0.10$, and $\Lambda \sim 10^5$

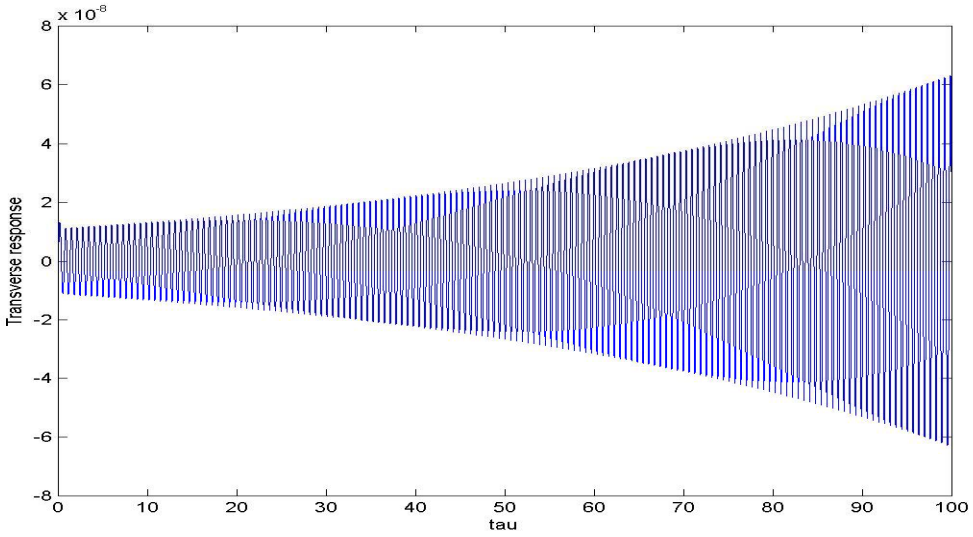

Fig. 6.6. $\tilde{\Delta}_{2N-1}$ vs. τ for $u = 5.60$, $\beta = 0.10$, and $\Lambda \sim 10^5$

When $\beta = 0.20$ Figure 6.7 shows the response to be stable when $u = 8.78$ and Figure 6.8 shows the response to be unstable at $u = 8.79$; therefore, the critical velocity can be approximated as $u = 8.785$. Compared with the value obtained in Table 5.5 ($u = 5.585$) and in Table 5.8 ($u = 5.601$), the percent error is 36.4% and .36.2% respectively.

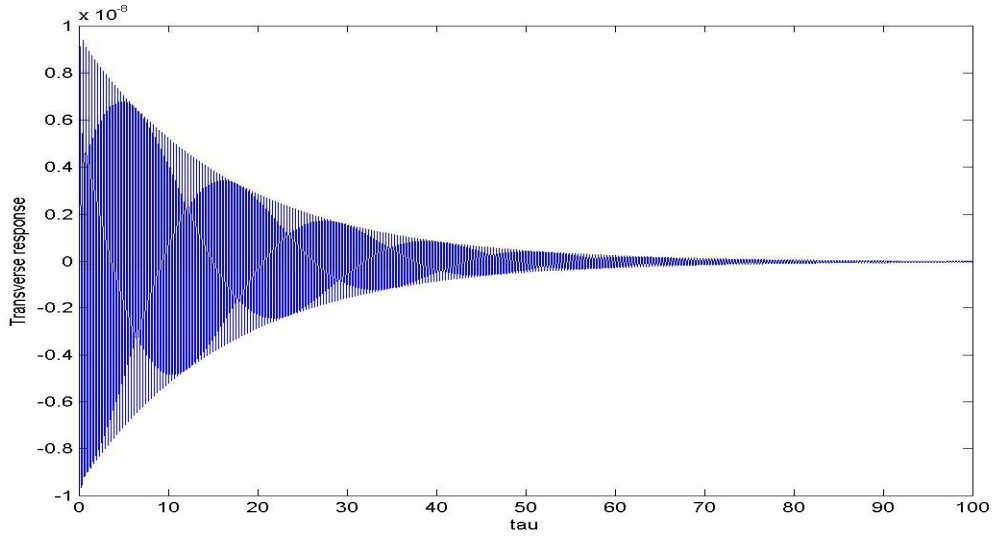

Fig. 6.7. $\tilde{\Delta}_{2N-1}$ vs. τ for $u = 8.78$, $\beta = 0.20$, and $\Lambda \sim 10^5$

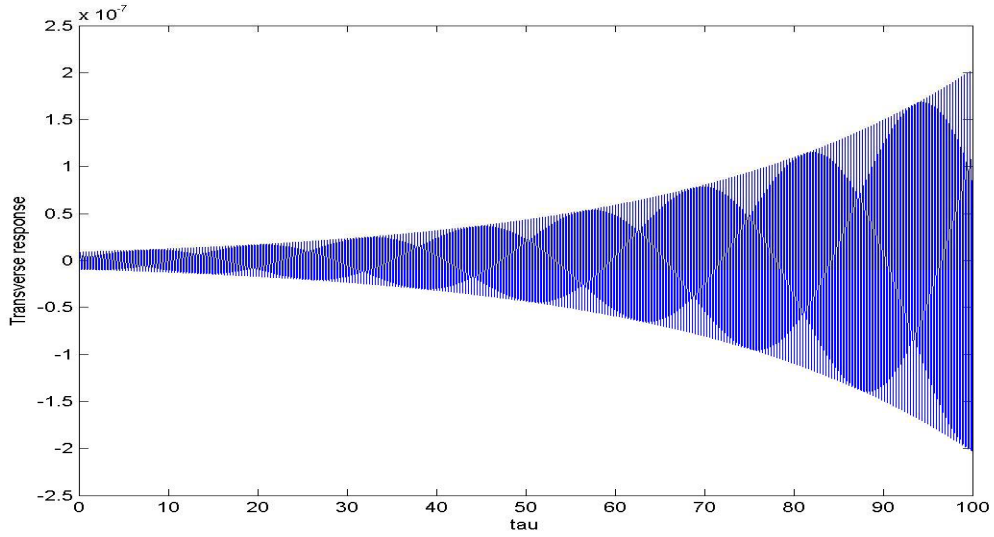

Fig. 6.8. $\tilde{\Delta}_{2N-1}$ vs. τ for $u = 8.79$, $\beta = 0.20$, and $\Lambda \sim 10^5$

As seen from Figures 6.1-6.8, the values of the critical velocities obtained from the Bubnov-Galerkin approximation (trigonometric\hyperbolic and polynomial) agree very well for $0.01 \le \beta \le 0.05$, fair for $\beta = 0.10$, and poor for $\beta = 0.20$ compared with

the exact numerical integration critical velocities. It was expected from the graphs created in the previous chapter that the results for $\beta > 0.3$ would be poor but unexpected for $\beta = 0.2$. This discrepancy is due firstly to the fact that the Bubnov-Galerkin approximation is simply an approximation and secondly due to the fact that the basis functions used in the Bubnov-Galerkin approximation were obtained from the non-fluid differential equations; i.e. the boundary conditions (essential and natural) were not satisfied exactly.

2. Numerically Integrated Results for a Moderately Thick and Thick Beam

The procedure for numerically integrating the time-dependent differential equations for a moderately thick and thick beam will be identical to the procedure for a thin beam. Once again, the non-dimensional fixed material parameter values used were $\Lambda \sim 10^2, 10^3$, $0.01 \le \beta \le 0.20$, $\gamma_0 = 1.0x10^{-4}$, and $\sigma = 0$. For the sake of brevity, only three values of the mass ratio will be considered, $\beta = 0.01, 0.10, 0.20$ The finite element values used again were $\Delta\tau = 1.0x10^{-3}$, $\left\{\tilde{\Delta}\right\}_0 = \{0\}$, $\left\{\dot{\tilde{\Delta}}\right\}_0 = \{0\}$, and $\left\{\ddot{\tilde{\Delta}}\right\}_0 = \{0\}$ with 50 elements integrated over 100 non-dimensional time units.

When $\beta = 0.01$ ($\Lambda \sim 10^3$), Figure 6.9 shows the response to be stable when $u = 4.29$ and Figure 6.10 shows the response to be unstable at $u = 4.30$; therefore, the critical velocity can be approximated as $u = 4.295$. This result is exactly the numerically integrated result when $\Lambda \sim 10^5$. Compared with the value obtained in Table 5.11 for the four-term trigonometric\hyperbolic approximation ($u = 4.186$) and in Table

5.15 for the four-term polynomial approximation ($u = 4.298$), the percent error is 6.6% and $7.0x10^{-2}$ % respectively.

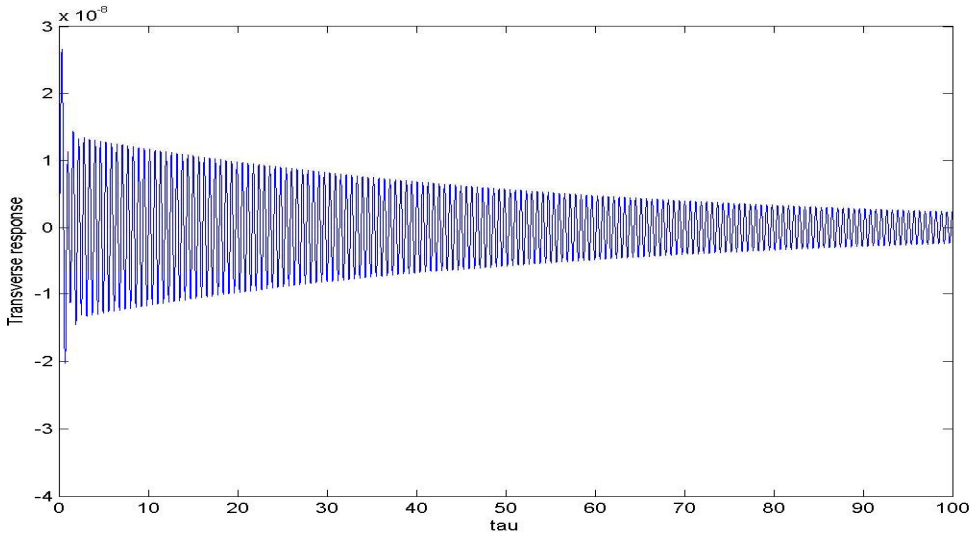

Fig. 6.9. $\tilde{\Delta}_{2N-1}$ vs. τ for $u = 4.29$, $\beta = 0.01$, and $\Lambda \sim 10^3$

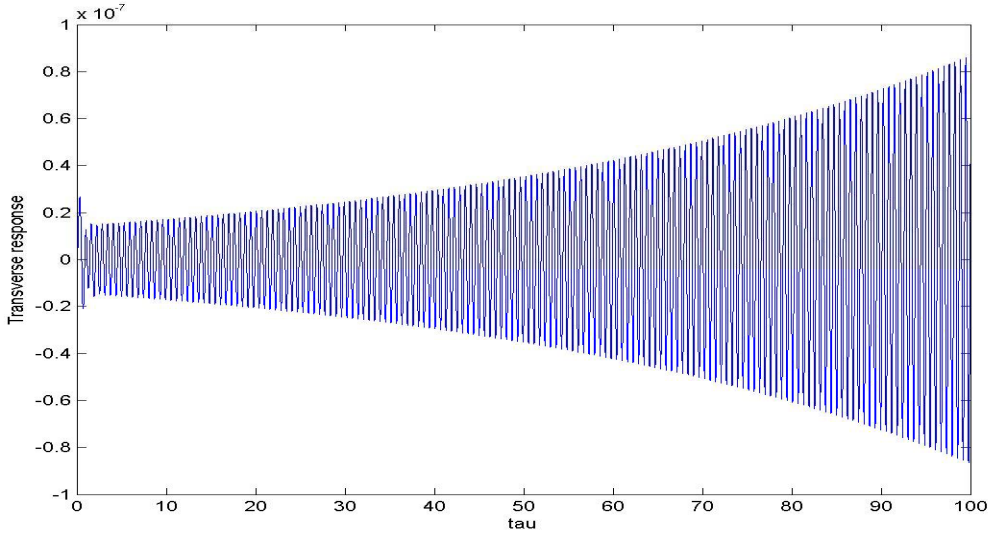

Fig. 6.10. $\tilde{\Delta}_{2N-1}$ vs. τ for $u = 4.30$, $\beta = 0.01$, and $\Lambda \sim 10^3$

When $\beta = 0.10$ ($\Lambda \sim 10^3$), Figure 6.11 shows the response to be stable when $u = 5.59$ and Figure 6.12 shows the response to be unstable at $u = 5.60$; therefore, the critical velocity can be approximated as $u = 5.595$. This result is again exactly the result obtained when $\Lambda \sim 10^5$ Compared with the value obtained in Table 5.11 for the four-term trigonometric\hyperbolic approximation ($u = 4.691$) and in Table 5.15 for the four-term polynomial approximation ($u = 4.805$), the percent error is 16.2% and 14.1% respectively.

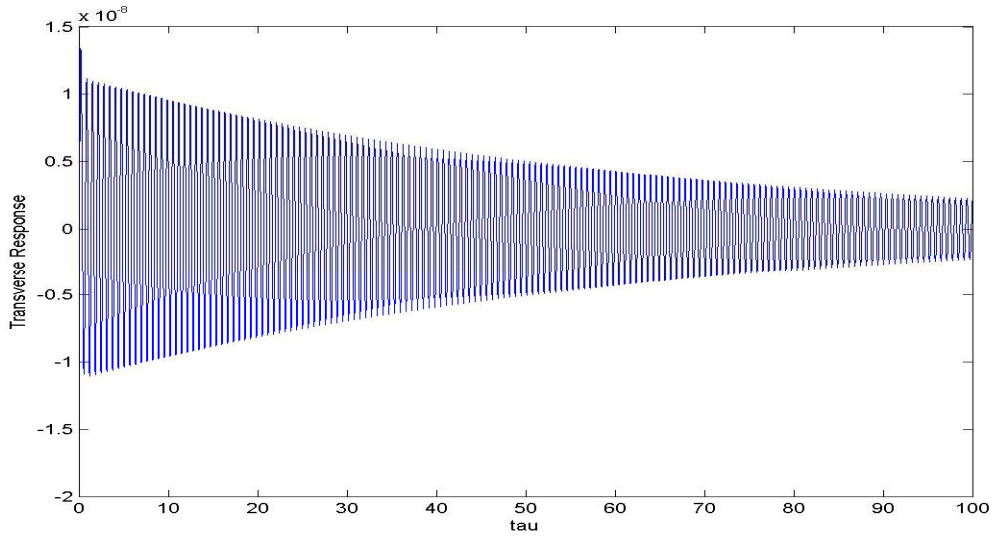

Fig. 6.11. $\tilde{\Delta}_{2N-1}$ vs. τ for $u = 5.59$, $\beta = 0.10$, and $\Lambda \sim 10^3$

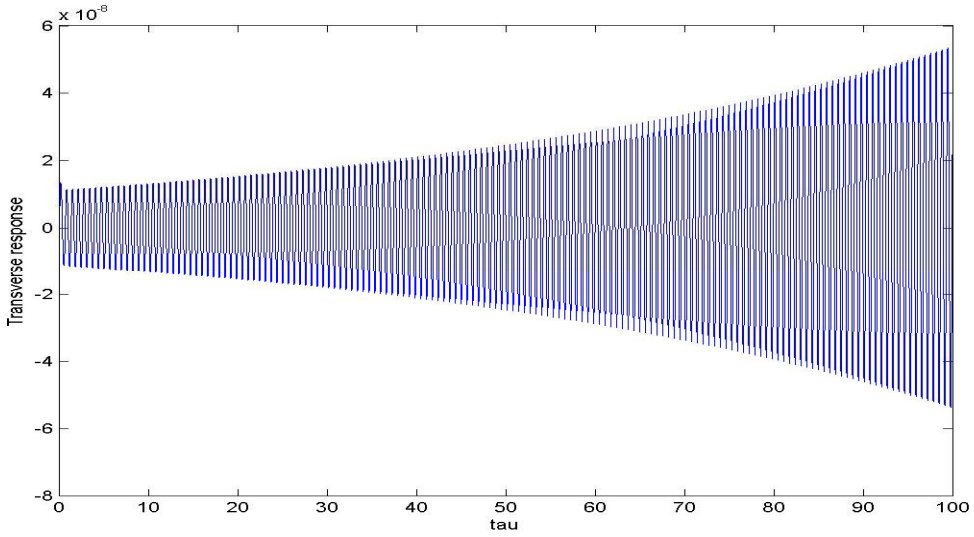

Fig. 6.12. $\tilde{\Delta}_{2N-1}$ vs. τ for $u = 5.60$, $\beta = 0.10$, and $\Lambda \sim 10^3$

When $\beta = 0.20$ ($\Lambda \sim 10^3$), Figure 6.13 shows the response to be stable when $u = 8.75$ and Figure 6.14 shows the response to be unstable at $u = 8.76$; therefore, the critical velocity can be approximated as $u = 8.755$. This result are very close to the result obtained when $\Lambda \sim 10^5$ ($u = 8.785$). Compared with the value obtained in Table 5.11 for the four-term trigonometric\hyperbolic approximation ($u = 5.523$) and in Table 5.15 for the four-term polynomial approximation ($u = 5.607$), the percent error is 36.9% and 36.0% respectively.

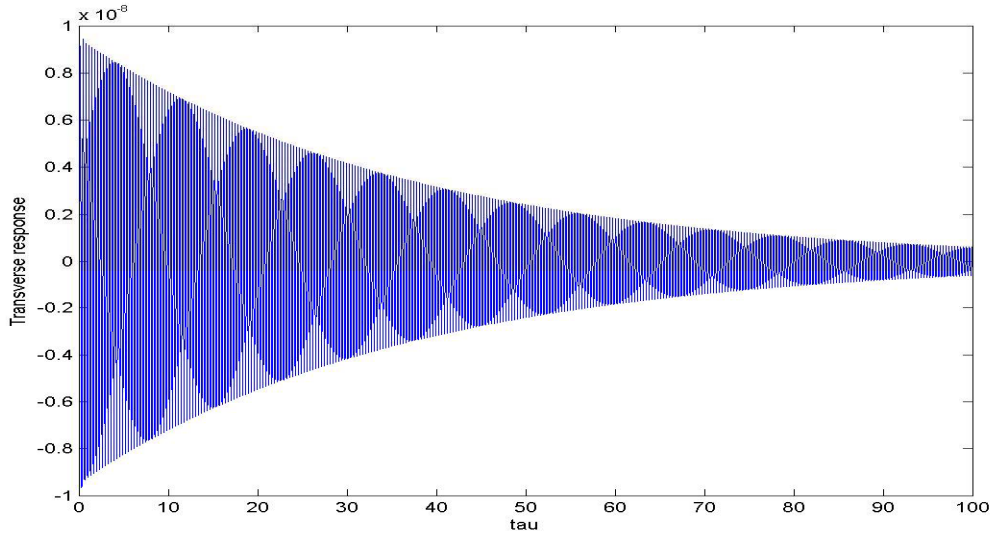

Fig. 6.13. $\tilde{\Delta}_{2N-1}$ vs. τ for $u = 8.75$, $\beta = 0.20$, and $\Lambda \sim 10^3$

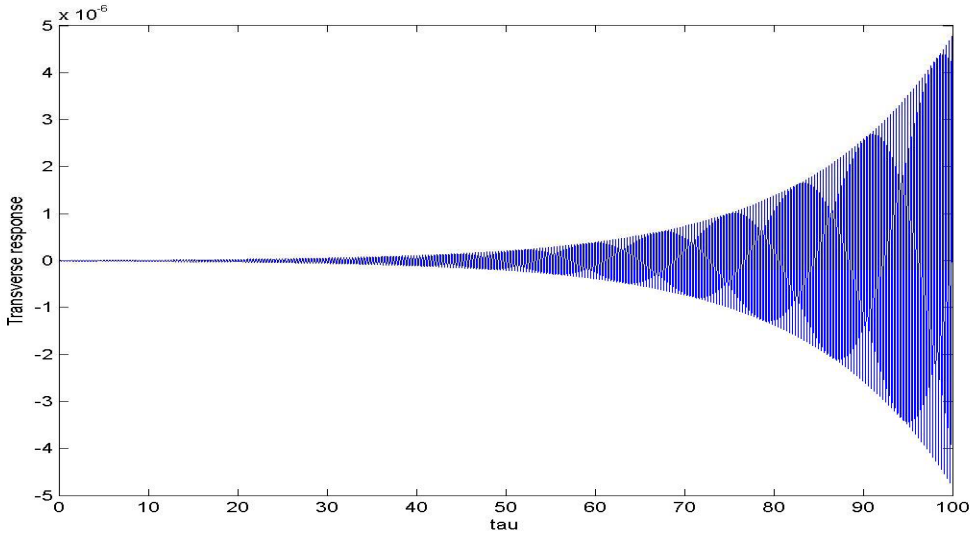

Fig. 6.14. $\tilde{\Delta}_{2N-1}$ vs. τ for $u = 8.76$, $\beta = 0.20$, and $\Lambda \sim 10^3$

As seen from Figures 6.9-6.14, the values of the critical velocities obtained from the Bubnov-Galerkin approximation (trigonometric\hyperbolic and polynomial) agree very well for $\beta = 0.01$, fair for $\beta = 0.10$, and poor again for $\beta = 0.20$ compared with the

exact numerical integration critical velocities. Also, the critical velocities obtained when $\Lambda \sim 10^5$ are exactly the same as those when $\Lambda \sim 10^5$ for $\beta = 0.01, 0.10$ and very close when $\beta = 0.20$. One can conclude that the slenderness ratio change from $\Lambda \sim 10^5$ to $\Lambda \sim 10^3$ has very little, or no effect on the critical velocity.

When $\beta = 0.01$ ($\Lambda \sim 10^2$), Figure 6.15 shows the response to be stable when $u = 4.22$ and Figure 6.16 shows the response to be unstable at $u = 4.23$; therefore, the critical velocity can be approximated as $u = 4.225$. This result is less than the numerically integrated result when $\Lambda \sim 10^5$ as expected from Figures 5.13 and 5.19. Compared with the value obtained in Table 5.12 for the four-term trigonometric\hyperbolic approximation ($u = 4.013$) and in Table 5.16 for the four-term polynomial approximation ($u = 4.343$), the percent error is 5.0% and 2.8% respectively.

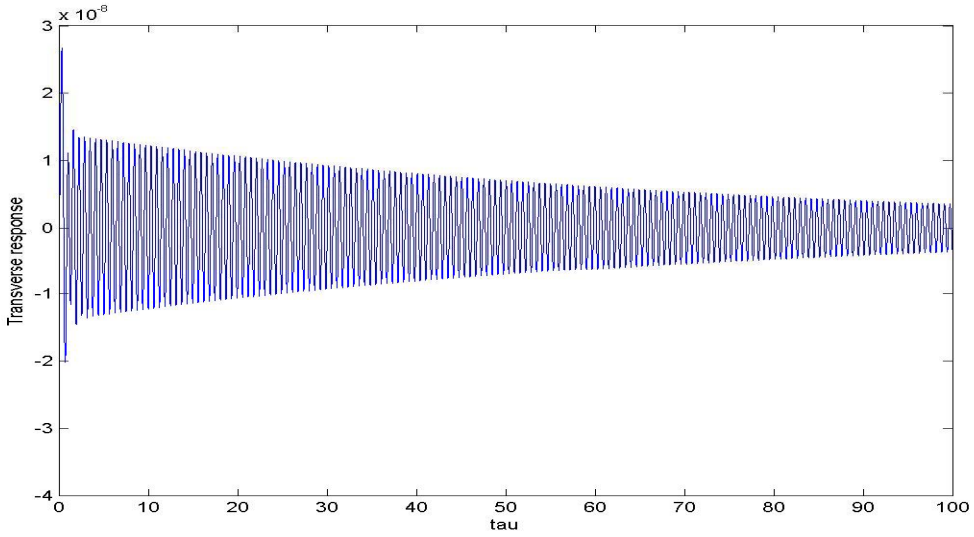

Fig. 6.15. $\tilde{\Delta}_{2N-1}$ vs. τ for $u = 4.22$, $\beta = 0.01$, and $\Lambda \sim 10^2$

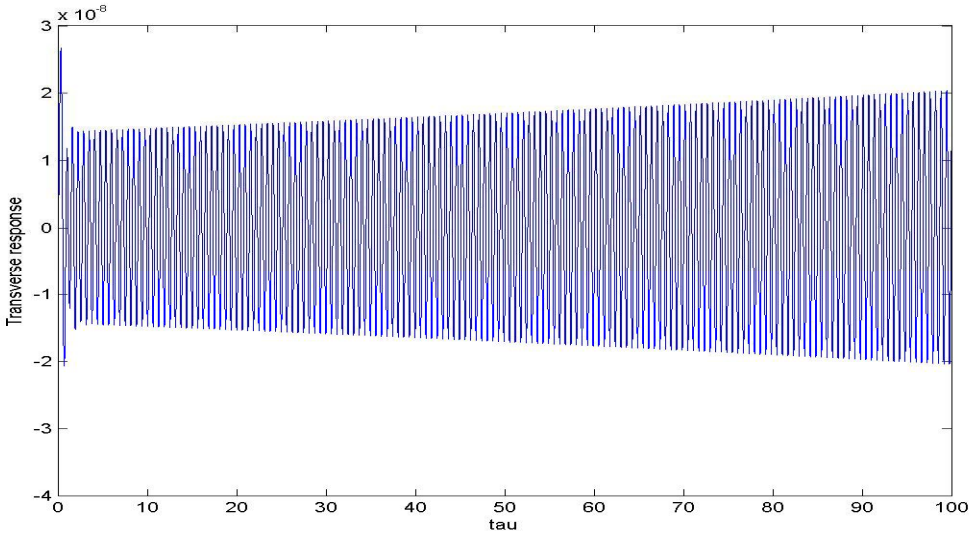

Fig. 6.16. $\tilde{\Delta}_{2N-1}$ vs. τ for $u = 4.23$, $\beta = 0.01$, and $\Lambda \sim 10^2$

When $\beta = 0.10$ ($\Lambda \sim 10^2$), Figure 6.17 shows the response to be stable when $u = 5.51$ and Figure 6.18 shows the response to be unstable at $u = 5.52$; therefore, the critical velocity can be approximated as $u = 5.515$. This result is again less than the numerically integrated result when $\Lambda \sim 10^5$. Compared with the value obtained in Table 5.12 for the four-term trigonometric\hyperbolic approximation ($u = 4.493$) and in Table 5.16 for the four-term polynomial approximation ($u = 4.806$), the percent error is 18.5% and 12.3% respectively.

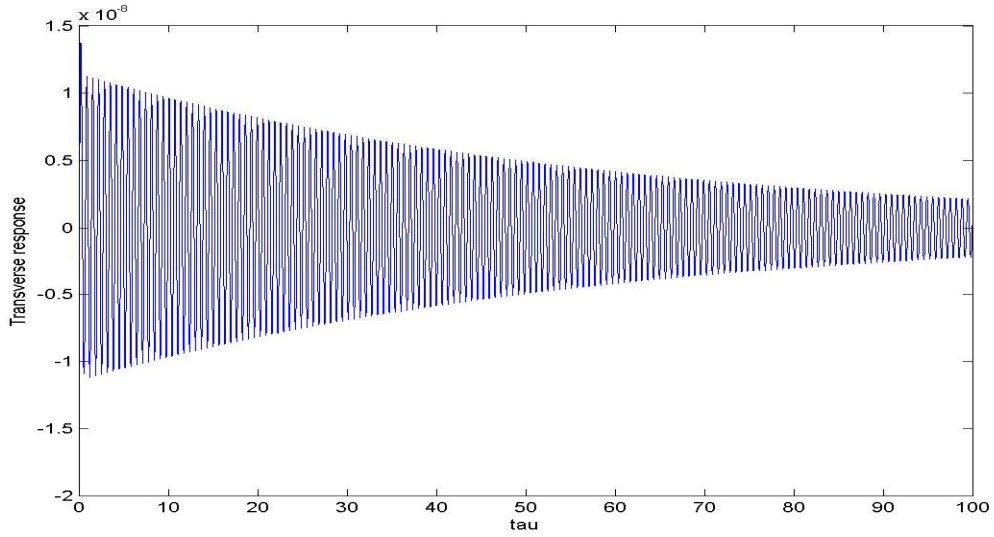

Fig. 6.17. $\tilde{\Delta}_{2N-1}$ vs. τ for $u = 5.51$, $\beta = 0.10$, and $\Lambda \sim 10^2$

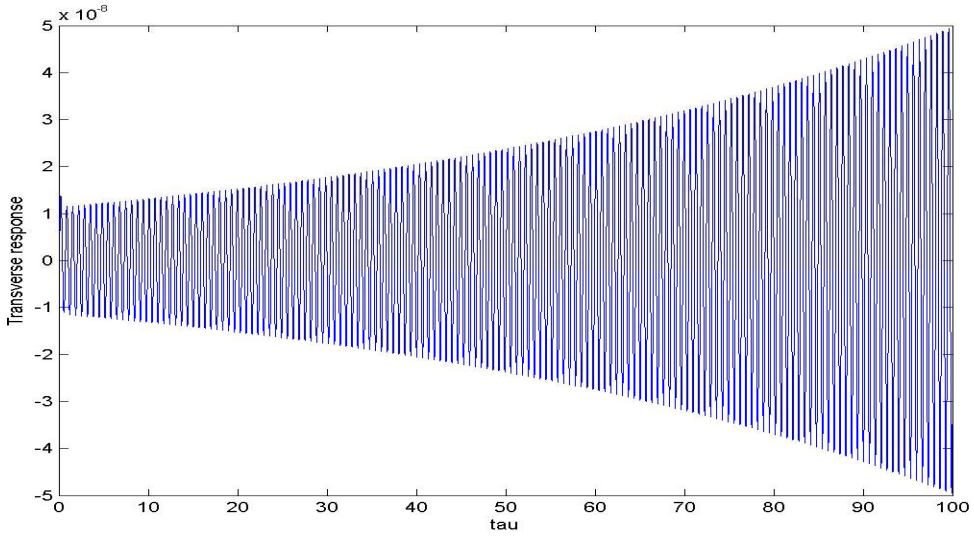

Fig. 6.18. $\tilde{\Delta}_{2N-1}$ vs. τ for $u = 5.52$, $\beta = 0.10$, and $\Lambda \sim 10^2$

When $\beta = 0.20$ ($\Lambda \sim 10^2$), Figure 6.19 shows the response to be stable when $u = 8.46$ and Figure 6.20 shows the response to be unstable at $u = 8.47$; therefore, the

critical velocity can be approximated as $u = 8.465$. This result is again less than the numerically integrated result when $\Lambda \sim 10^5$. Compared with the value obtained in Table 5.12 for the four-term trigonometric\hyperbolic approximation ($u = 5.279$) and in Table 5.16 for the four-term polynomial approximation ($u = 5.490$), the percent error is 37.6% and 35.1% respectively.

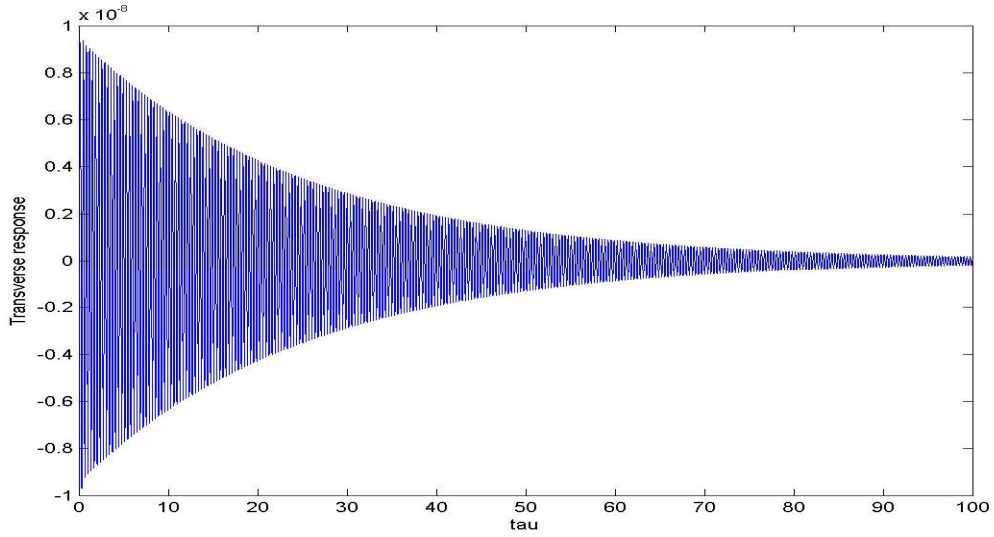

Fig. 6.19. $\tilde{\Delta}_{2N-1}$ vs. τ for $u = 8.46$, $\beta = 0.20$, and $\Lambda \sim 10^2$

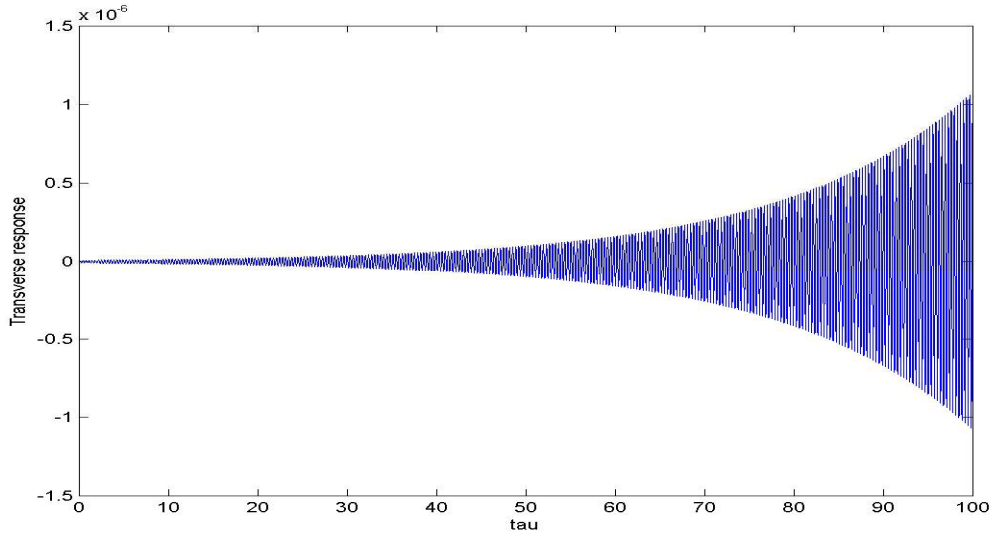

Fig. 6.20. $\tilde{\Delta}_{2N-1}$ vs. τ for $u = 8.47$, $\beta = 0.20$, and $\Lambda \sim 10^2$

The critical velocities obtained from numerical integration and from the Bubnov-Galerkin approximation agreed well for $\beta < 0.10$ and not so well for $\beta \geq 0.10$. The statement in the previous chapters about the linear model being poor for higher ranges of β ($\beta > 0.30$) is reinforced by the current numerical integration results. Therefore, it can now be stated that the linear model is only valid for $\beta < 0.10$ instead of $\beta < 0.30$ for all slenderness ratios ($\Lambda \sim 10^5, 10^3, 10^2$). It was a surprising result that the polynomial Bubnov-Galerkin basis function gave a better estimate of the critical velocity than the trigonometric\hyperbolic basis functions.

Looking back at Figures 5.9-5.20, it was anticipated that the change in critical velocity in going from $\Lambda \sim 10^5$ to $\Lambda \sim 10^3$ would be very small and from $\Lambda \sim 10^5$ to $\Lambda \sim 10^2$ would be fair. From the numerical integration results, the $\Lambda \sim 10^3$ critical velocities were identical (or very close with two significant digits accuracy) with

$\Lambda \sim 10^5$ critical velocities. The $\Lambda \sim 10^2$ critical velocities were however smaller than the $\Lambda \sim 10^5$ critical velocities as expected from Figures 5.9-5.20. Therefore, the effect of shear deformation overall lowers the critical velocities and has a noticeable effect only when the beam is thick ($\Lambda \sim 10^2$)

CHAPTER VII

CONCLUSION

The primary aim of this study, as stated in Chapter I, was to present a complete energy formulation via the principle of virtual work was given along with the dimensional and non-dimensional governing differential equations of motion for linear Timoshenko beam theory governing fluid-conveying pipes that undergo bending. This is fulfilled in the preceding chapters.

In addition, the eigenvalue problem was formulated via the Bubnov-Galerkin method using the basis functions (polynomial and trigonometric/hyperbolic) for the non-fluid beam; i.e. the boundary conditions (essential and natural) for the non-fluid beam were met instead of the actual boundary conditions for the fluid beam. The stability of the resulting equation (depending on how many terms were taken in the approximation) was studied via the Routh-Hurwitz stability criteria and the velocity at which the system goes unstable (i.e. the critical velocity) was ascertained for each value of the mass ratio β. When the number of terms increased in the approximation, "jumps" appeared around certain values of ($\beta = 0.3, 0.8$ for the four-term approximation). Along with more jumps appearing when the terms increased, the critical velocities increased when $\beta > 0.3$; i.e. the system was beginning to diverge after the approximate value $\beta = 0.3$. Vittori [3] also observed this phenomenon. These jumps and divergence also appeared for each value of the slenderness ratio ($\Lambda \sim 10^5, 10^3, 10^2$) studied. From these results, it is clear that the linear model is invalid for higher values of β.

Finally, a time-dependent Finite Element model of the non-dimensional equations of motion was formulated using [12] super-convergent spatial shape functions. Typical element non-dimensional mass, damping, and stiffness matrices were explicitly given along with accompanying boundary terms. The conventional shear force and moment boundary terms appeared along with two unusual boundary terms. These boundary terms represent the energy transferred to the beam from the fluid due to the free right end (proven by Benjamin [2]). These boundary terms were also shown to contribute only to outlet of the pipe (i.e. the second node of the right-most element). After a simple assembly, the resulting sets of coupled time-dependent ordinary differential equations were numerically integrated via the Newmark time marching scheme. The right-most transverse degree of freedom was plotted versus time to determine whether or not the system was stable or unstable. It was seen that the critical velocity for each value of Λ was reasonably close to the critical velocity obtained from the Bubnov-Galerkin approximation for very small values of β ($\beta < 0.1$). Therefore, the aforementioned statement about the linear model being invalid for $\beta > 0.3$ can further be refined by saying the linear model is invalid for $\beta > 0.1$.

When comparing critical velocities for the different slenderness ratios, the numerical integration results for $\beta < 0.1$ were identical for $\Lambda \sim 10^5$ and $\Lambda \sim 10^3$. When $\Lambda \sim 10^2$ however, the critical velocities were slightly lower. These slightly lower critical velocities were to be expected from examining Figures 5.9-5.20; in these figures, the $\Lambda \sim 10^3$ and $\Lambda \sim 10^5$ critical velocity points are right on top of each other and the

$\Lambda \sim 10^2$ critical velocity points noticeably slightly lower than the $\Lambda \sim 10^5$ critical velocity points.

The next step in further work will be to develop the non-linear equations of motion, study interesting characteristics by various non-linear methods, formulate the accompanying finite element model, and numerically solve the governing equations. It is anticipated that the response will go into a limit cycle which has been shown in other researcher's work.

REFERENCES

1. M.P. Paidoussis and G.X. Li 1993 *Journal of Fluids and Structures* **7**, 137-204. Pipes Conveying Fluid: A Model Dynamical Problem.

2. T.B. Benjamin 1961 *Proceedings of the Royal Society of London* **261**, 457-486. Dynamics of a System of Articulated Pipes Conveying Fluid I. Theory.

3. P. Vittori 2004, M.S. Thesis, College of Engineering, Florida Atlantic University. Dynamic Stability of Fluid-Conveying Pipes on Uniform and Non-Uniform Elastic Foundation.

4. B.E. Laithier 1979, Ph.D. Dissertation, Department of Mechanical Engineering, McGill University. Dynamics of Timoshenko Tubular Beams Conveying Fluid.

5. R.H. Long 1995 *Journal of Applied Mechanics* **22**, 65-68. Experimental and Theoretical Study of Transverse Vibration of a Tube Containing Flowing Fluid.

6. M. Becker, W. Hauger and W. Winzen 1978 *Archives of Mechanics* **30**, 757-768. Exact Stability Analysis of Uniform Cantilevered Pipes Conveying Fluid or Gas.

7. D.W. Dareing 1976 *Journal of Petroleum Technology.* Natural Frequencies of Marine Drilling Risers.

8. A.D. Dimarogonas and S. Haddad 1992 *Vibration for Engineers*. Englewood Cliffs, NJ: Prentice-Hall.

9. D. Escobar and E.C. Ting 1986 *PVP* **101**, 61-72. A Finite Element Computational Procedure for the Transient and Stability Behaviours of Fluid-Conveying Structures.

10. A.K. Kohli and B.C. Nakra 1984 *Journal of Sound and Vibration* **93**, 307-311. Vibration Analysis of Straight and Curved Tubes Conveying Fluid by Means of Straight Beam Finite Elements.

11. M.P. Paidoussis 1975 *Journal of Mechanical Engineering Science* **17**, 19-25. Flutter of Conservative Systems of Pipes Conveying Incompressible Fluid.

12. J.N. Reddy 2002 *Energy Principles and Variational Methods in Applied Mechanics (2nd Ed.).* Hoboken, NJ: John Wiley & Sons Inc.

13. M.M. Stanisic, J.A. Euler and S.T. Montgomery 1974 *Engineering Archive* **43**, 295-305. On a Theory Concerning the Dynamical Behavior of Structures Carrying Moving Masses.

14. M.P. Paidoussis and B.E. Laithier 1976 *Journal of Mechanical Engineering Science* **18**, 210-220. Dynamics of Timoshenko Beams Conveying Fluid.

15. B.E. Lathier and M.P. Paidoussis 1981 *Journal of Sound and Vibration* **79**, 175-195. The Equations of Motion of Initially Stressed Timoshenko Tubular Beams Conveying Fluid.

16. G.L Anderson 1972 *Journal of Sound and Vibration* **27**, 279-296. Application of a Variational Method to Dissipative, Non-Conservative Problems of Elastic Stability.

17. M.P. Paidoussis, T.P. Luu and B.E. Laithier 1986 *Journal of Sound and Vibration* **106**, 311-331. Dynamics of Finite-Length Tubular Beams Conveying Fluid.

18. A. Pramila, J. Laukkanen and S. Liukkonen 1991 *Journal of Sound and Vibration* **144**, 421-425. Dynamics and Stability of Short Fluid-Conveying Timoshenko Element.

19. C. Chu and Y. Lin 1995 *Shock and Vibration* **2,** 247-255. Finite Element Analysis of Fluid-Conveying Timoshenko Pipes.

20. Y.H. Lin and Y.K. Tsai 1997 *International Journal of Solid Structures* **34**, 2945-2956. Nonlinear Vibrations of Timoshenko Pipes Conveying Fluid.

21. C.P. Stack, R.B. Garnett and G.E. Pawlas 1993 *AIAA/ASME Structures, Structural Dynamics & Materials Conference*, 2120-2129. A Finite Element for the Vibration Analysis of a Fluid-Conveying Timoshenko Beam.

22. J.N. Reddy and C.M. Wang 2004, Centre for Offshore Research and Engineering (CORE), The National University of Singapore. Dynamics of Fluid-Conveying Beams: Governing Equations and Finite Element Models.

23. W.S. Edelstein, S.S. Chen and J.A. Jendrzejcyk 1986 *Journal of Sound and Vibration* **107**, 121-129. A Finite Element Computation of the Flow-Induced Oscillations in a Cantilevered Tube.

24. P.J. Holmes 1978 *Journal of Applied Mechanics* **45**, 619-622. Pipes Supported at Both Ends Cannot Flutter.

25. M Langthjem 1995 *Mechanical Structures and Machinery* **23**, 343-376. Finite Element Analysis and Optimization of a Fluid-Conveying Pipe.

26. R.E. Nickel and G.A. Secor 1972 *International Journal for Numerical Methods in Engineering* **5**, 243-253. Convergence of Consistently Derived Timoshenko Beam Finite Elements.

27. J. Rousselet and G. Herrmann 1981 *Journal of Applied Mechanics* **48**, 943-947. Dynamics Behaviour of Continuous Cantilevered Pipes Conveying Fluid Near Critical Velocities.

28. C. Semler, X. Li and M.P. Paidoussis 1994 *Journal of Sound and Vibration* **169**, 577-598. The Non-Linear Equations of Motion of Pipes Conveying Fluid.

29. J.N. Reddy 2006 *An Introduction to the Finite Element Method (3rd Ed.)*. Boston, MA: McGraw-Hill.

30. G.R. Cowper 1966 *Journal of Applied Mechanics* **33**, 335-340. The Shear Coefficient in Timoshenko's Beam Theory.

31. J.P. Charpie 1991, Ph.D. Dissertation, Department of Science and Mechanics, The Pennsylvania State University. An analytic Model for the Free In-Plane Vibration of Beams of Variable Curvature and Thickness.

32. D.B. McIver 1973 *Journal of Engineering Mathematics* **7**, 249-261. Hamilton's Principle for Systems of Changing Mass.

APPENDIX A

ROUTH-HURWITZ STABILITY CRITERIA

Developed by Routh in 1875 and modified by Hurwitz in 1895, the Routh-Hurwitz stability criteria determine the stability of a polynomial equation without actually computing the roots. Suppose an n^{th} degree polynomial is of the form [3]

$$f(s) = a_0 s^n + a_1 s^{n-1} + a_2 s^{n-2} + \cdots + a_{n-1} s + a_n \tag{A.1}$$

then its roots are generally of the complex form. The stability of (A.1) is solely determined by whether or not the real part of one root is positive. If the real part of at least one root of is positive, the polynomial in (A.1) will be unstable. The Routh-Hurwitz stability criteria says that the number of sign changes in the first column of a Hurwitz array is equal to the number of roots with positive real parts; thus, a system will be stable is there are no sign changes in the first column.

In order to apply the stability criteria, the first necessary condition that the coefficients in (A.1) are positive. The second necessary condition is that the coefficients of (A.1) are different from zero. The Hurwitz array is of form

$$\begin{array}{c|ccccc} s^n & a_0 & a_2 & a_4 & \cdots & a_n \\ s^{n-1} & a_1 & a_3 & a_5 & \cdots & a_{n-1} \\ s^{n-2} & b_1 & b_2 & b_3 & \cdots & \cdots \\ s^{n-3} & c_1 & c_2 & c_3 & \cdots & \cdots \\ s^{n-4} & \vdots & \vdots & \vdots & \ddots & \cdots \\ \vdots & & & & & \\ s^1 & & & & & \\ s^0 & & & & & \end{array} \tag{A.2}$$

where the a_i's are the polynomial coefficients and

$$b_1 = -\frac{1}{a_1}\begin{vmatrix} a_0 & a_2 \\ a_1 & a_3 \end{vmatrix}, b_2 = -\frac{1}{a_1}\begin{vmatrix} a_0 & a_4 \\ a_1 & a_5 \end{vmatrix}, b_3 = -\frac{1}{a_1}\begin{vmatrix} a_0 & a_6 \\ a_1 & a_7 \end{vmatrix}$$
$$c_1 = -\frac{1}{b_1}\begin{vmatrix} a_1 & a_3 \\ b_1 & b_2 \end{vmatrix}, c_2 = -\frac{1}{b_1}\begin{vmatrix} a_1 & a_5 \\ b_1 & b_3 \end{vmatrix}, \ldots \tag{A.3}$$

Once the terms in (A.3) are evaluated, the first column of (A.2) is inspected and the stability is determined by the number of sign changes. Because of the necessary condition of positive coefficients in (A.1), it is necessary and sufficient condition for stability that the rest of the terms in the first column of (A.2) have positive signs; no roots will have positive real parts.

A special case to consider is when the first element of a row in (A.2) is zero but some other elements are non-zero [3]. In this case, replace the zero element by a small number ε. The number ε should be treated as the same sign as the element above. Once the table is completed, the results should be interpreted as $\varepsilon \to 0$.

An alternative to the aforementioned Hurwitz array in (A.2) are Hurwitz determinants. This procedure is somewhat simpler when writing a program. The first five Hurwitz determinants are

$$T_0 = a_0, T_1 = a_1, T_2 = \begin{vmatrix} a_1 & a_0 \\ a_3 & a_2 \end{vmatrix}, T_3 = \begin{vmatrix} a_1 & a_0 & 0 \\ a_3 & a_2 & a_1 \\ 0 & a_4 & a_3 \end{vmatrix}, T_4 = \begin{vmatrix} a_1 & a_0 & 0 & 0 \\ a_3 & a_2 & a_1 & 0 \\ 0 & a_4 & a_3 & a_2 \\ 0 & 0 & 0 & a_4 \end{vmatrix} \tag{A.4}$$

and for $n > 4$

$$T_n = \begin{vmatrix} a_1 & a_3 & a_5 & a_7 & \cdots & a_{2n-1} \\ a_0 & a_2 & a_4 & a_6 & \cdots & a_{2n-2} \\ 0 & a_1 & a_3 & a_5 & \cdots & a_{2n-3} \\ 0 & a_0 & a_2 & a_4 & \cdots & a_{2n-4} \\ \vdots & \vdots & \vdots & \vdots & \ddots & \vdots \\ 0 & 0 & 0 & 0 & 0 & a_n \end{vmatrix} \tag{A.5}$$

In forming the *nxn* determinant of (A.5), one should go left-to-right and up-to-down filling in the slots until there is no more available slots to fill. Also one should replace the elements that don't exist by zeros.

Lienard and Shippart modified the Routh-Hurwitz criteria in 1914. They stated that the polynomial in (A.1) is stable only if every coefficient $(a_i's)$ and the determinants $T_{n-1}, T_{n-3}, T_{n-5}, \ldots$ were positive. This technique cut the calculations approximately in half [32].

APPENDIX B

DERIVATION OF SUPER-CONVERGENT SHAPE FUNCTIONS

Recall from (3.47) and (3.48)

$$\bar{M}_{xx} = \frac{\partial \phi}{\partial \xi} \tag{B.1}$$

$$\bar{Q}_x = \Lambda \left(\frac{\partial \eta}{\partial \xi} + \phi \right) \tag{B.2}$$

and from the non-dimensional Timoshenko beam equilibrium equations (without fluid)

$$\frac{d\bar{M}_{xx}}{d\xi} - \bar{Q}_x = 0 \tag{B.3}$$

$$\frac{d\bar{Q}_x}{d\xi} = 0 \tag{B.4}$$

Re-writing (3.4) in non-dimensional variables and using (B.2) and (B.4), we obtain

$$\gamma_{xz} = \frac{\partial \eta}{\partial \xi} + \phi = b_0 = const. \tag{B.5}$$

The non-dimensional transverse deflection is interpolated as a cubic polynomial of the form

$$\eta = a_0 + a_1 \xi + a_2 \xi^2 + a_3 \xi^3 \tag{B.6}$$

and its derivatives are of the form

$$\begin{aligned} \eta' &= a_1 + 2a_2 \xi + 3a_3 \xi^2 \\ \eta'' &= 2a_2 + 6a_3 \xi \\ \eta''' &= 6a_3 \end{aligned} \tag{B.7}$$

where $(\cdot)' = \frac{d}{d\xi}$. Substituting (B.5) into (B.1) and changing partial derivatives into ordinary derivatives we obtain

$$\bar{M}_{xx} = \frac{d\phi}{d\xi} = \frac{d}{d\xi}\left(b_0 - \frac{d\eta}{d\xi}\right) = -\eta'' \tag{B.8}$$

Using (B.2), (B.3), and (B.5) we get the relationship

$$\frac{d\bar{M}_{xx}}{d\xi} = \bar{Q}_x = \Lambda\gamma_{xz} \tag{B.9}$$

along with (B.8) from which we can say

$$\gamma_{xz} = -\frac{1}{\Lambda}\eta''' = -\frac{6}{\Lambda}a_3 \tag{B.10}$$

where now the rotation can be written as

$$\phi = \gamma_{xz} - \frac{d\eta}{d\xi} = -\left(a_1 + 2a_2\xi + \left(3\xi^2 + \frac{6}{\Lambda}\right)a_3\right) \tag{B.11}$$

Now the four constants, $a_0, \cdots, a_4$ can be written in terms of the nodal displacements and rotations at the left and right ends of a non-dimensional element length *h* through the equations

$$\begin{aligned}
&\eta(0) = a_0 = \eta_1 = \Delta_1 \\
&\eta(h) = a_0 + a_1 h + a_2 h^2 + a_3 h^3 = \eta_2 = \Delta_2 \\
&\phi(0) = -\left(a_1 + \frac{6}{\Lambda}a_3\right) = \phi_1 = \Delta_3 \\
&\phi(h) = -\left(a_1 + 2a_2 h + \left(3h^2 + \frac{6}{\Lambda}\right)a_3\right) = \phi_2 = \Delta_4
\end{aligned} \tag{B.12}$$

or in matrix from

$$\begin{bmatrix} 1 & 0 & 0 & 0 \\ 1 & h & h^2 & h^3 \\ 0 & -1 & 0 & -\frac{6}{h} \\ 0 & -1 & -2h & -\left(3h^2+\frac{6}{\Lambda}\right) \end{bmatrix} \begin{Bmatrix} a_0 \\ a_1 \\ a_2 \\ a_3 \end{Bmatrix} = \begin{Bmatrix} \Delta_1 \\ \Delta_2 \\ \Delta_3 \\ \Delta_4 \end{Bmatrix} \tag{B.13}$$

The matrix of (B.13) must be inverted to solve for $a_0,\cdots,a_4$ in terms of $\Delta_1,\cdots,\Delta_4$. Once these constants are solved for, $a_0,\cdots,a_4$ are substituted back into (B.6) and (B.11). After gathering terms with respect to $\Delta_1,\cdots,\Delta_4$ and making the substitution $\mu = 1+\frac{12}{\Lambda}$ and $\zeta = \frac{\xi}{h}$, one arrives at(6.13)-(6.14). The super-convergent shape functions in (6.13)-(6.14) also have the property

$$\begin{aligned} \eta(0) &= \Delta_1 \\ \phi(0) &= \Delta_2 \\ \eta(h) &= \Delta_3 \\ \phi(h) &= \Delta_4 \end{aligned} \tag{B.14}$$

APPENDIX C

1-D FINITE ELEMENT PROGRAM

```
%%%%%%%%%%%%%%%%%%%%%%%%%%%%%%%%%%%%%%%%%%%%%%%%%%%%%%%%%%%%%%%%%%%%%%%%%
%%%%%%%1-D FINITE ELEMENT PROGRAM FOR AN ELASTIC TIMOSHENKO Pipe%%%%%%
%%%%%%%%%%%%%%%%%%%%%%%%%%%%%%%%%%%%%%%%%%%%%%%%%%%%%%%%%%%%%%%%%%%%%%%%%

%Clear workspace and Command Window
clear;
clc;

%Finite Element Parameters
NE=50                   %Number of Elements
Time=100;               %Total Time
DeltaT=1.0E-3;          %Time Step
u_disp_init=0.0;        %Initial Displacement
u_vel_init=0.0;         %Initial Velocity
u_acc_init=0.0;         %Initial Acceleration

%Parameters of the System
Lambda=10E5;            %Slenderness Ratio
u=4.29;                 %Non-Dimensional Velocity
beta=0.01;              %Mass Ratio
sigma=0.0;              %Rotary Inertia Constant
gamma1=1E-4;            %Forcing Amplitude

%Begin Calculation Timer
tic

%Number of Nodes(NN) and Dof(NDOF) in the model
NN=NE+1;
NDOF=2*NN;

%Nodal Coordinates
z=zeros(NN,1);
for i=1:1:NN
    z(i,1)=(1/(NE))*(i-1);
end

%Length of each element
L=zeros(NE,1);
for i=1:1:NE
    L(i,1)=z(i+1,1)-z(i,1);
end
h=L(1,1);

%Element Connectivity Matrix
con1=zeros(1,NE);
con2=con1;
for j=1:1:NE
```

```
    con1(1,j)=j;
    con2(1,j)=j+1;
end
econ=[con1;con2];

%Local [M] Matrices
M_local=zeros(4,4,NE);
m1=1/(420*h*(Lambda+12)^2);
for n=1:1:NE

M_local(1,1,n)=(156*h^2+504*sigma)*Lambda^2+3528*h^2*Lambda+20160*h^2;
M_local(1,2,n)=-2*h*(21*sigma+11*h^2)*Lambda^2-2*h*(231*h^2-
1260*sigma)*Lambda-2520*h^3;
M_local(1,3,n)=(54*h^2-504*sigma)*Lambda^2+1512*h^2*Lambda+10080*h^2;
M_local(1,4,n)=h*(-
42*sigma+13*h^2)*Lambda^2+h*(378*h^2+2520*sigma)*Lambda+2520*h^3;

M_local(2,1,n)=M_local(1,2,n);
M_local(2,2,n)=4*h^2*(14*sigma+h^2)*Lambda^2+4*h^2*(210*sigma+21*h^2)*L
ambda+4*h^2*(5040*sigma+126*h^2);
M_local(2,3,n)=-h*(-42*sigma+13*h^2)*Lambda^2-
h*(378*h^2+2520*sigma)*Lambda-2520*h^3;
M_local(2,4,n)=-h^2*(3*h^2+14*sigma)*Lambda^2-
h^2*(840*sigma+84*h^2)*Lambda-h^2*(-10080*sigma+504*h^2);

M_local(3,1,n)=M_local(1,3,n);
M_local(3,2,n)=M_local(2,3,n);
M_local(3,3,n)=(156*h^2+504*sigma)*Lambda^2+3528*h^2*Lambda+20160*h^2;
M_local(3,4,n)=2*h*(21*sigma+11*h^2)*Lambda^2+2*h*(231*h^2-
1260*sigma)*Lambda+2520*h^3;

M_local(4,1,n)=M_local(1,4,n);
M_local(4,2,n)=M_local(2,4,n);
M_local(4,3,n)=M_local(3,4,n);
M_local(4,4,n)=4*h^2*(14*sigma+h^2)*Lambda^2+4*h^2*(210*sigma+21*h^2)*L
ambda+4*h^2*(5040*sigma+126*h^2);

end

%Global [M] Matrix
M=zeros(NDOF,NDOF);
for n=1:1:NE
    for i=1:1:2
        for j=1:1:2
            ii=econ(i,n);
            jj=econ(j,n);
            M(2*ii-1,2*jj-1)=M(2*ii-1,2*jj-1) + M_local(2*i-1,2*j-1,n);
            M(2*ii-1,2*jj)  =M(2*ii-1,2*jj)   + M_local(2*i-1,2*j,n);
            M(2*ii,2*jj-1)  =M(2*ii,2*jj-1)   + M_local(2*i,2*j-1,n);
            M(2*ii,2*jj)    =M(2*ii,2*jj)     + M_local(2*i,2*j,n);
        end
    end
end
```

```
M=m1*M;

%Local [C] Matrices
C_local=zeros(4,4,NE);
c1=-(sqrt(beta)*u)/(30*(Lambda+12));
c33=(sqrt(beta)*u)/c1;

for n=1:1:NE

C_local(1,1,n)=0  ;
C_local(1,2,n)=-6*h*(Lambda+10);
C_local(1,3,n)=30*Lambda+360;
C_local(1,4,n)=6*h*(Lambda+10);

C_local(2,1,n)=-C_local(1,2,n);
C_local(2,2,n)=0;
C_local(2,3,n)=-6*h*(Lambda+10);
C_local(2,4,n)=-h^2*Lambda;

C_local(3,1,n)=-C_local(1,3,n);
C_local(3,2,n)=-C_local(2,3,n);
C_local(3,3,n)=0  ;
C_local(3,4,n)=-6*h*(Lambda+10);

C_local(4,1,n)=-C_local(1,4,n);
C_local(4,2,n)=-C_local(2,4,n);
C_local(4,3,n)=-C_local(3,4,n);
C_local(4,4,n)=0;

end

C_local(3,3,NE)=C_local(3,3,NE) - c33  ;

%Global [C] Matrix
C=zeros(NDOF,NDOF);
for n=1:1:NE
    for i=1:1:2
        for j=1:1:2
            ii=econ(i,n);
            jj=econ(j,n);
            C(2*ii-1,2*jj-1)=C(2*ii-1,2*jj-1) + C_local(2*i-1,2*j-1,n);
            C(2*ii-1,2*jj)  =C(2*ii-1,2*jj)   + C_local(2*i-1,2*j,n);
            C(2*ii,2*jj-1)  =C(2*ii,2*jj-1)   + C_local(2*i,2*j-1,n);
            C(2*ii,2*jj)    =C(2*ii,2*jj)     + C_local(2*i,2*j,n);
        end
    end
end
C=c1*C;

%Local [K] Matrices
K_local=zeros(4,4,NE);
k1=(1/(30*h^3*(Lambda+12)^2));
```

```
kc=u^2/(h*(Lambda+12));

k31=-12*kc/k1;
k32=6*h*kc/k1;
k33=12*kc/k1;
k34=-h*(Lambda+6)*kc/k1;

for n=1:1:NE

K_local(1,1,n)= (360-36*u^2*h^2)*Lambda^2+(-
720*u^2*h^2+4320*h^2)*Lambda-4320*u^2*h^2  ;
K_local(1,2,n)= 3*h*(u^2*h^2-60)*Lambda^2-2160*h^3*Lambda  ;
K_local(1,3,n)= (-360+36*u^2*h^2)*Lambda^2+(720*u^2*h^2-
4320*h^2)*Lambda+4320*u^2*h^2 ;
K_local(1,4,n)= 3*h*(u^2*h^2-60)*Lambda^2-2160*h^3*Lambda ;

K_local(2,1,n)= K_local(1,2,n);
K_local(2,2,n)= -4*h^2*(u^2*h^2-30)*Lambda^2-4*h^2*(-180+15*u^2*h^2-
270*h^2)*Lambda-4*h^2*(-1080+90*u^2*h^2);
K_local(2,3,n)= -3*h*(u^2*h^2-60)*Lambda^2+2160*h^3*Lambda;
K_local(2,4,n)= h^2*(u^2*h^2+60)*Lambda^2+h^2*(1080*h^2-
720+60*u^2*h^2)*Lambda+h^2*(-4320+360*u^2*h^2);

K_local(3,1,n)= K_local(1,3,n)     ;
K_local(3,2,n)= K_local(2,3,n)  ;
K_local(3,3,n)= (360-36*u^2*h^2)*Lambda^2+(-
720*u^2*h^2+4320*h^2)*Lambda-4320*u^2*h^2;
K_local(3,4,n)= -3*h*(u^2*h^2-60)*Lambda^2+2160*h^3*Lambda;

K_local(4,1,n)= K_local(1,4,n);
K_local(4,2,n)= K_local(2,4,n);
K_local(4,3,n)= K_local(3,4,n);
K_local(4,4,n)= -4*h^2*(u^2*h^2-30)*Lambda^2-4*h^2*(-180+15*u^2*h^2-
270*h^2)*Lambda-4*h^2*(-1080+90*u^2*h^2);

end

K_local(3,1,NE)=K_local(3,1,NE) + k31 ;
K_local(3,2,NE)=K_local(3,2,NE) + k32;
K_local(3,3,NE)=K_local(3,3,NE) + k33;
K_local(3,4,NE)=K_local(3,4,NE) + k34;

%Global [K] Matrix
K=zeros(NDOF,NDOF);
for n=1:1:NE
    for i=1:1:2
        for j=1:1:2
            ii=econ(i,n);
            jj=econ(j,n);
            K(2*ii-1,2*jj-1)=K(2*ii-1,2*jj-1) + K_local(2*i-1,2*j-1,n);
            K(2*ii-1,2*jj)  =K(2*ii-1,2*jj)   + K_local(2*i-1,2*j,n);
            K(2*ii,2*jj-1)  =K(2*ii,2*jj-1)   + K_local(2*i,2*j-1,n);
```

```
            K(2*ii,2*jj)    =K(2*ii,2*jj)     + K_local(2*i,2*j,n);
        end
    end
end
K=k1*K;

%Local {f} Vectors
f_local=zeros(4,1,NE);
f1=((gamma1*h)/12);

for n=1:1:NE
    for i=1:1:4
        f_local(1,1,n)=6;
        f_local(2,1,n)=-h;
        f_local(3,1,n)=6;
        f_local(4,1,n)=h;
    end
end

%Global {f} Vector
f=zeros(NDOF,1);
for n=1:1:NE
    for i=1:1:2
        ii=econ(i,n);
        f(2*ii-1,1)=f(2*ii-1,1) + f_local(2*i-1,1,n);
        f(2*ii,1)  =f(2*ii,1)   + f_local(2*i,1,n);
    end
end
f=f1*f;

%Condensed [M], [C], [K] Matrices
for i=1:1:(NDOF-2)
    for j=1:1:(NDOF-2)
        K_cond(i,j)=K(i+2,j+2);
        M_cond(i,j)=M(i+2,j+2);
        C_cond(i,j)=C(i+2,j+2);
    end
end

%Condensed {f} Vector
for i=1:1:(NDOF-2)
    f_cond1(i,1)=f(i+2,1);
end


%Time Step Parameters
alpha=0.5;
gamma=0.5;

a1=alpha*DeltaT;
a2=(1-alpha)*DeltaT;
a3=2/(gamma*(DeltaT)^2);
```

```
a4=2/(2*gamma*DeltaT);
a5=(1/gamma) -1;
a6=2*alpha/gamma -1;
a7=(DeltaT/2)*(2*alpha/gamma -2);

%Time Step Approximation
u_plot=zeros(ceil(Time/DeltaT),1);

K_hat=(K_cond + a3*M_cond + a5*C_cond);
K_hat_inv=inv(K_hat);

%Initial Displacement, Velocity, and Acceleration for the first time
step
u_disp_star=u_disp_init*ones(NDOF-2,1);
u_vel_star=u_vel_init*ones(NDOF-2,1);
u_acc_star=u_acc_init*ones(NDOF-2,1);

%Initial Displacement, Velocity, and Acceleration for the second time
step
u_disp=K_hat_inv*(f_cond1 + M_cond*(a3*u_disp_star + a4*u_vel_star +
a5*u_acc_star) + C_cond*(a5*u_disp_star + a6*u_vel_star +
a7*u_acc_star));
u_acc=a3*(u_disp-u_disp_star) - a4*u_vel_star - a5*u_acc_star;
u_vel=u_vel_star + a2*u_acc_star + a1*u_acc;

%First value of the last node's deflection
u_disp_first=u_disp(NDOF-3,1);

for i=2:1:ceil(Time/DeltaT)
    u_disp_1=u_disp;
    u_vel_1=u_vel;
    u_acc_1=u_acc;

    u_disp = K_hat_inv*( M_cond*(a3*u_disp_1 + a4*u_vel_1 + a5*u_acc_1)
+ C_cond*(a5*u_disp_1 + a6*u_vel_1 + a7*u_acc_1));
    u_acc= a3*(u_disp - u_disp_1) - a4*u_vel_1 - a5*u_acc_1;
    u_vel= u_vel_1 + a2*u_acc_1 + a1*u_acc;

%Second, Third,...value of the last node's deflection
u_plot(i,1)=u_disp(NDOF-3,1);

end

u_plot(1,1)=u_disp_first;

t=zeros(ceil(Time/DeltaT),1);
for i=1:1:ceil(Time/DeltaT)
    t(i,1)=DeltaT*(i-1);
end

plot(t,u_plot)
```

```
%End Calculation Timer
toc
```

VITA

Ryan Curtis Petrus received his Bachelor of Science degrees in Mathematics and Statistics, and Physics at Louisiana Tech University in 2004. Shortly after receiving these dual degrees, he entered the Mechanical Engineering graduate program at Texas A&M University in 2004. He graduated with his Master of Science degree in May 2006. His research interests are structural and vibration analysis of solid mechanics.

Mr. Petrus may be reached at 8400 Old Monroe Rd., Bastrop, LA 71220. His email address is ryanpike21@hotmail.com.